MITIGATION OF HARMONICS AND VOLTAGE VARIATION IN GRID CONNECTED WIND POWER SYSTEM USING STATIC SYNCHRONOUS COMPENSATOR

CASE STUDY: ADAMA- II WIND FARM

A THESIS SUBMITTED

IN PARTIAL FULFILLMENT OF THE REQUIREMENTS

FOR THE DEGREE OF

MASTER OF SCIENCE

IN

POWER SYSTEM AND ENERGY ENGINEERING

BY

LIULSEGED EPHREM

DEPARTMENT OF ELECTRICAL AND COMPUTER ENGINEERING,

FACULITY OF ELECTRICAL ENGINEERING, INSTITUE OF TECHNOLOGY (IOT),

SCHOOL OF GRADUTE STUDIES

HAWASSA UNIVERSITY

HAWASSA, ETHIOPIA

ADVISOR: Mr. TEWODROS TESFAYE

CO-ADVISOR: Mr. ISSAIAS GIDAY

JULY 17, 2020

HAWASSA UNIVERSITY

SCHOOL OF GRADUATE STUDIES

EXAMINERS' APPROVAL SHEET

We, the undersigned, members of the Board of Examiners of the final Master's degree open defense, by **Liulseged Ephrem** have read and evaluated his thesis entitled **"Mitigation of Harmonics and Voltage Variation in Grid Connected Wind Power System Using Static Synchronous Compensator (Case study: Adama-II Wind Farm)''** and examined the candidate. This is, therefore, to certify that the thesis has been accepted in partial fulfillment of the requirement for the degree of Master of Science in Electrical Engineering with Specialization in Power System and Energy Engineering.

Mr. Tefera Tadesse	_____	_____
Name of the Chair Person	Signature	Date
Dr. Baseem Khan	_____	_____
Name of Internal Examiner	Signature	Date
Dr. Friehun Taffesse	_____	_____
Name of External Examiner	Signature	Date
Mr. Tewodros Tesfaye	_____	_____
Name of Principal Advisor	Signature	Date
Mr. Issaias Gidey	_____	_____
Name of the Co-Advisor	Signature	Date
_____	_____	_____
SGC	Signature	Date

DECLARATION

I hereby declare that this submission is my own work towards the degree of Master of Science and that to the best of my knowledge, it contains no material previously published by another person nor material which has been accepted for the award of any other degree at any University, except where due acknowledgment has been made in the text.

Liulseged Ephrem	_____	_____
Student	Signature	Date
Certified by:		
Mr. Tewodros Tesfaye	_____	_____
Advisor	Signature	Date
Mr. Issaias Gidey	_____	_____
Co-Advisor	Signature	Date

ACKNOWLEDGEMENTS

First of all, I thank the Almighty God! who has endowed me with all the strength, patience and time to complete this thesis.

This thesis has been carried out at the department of electrical and computer engineering at Hawassa university-institute of technology (IOT). The financial support provided by Hawassa university via school of graduate studies is gratefully acknowledged.

I would like to thank Mr. Issaias Gidey, coordinator of the power system and energy engineering for continuous guidance and motivation to complete the thesis work.

I would like to thank my supervisors Mr. Tewodros Tesfaye and Mr. Issaias Gidey for help, inspiration, and encouragement. Thanks goes to my fellow MSc. students who have assisted me during my thesis work.

I would like to acknowledge Ethiopian Electric Power chief executive officer, Mr Andewalem Andarge, for granting permission to access Adama wind farms to collect all the necessary data for my research work. And I would also like to acknowledge the Adama II substations staffs, specially Mr Mohammed Awol, who is the technical operation manager, for kind provision of data and information.

Finally, I would like to thank my family for their love and support; and Wolaita Sodo University for giving me the chance to upgrade my academic status and for their financial sponsorship.

ABSTRACT

Recently the demand for renewable energy in general and that of wind energy specifically are increasing. The challenges to this energy related with power quality issues especially harmonics and voltage variations are increasing during the integration of large-scale wind power. Power electronics device plays major role in harmonic and voltage variation problems when integrating wind energy to the grid. Adama-II wind farm is set up with variable speed wind turbines coupled with doubly fed induction generator (DFIG) type. To solve these problems, Adama-II wind farm has 3^{rd} and 5^{th} harmonic branch of TKMCR static dynamic Var compensation device and magnetically coupled reactor type SVC which act as a harmonic mitigation, reactive power compensator and voltage regulator. However, they have problems like, sudden changes in capacitors, limited life of operation and low response time. Due to advantages of fast response time, better voltage support and reactive power support static synchronous compensator (STATCOM) is used in this thesis. In this regard, 3 MVAr average rated capacity of static synchronous compensator is needed to mitigate the harmonics and voltage variations at point of coupling (PCC). As FFT analysis shows, due to both back-to-back VSC of DFIG and non-linear load that are connected at PCC, total harmonic distortion of current and voltage at Point of common coupling without connection of static synchronous compensator are 30.21 % and 5.18 % respectively. But after the connection of static synchronous compensator, the total harmonic distortion of current and voltage are reduced to the value 3.39 % and 0.25% respectively. When STATCOM is connected at PCC, the voltage is recovered to the value of 1.048 pu from drop of 0.736 pu due to the connection of nonlinear load and to the value 0.9957pu from drop of 0.6885pu due to linear load. Effectiveness of the developed static synchronous compensator scheme relieves the point of common coupling voltage and current from harmonics distortion to comply with 3% and 5% specified by IEEE 519-1992. For validation of the developed system, MATLAB Power software is used for harmonic and voltage dip analysis. The result analysis by using SVC and STATCOM has been carried and STATCOM performed more than SVC in mitigating harmonics and voltage variation of grid connected wind power.

Keywords*:* *static synchronous compensator, doubly-fed induction generator, total harmonic distortion, voltage variation.*

TABLE OF CONTENTS

LIST OF FIGURES

LIST OF TABLES

ABBRIVATIONS

ASVC	Advanced Static VAr Compensator
AC	Alternating Current
ASD	Adjustable Speed Driver
BESS	Battery Energy Storage System
CVDPC	Combination of Vector Direct Power Control
DTC	Direct Torque Control
DFIM	Doubly Fed Induction Machine
DPC	Direct Power Control
DFIG	Doubly Fed Induction Generator
DC	Direct Current
DDSG	Direct Drive Synchronous Generator
FFT	Fast Fourier Transformer
FACTS	Flexible AC Transmission Systems
FSWT	Fixed Speed Wind Turbine
FLC	Fuzzy Logic Controller
GSC	Grid-Side Converter
HCC	Hysteresis Current Controller
IGBT	Insulated Gate Bipolar Transistor
IEEE	Institute of Electrical and Electronic Engineering
IEC	International Electro-Electrotechnical Commissioning
LPF	Low Pass Filter
MCR	Magnetically Coupled Reactors
MPPT	Maximum Power Point Tracking
PCC	Point of Common Coupling
PI	Proportional-Integral
PLL	Phase-Locked Loop
PMSG	Permanent Magnet Synchronous Generator
PT	Potential Transformer
PV	Photovoltaic
PWM	Pulse Width Modulation

RPM	Rotations Per Minute
RSC	Rotor Side Converter
SE	Sany Electric
SVC	Static VAr Compensator
SCIG	Squirrel Cage Induction Generator
STATCOM	Static Synchronous Compensator
SSSC	Static Synchronous Series Compensator
SLGF	Single Line to Ground Fault
SMC	Sliding Mode Control
SVOC	Stator Voltage Oriented Control
TCR	Thyristor Control Reactor
TCSC	Thyristor Controlled Series Compensator
THD	Total Harmonic Distortion
TSR	Tip Speed Ratio
UPFC	Unified Power Flow Controller
VAWT	Vertical Axis Wind Turbine
VSC	Voltage Source Converter
VSIGs	Variable Speed Induction Generators
VFC	Variable Frequency Converter
VSWT	Variable-Speed Wind Turbine
WEG	Wind Energy Generation
WECC	Western Electricity Coordinating Council
WECS	Wind Energy Conversion System
WF	Wind Farm
WTG	Wind Turbine Generation
3Φ	Three-phase

CHAPTER ONE

INTRODUCTION

1.1 Background

A global transition to renewable energy resources is well suited to meet the need for power in remote areas which lack grid and road infrastructure. The support for the use of renewable energy resources is increasing as global warming is a major environmental concern, and it offers an alternative for future energy supply [1]. To have sustainable growth and social progress, it is necessary to meet the energy need by utilizing renewable energy resources like wind, solar, biomass, hydro, co-generation, etc. [2]. In sustainable energy system, energy conservation and the use of renewable energy source are the key factors that drive the system. The need to integrate the renewable energy like wind energy into power system is to mitigate the impact on the environmental pollution by the conventional power generation system [3].

Wind energy is one of the most promising renewable energy resources for generating electricity due to its cost competitiveness compared to other conventional types of energy resources. The wind is a free, clean and inexhaustible energy source. Wind energy conversion is the fastest-growing source of new electric generation in the world [4].

Increased rate of depletion of fossil energy resources in one hand and growing energy demand on the other hand has initiated considerable research activity worldwide to explore means for tapping of renewable energy resources. Many different concepts have been developed and tested over years. Activities in this field were encouraged by the oil crisis in 1973. During the last two decades, the production of wind turbines has grown in size from 20 kW to 2 MW [5]. Many improvements and innovations have been made since the wind turbines began to become important as an alternative method of generating electricity from the 1980s [6]. The first wind turbine in the world was designed and built by Charls Brush in 1988. It generated 12 MW power [7].

The first use of wind power was to sail Ships in the Nile some 5,000 year ago. Many civilizations used wind power for transportation and other purposes. The Europeans used it to grind grains and pump water in the 1700s and 1800s. The first windmill to generate electricity in the rural U.S.A. was installed in 1890. An experimental grid connected turbine with as large a capacity as 2 MW was installed in 1979 on Howard Knob Mountain near Boone, NC, and a 3 MW turbine was

installed in 1988 on Berger Hill in Orkney, Scotland [8]. According to the Global Wind Energy Association, the global wind power installed capacity was 486.66 GW by the end of 2016. Among all the countries, China has installed 149 GW wind power by the end of 2016 [9], ranking No.1 in the world. In India Out of total installed generation capacity of renewable power as on March 2012 wind power accounted for about 65.65%. According to Global Wind Statistics Egypt is the second wind power produced country following South Africa in 2016 over all Africa country [10].

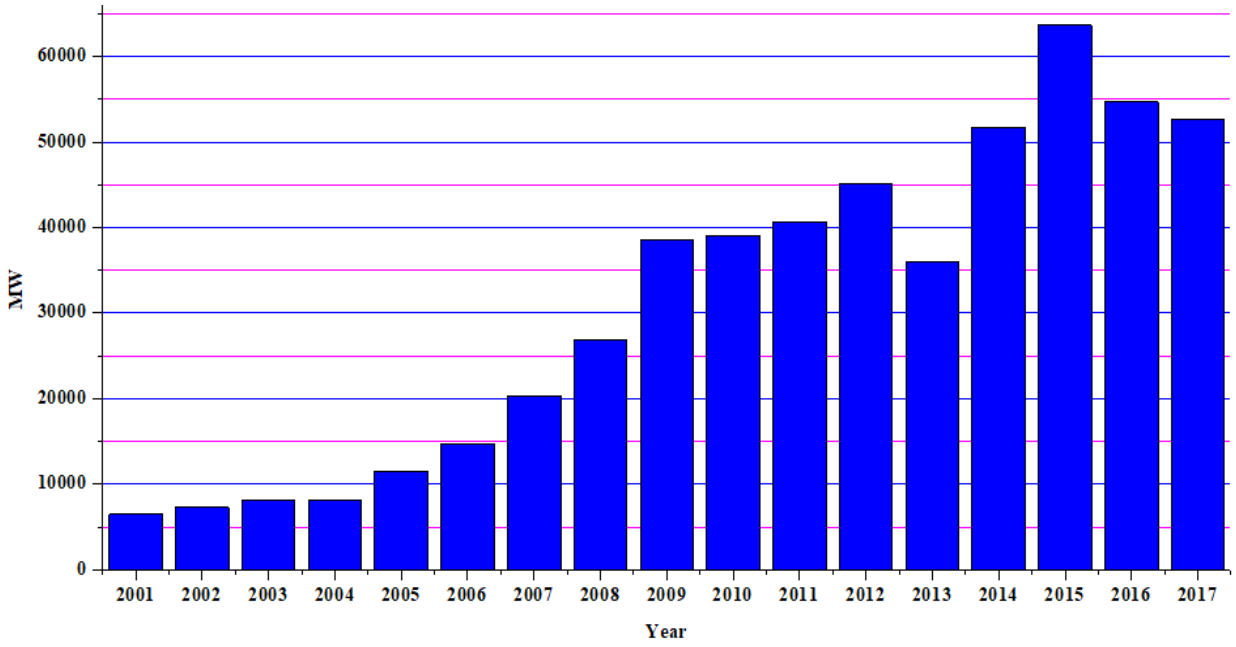

Figure 1-1: Global annual installed wind capacity 2001-2017 [10].

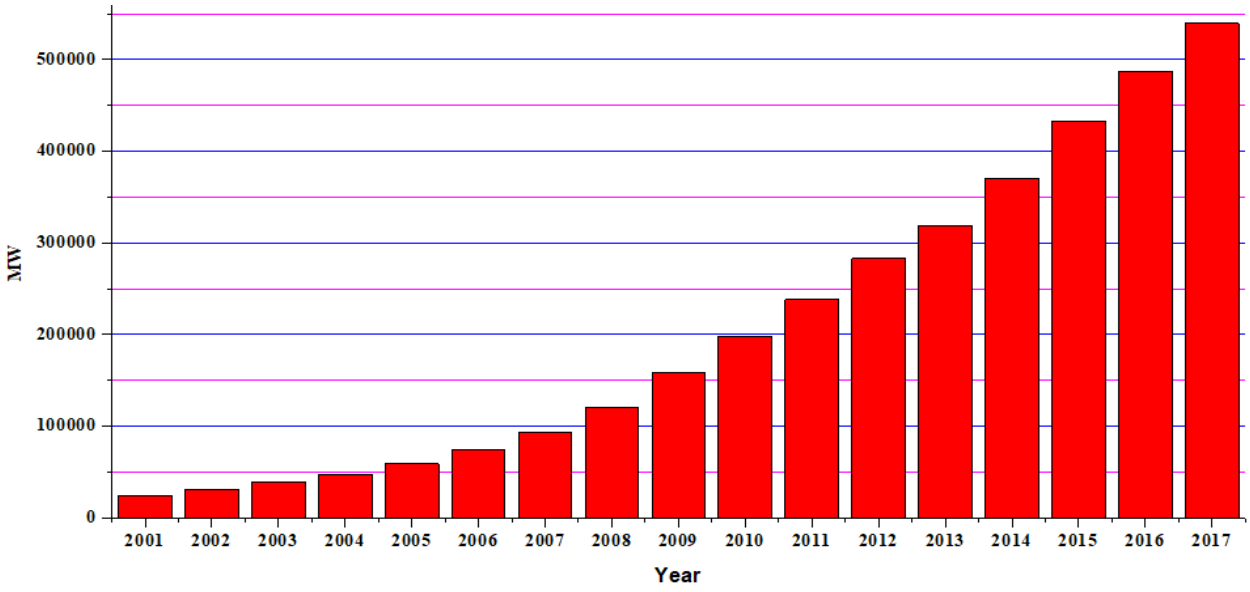

Figure 1-2: Global cumulative installed wind capacity 2001-2017 [10].

Table 1-1: Top 10 New Installed Capacity Jan-Dec 2017 [10].

Contry	MW	%share
PR chaina*	19,500	37
US	7,017	13
Germany	6,581	13
United Kingdome	4,270	8
India	4,148	8
Brazil*	2,022	4
France	1,694	3
Turkey	766	1
Mexico	478	1
Belgium	467	1
Rest of the world	5,630	11
Total top 10	49,943	89
World Total	52,573	100

Table 1-2: Top 10 Cumulative Capacity Dec 2017 [10].

Contry	MW	%share
PR chaina*	188,232	35
US	89,077	17
Germany	56,132	10
India	32,848	6
Spain	23,170	4
United Kingdome	18,872	3
France	13,759	3
Brazil*	12,763	2
Canada	12,239	2
Italy	9,479	2
Rest of the world	83,008	15
Total top 10	453,572	85
World Total	539,581	100

Table 1-3: Global Installed Wind Power Capacity (MW)-Regional Distribution [10].

		End of 2016	New of 2017	Total of 2016
Africa &Middle East	South Africa	1,473	621	2,094
	Egypt	810	-	810
	Morocco	787	-	787
	Ethiopia	324	-	324
	Tunisia	245	-	245
	Jordan	119	-	119
	Other	159	-	159
	Total	3,917	621	4,538

1.1.1 Description of Wind Power in Ethiopia

The renewable energy potential in Ethiopia includes: hydro power, wind power, solar power, geothermal power and biomass. Ethiopia has huge renewable energy potential and lately investing aggressively in energy generation and transmission network. Ethiopia is using wind power plants in addition to the existing hydro power plants to supply increasing load demand to insure sustainable development. Consequently, large scale wind farms are going to be integrated to Ethiopian Electric Power Grid. Technically, wind energy could be the second most important resource next to hydro power for power generation. Ethiopia has great wind energy potential. According to [11] study statistics, the capacity of 18,645 MW, 4,925 MW Power, and 2,005 MW with wind speed of 7.5~8 m/s,8~8.8 m/s, and more than 8.8 m/s respectively at a height of 50 m can be generated. This shows that there is a favorable condition to construct large scale wind farm

The [12] shows that, from less than 300 MW of installed capacity 13 years ago, Ethiopia has now installed 4,284 MW of power generation capacity. Of this, 3,810 MW is from hydro installations, 324 MW from wind, 7 MW is geothermal energy and there is also 143 MW of diesel power generation. However, the total renewable energy resources potentials are: Hydro power ~ 45,000 MW, wind~10,000 MW, solar~5,000 MW, geothermal potential ~ 5,000 to 10,000 MW and others. Based on the government's energy plan for the years up to 2020, Ethiopia has prioritized 300 MW of solar PV projects dispersed across three sites; 820 MW of wind power to be located in four sites; 570 MW of geothermal power to be developed in four sites; and an extra 3,879 MW of new hydro plants in eight different sites. Ethiopia is seeking to tender up to 500 MW of solar PV via the scaling solar program and the first such tender will before a capacity of 200 MW to 250 MW. Currently, Ethiopia has three wind power plant stations namely: Adama-I (51 MW) Ashegoda (120 MW) and Adama II-(153 MW).

Adama-II power project is located in the middle of Ethiopia, about 95 kilometers from Addis Ababa, 7 kilometers west of Nazret (Adama), and 3.5 kilometers west of Adama-I wind power project. The total number of wind turbines are 102, and arranged in 8 groups. The construction was started by HYDROCHINA-CGCOC in 2012 and started operation in 2015. The total investment of the project amounts to 352.69 million$, the unit power investment amounts to 2,255$/kw. Each turbine can generate 1.5 MW, the total installed capacity of 153 MW with an annual energy output of 476.665 GWh and an equivalent average full load time of 3,115 h with a

capacity factor of 0.35. The central geographical position of the wind power project site is 39^0 12' 10" E 8°, 34' 18" N and the elevation is 1,741~2,173 m from sea level. The ground surface of Adama-II wind power project site is mainly of grass and small shrubs combined with less gravel [13].

Figure 1-3: View of Adama-II wind farm [13].

1.1.2 Integration of Wind Power

Incorporating large amount of wind energy in power network will result in fluctuating real power injection and varying reactive power absorption which leads to voltage fluctuations and affect the stability and power quality of the system [14]. The integration of wind energy into existing power system presents a technical challenge and that requires consideration of voltage regulation, stability, power quality problems [15].

There are broadly two generation concepts in wind energy systems, one with asynchronous generator and the other with synchronous generator. Both are based on variable-speed generators and use blade angle adjustment (pitch control) as power limiters [16]. In view of the variable speed operation potential, DFIG is becoming popular generator used for wind power. Control of the voltage of the DFIG wind farm has been identified as the latest challenge with the present requirements of grid code. DFIG is a wound rotor induction motor with rotor insertion. The speed

of the DFIG can be controlled by inserting changeable voltage of slip frequency to the machine rotor [17]. Conceptually in DFIG the induction generator is connected at the stator terminals as well as at the rotor mains via a partially rated variable frequency AC/DC/AC converter. The VFC consists of RSC and GSC connected back-to-back by a DC-link capacitor. When DFIG based wind turbine is connected to weak power network characterized by the short circuit ratios, then during a grid disturbance or heavy load operation near PCC due to the small power capacity of GSC, it cannot provide sufficient reactive power and voltage support and there can be a risk of voltage instability, disconnection of wind turbine from the network and damages incur on the DFIG power electronic converters due to the high voltage induced in it [18].

1.1.3 Power Quality Problem

Injection of alternative energy into a utility grid results in violation of power quality because of the fluctuating nature of the wind [19]. Power quality can be defined as "any power problem manifested in voltage, current and frequency those results in failure or maloperation of the customer equipment". The power quality is an essential customer-focused measure and is greatly affected by the operation of a distribution and transmission network. The main power quality issues are voltage sag, swell, flickers, harmonics etc. [20]. Today in wind turbine generating system pulse-controlled inverters are used. Due to the improvement in switching techniques, the voltage and current at the point of common connection can be made in sinusoidal form and at unity power factor so as to improve the power quality at PCC [21]. Harmonics, voltage sag/swell and persistent quasi steady state harmonics and dynamic switching excursions can result in electric equipment failure, malfunction, hot neutral, ground potential use, fire and shock hazard in addition to poor power factor and inefficient utilization of electric energy manifested in increased reactive power supply to the hybrid load, poor power factor and severely distorted voltage and current waveforms [22].

Power quality indices have to be maintained in a power system according to the standards of EN50160 and IEC61400-21. These standards define the measurement and assessment of the power quality characteristics of the grid-connected wind generation and are widely accepted by the wind turbine manufacturers and utilities. The important factors to be considered in power quality measurements are the active power, reactive power, variation in voltage, flicker, harmonics, and transient response due to switching operation [23].

Power quality refers to maintaining a sinusoidal waveform of bus voltages at rated voltage and frequency. The waveform of electric power at generation stage is purely sinusoidal and free from any distortion. Different types of linear and nonlinear loads such as the solid-state controllers etc. connected to the bus may distort the waveform. These distortions may propagate all over the electrical network [24]. Any significant deviation in the waveform magnitude, frequency, or purity is a potential power quality problem. Of course, there is always a close relationship between voltage and current in any practical power system. Although the generators may provide a near-perfect sine-wave voltage, the current passing through the impedance of the system can cause a variety of disturbances to the voltage.

Power quality is often considered as a combination of voltage and current quality. In most of tire cases, it is considered that the network operator is responsible for voltage quality at the PCC while the customer's load often influences the current quality at the point of common coupling [25].

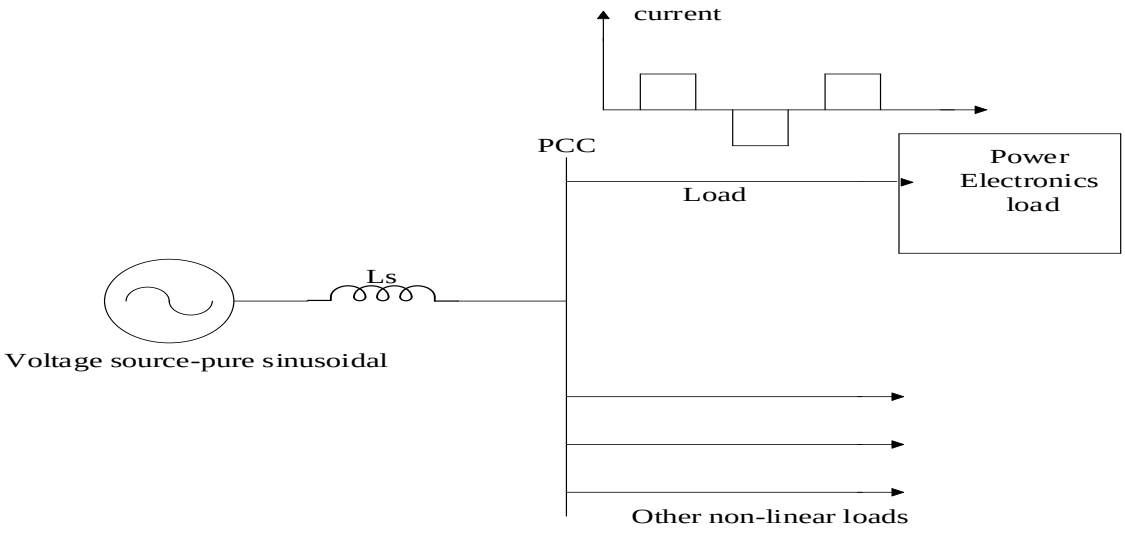

Figure 1-4: Source current distortion at PCC.

Power quality problems are classified in two main groups as steady-state and transients. Power system harmonics and voltage unbalance can be given as examples of power quality problems in the steady state. Voltage dips, spikes and surges are examples which tend to occur over short time intervals, and classified as transients. Of all these, harmonic distortion and voltage dips are the most important power quality problems facing industrial and large commercial customers [26]. Power quality problems in electrical systems mainly include voltage sag, voltage swell, voltage

and current unbalance, flicker, harmonics, and power interruption. These may cause abnormal operation of the facilities or even trip the protection devices.

The wide use of nonlinear loads (ASD, Computers, Laser printers, SMPS, Rectifier etc.) connected to power distribution system or inverter-based application, causes significant power quality degradation in the grid integrated system in terms of current/voltage harmonic, power factor and resonance problem. Thus, a proper control scheme is necessary under normal operating conditions to allow the proper control over the active power production [27].

I. Voltage Sag/Dip

A voltage sag is a short duration phenomenon at power system frequency resulting in a decrease in the RMS voltage magnitude from 10% to 90%. It typically lasts about half a cycle to a minute. Loads such as adjustable speed drives, process control equipment and computers are sensitive to these voltage sags. These loads may trip or mis operate even for voltage sag of 10% and lasting two cycles. Process industry applications such as paper mills and semiconductor fabrication plants take a lot of time to restart when tripped. Since they are production oriented, the impact of the voltage sag is enormous [28]. Sags are usually caused by system faults, and are also often the result of switching on loads with heavy startup currents [29].

II. Harmonic Distortion

Harmonic distortion is one of the main power quality disturbances frequently encountered by the utilities. The harmonic disturbances in the power supply are caused by the non-linear characteristics of the loads. The presence of harmonics leads to transformer heating, electromagnetic interference and solid-state device malfunction. Hence, it is necessary to reduce the dominant harmonics below 5% as specified in IEEE 519-1992 harmonic standard [30]. The harmonic voltage and current should be limited to the acceptable level at the point of wind turbine connection to the network. To ensure the harmonic voltage within limit, each source of harmonic current can allow only a limited contribution, as per the IEC-61400-36 guideline. The rapid switching gives a large reduction in lower order harmonic current compared to the line commutated converter, but the output current will have high frequency current and can be easily filtered [31].

1.1.4 Flexible AC Transmission Systems (FACTS)

Flexible alternating-current transmission systems are defined by the IEEE as “AC transmission systems incorporating power electronics-based and other static controllers to enhance controllability and increase power transfer capability” [32]. Flexible AC Transmission Systems, called FACTS, got in the recent years a well-known term for higher controllability in power systems by means of power electronic devices. Several FACTS devices have been introduced for various applications worldwide. A number of new types of devices are in the stage of being introduced in practice. In most of the applications the controllability is used to avoid cost intensive or landscape requiring extensions of power systems, for instance like upgrades or additions of substations and power lines. FACTS devices provide a better adaptation to varying operational conditions and improve the usage of existing installations. The basic applications of FACTS devices are Power flow control, increase of transmission capability, Voltage control, Reactive power compensation, Stability improvement, Power quality improvement, Power conditioning, Flicker mitigation, Interconnection of renewable and distributed generation and storages. The influence of FACTS devices are achieved through switched or controlled shunt compensation, series compensation or phase shift control. The devices work electrically as fast current, voltage or impedance controllers. The power electronics allows very short reaction times down to far below one second [33].

FACTS devices are classified as thyristor-based devices and voltage source converter devices. Although voltage source converters require GTO, IGBT or MCT switches, which makes them more expensive than thyristor-based devices, but they have many technical advantages over the thyristor-based devices like their faster response, less volume occupation and better performance in a critical situation [34].

Largely powerful wind power stations are manufactured as and they facilitate power systems. However, variable speed of wind leads in power loss, frequency change, voltage flicker, potential difference and power changes. So, instability problems occur in the power systems which are connected to wind power station. FACTS equipments are used to resolve of those problems. Generally, FACTS devices are composed of STATCOM, SVC, SSSC, TCSC and UPFC [35].

Based on the rotational speed, two popular wind-turbine operating concepts are realized. First, the FSWT systems that utilizes a SCIG directly connected to the grid. Second, the VSWT systems that

utilizes either DFIG or direct drive synchronous generator [36]. In case of fixed-speed wind turbine operation, all the fluctuation in the wind speed are transmitted as fluctuation in the mechanical torque, electrical power on the grid and leads to large voltage fluctuations. Thus, the network needs to manage, the excessive voltage transients which are to be avoided. Today in the variable-speed wind turbine designs, power electronics converters are mostly used. Thus, the issue of harmonics distortion of the network voltage should be considered [37].

I. Static VAr Compensator

This device, which has been in use since the 1970s, is a combination of thyristor-switched capacitor banks and thyristor-controlled inductor banks. At low system voltage conditions, the device generates reactive power, that is, delivers capacitive current, whereas during high voltage conditions it absorbs reactive power, behaving like an inductor. Commonly the devices have a steady-state rating and a transient rating (in the absorbing direction only) with the aim of rescuing a dangerously high voltage condition and allowing time for other system action. A problem with the device is that its capacitive contribution is most effective at higher voltage. Below 0.9 pu voltage, it falls off linearly to 0 at zero voltage, as shown in Figure 1.5 [38].

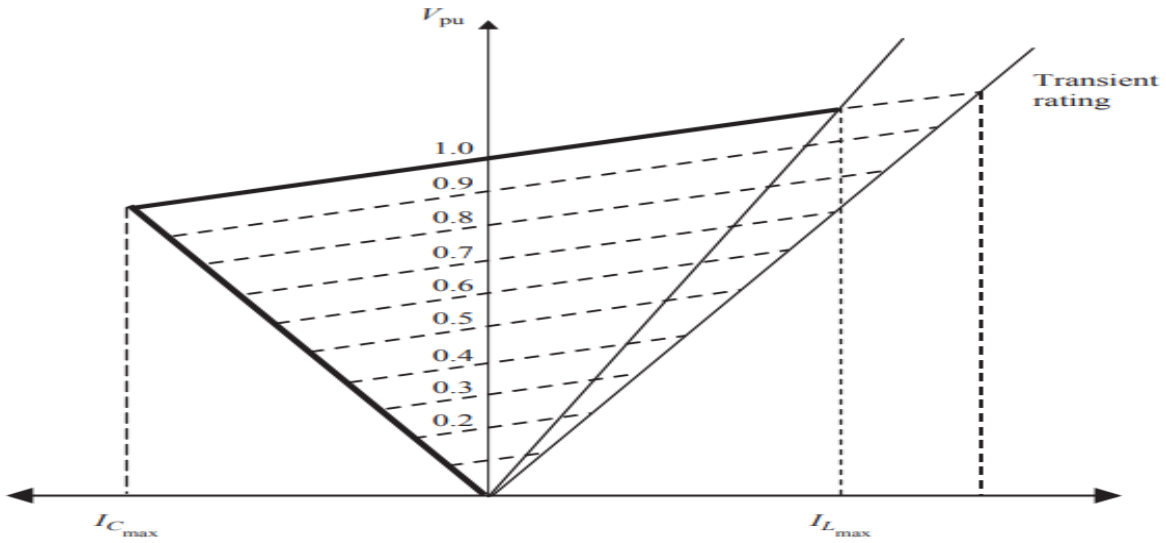

Figure 1-5: SVC operating chart [40].

II. Static Synchronous Compensator

This device, formerly known as the advanced static VAr compensator, is based on a voltage source converter rather than a thyristor-controlled capacitance. It has transient capability in both the capacitive and inductive quadrants. Being based on voltage source converter technology, the

device can also act as an active harmonic filter [38]. The concept of the STATCOM was proposed by Gyugyi in 1976 [39].

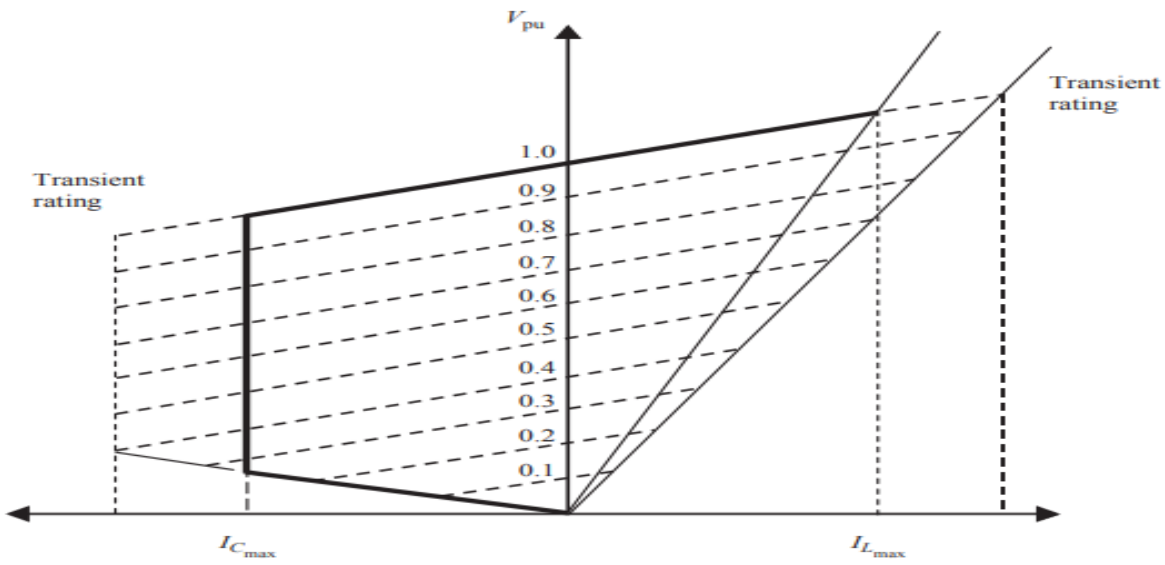

Figure 1-6: STATCOM operating chart [40].

1.2 Statement of the Problem

The penetration of wind power into the grid is important to handle the required load demand. However, due to the intermittent nature of wind and presence of frequency converters, injection of wind power affects the power quality of the grid. Due to the variation in wind speed, power output of wind turbines varies considerably. Adama-II wind turbine is installed with variable-speed DFIG. These variation in power output and reactive power requirement of DFIG causes steady state voltage variation at PCC. In DFIG, the stator is connected directly to the grid whereas the rotor is fed through back-to back bidirectional converter. AC/DC/AC frequency converter and other nonlinear loads, that are connected at PCC of the network, inject harmonic distortion in to the grid. This harmonics distortion affects the wave shape, purity, magnitude and power factor of the voltage and current at PCC. Thus, it degrades the power quality of the grid. Voltage sags typically tend to deteriorate the performance of the power converters and electrical machines connected to the AC network. If these power quality problems occur continuously in a system, they can cause loss of production, failure or mal-function of end user equipment. But according to the guidelines IEC 61400 or IEEE STD 519-1992, THD at PCC must be limited within the acceptable standard. To solve these problems, Adama-II wind farm are using of TKMCR static dynamic Var compensation device and magnetically coupled reactor type SVC which act as a

reactive power compensator and voltage regulator. However, they have problems like, sudden changes in capacitors, limited life of operation and low response time. To alleviate these problem STATCOM is used in this thesis. The advantages of STATCOM include fast response time, better voltage support and reactive power support.

1.3 Objectives of the Thesis

1.3.1 General Objective

The main objective of this thesis is harmonics and voltage variation mitigation of grid connected wind power system using static synchronous compensator control scheme.

1.3.2 Specific Objectives

The specific objectives include the following:

i. To model doubly-fed induction generator wind turbine of Adama II wind farm.
ii. To model static synchronous compensator of FACTS device.
iii. To analyze the total harmonics distortion at PCC due to the connection of both back -to-back VSC of DFIG and nonlinear loads at PCC, and compare the results with IEEE-519 standard.
iv. To improve the voltage dip/sag at PCC of grid connected wind power due to the connection of both linear and nonlinear loads at PCC.
v. To implement the developed system by using MATLAB/SIMULINK in power system block set.

1.4 Scope of the Thesis

This thesis is conducted to mitigate the harmonics and voltage variation problems of grid connected Adama II wind farm. The voltage variation at PCC is studied during a three-phase symmetrical fault in grid network. The THD harmonic distortion of voltages and currents, due to the AC/DC/AC frequency converter and nonlinear local loads, are analyzed at PCC of the network. The studied system model consists: three-phase 230KV grid, DFIG type wind turbine, local nonlinear loads and STATCOM with capacitor as energy storage device at DC-bus. The STATCOM is connected at PCC in shunt to inject reactive power to control the voltage and mitigate harmonics at PCC.

CHAPTER TWO

LITREATURE REVIEW

2.1 Related work

More research has been done on FACTS devices and discussed on controllers like Static Var Compensator and Static Synchronous Compensator to improve power quality of grid connected wind power system. Conventionally, the researcher worked on mitigation of the major power quality problems like voltage sag/dip and harmonics using capacitor, filters and SVC.

Azad et al., (2014) [41] studied on improving voltage profile of a grid connected to wind farm using static var compensator. The variations in the load and in the speed of wind give fluctuations in the voltage generated by the squirrel cage induction generator and hence in grid voltage also. The variation in the voltage of grid is controlled by SVC which is shunt connected TCR and Fixed Capacitor. TCR is automatically operated by fuzzy logic controller. Due to the absorption of reactive power by the WEG, the grid voltage drops. To prevent this, reactive power has to be compensated at the WEG end. So, the System is modeled in MATLAB and considerable improvement in grid voltage is achieved by compensating the reactive power.

Kadam., (2013) [42] analyzed the mitigation of voltage sag in grid connected wind farm system using STATCOM. Issue related to fixed speed wind turbine equipped with squirrel cage induction generators is the fault ride through capability. Fixed speed Squirrel Cage Induction Generator is modeled using PSCAD software. They focused on the major power quality problems such as voltage sag during three phase symmetrical and unsymmetrical faults occurrence at different locations of the system network. They analyzed the voltage sag by creating symmetrical and asymmetrical fault at three different locations like at generator, load & grid side. They also analyzed the voltage swell due to symmetrical fault at the same three different locations mentioned above. They showed that the designed wind farm with STATCOM responded well in mitigating voltage sag caused by symmetrical and asymmetrical faults whereas voltage swell caused by symmetrical fault.

Sahu et al., (2013) [43] performed the power quality enhancement of power transmission system using Static Var compensation with PID controller. They worked on power quality problems specially on voltage sag and voltage flicker. Their work result shows: SVC considered source end

and load end transmission line, and different switch modes result different effect especially when fault. The effects on power compensation line power, bus voltages rotor deviations angular velocity and terminal voltages of power system using SVC installed at source end and load end for the same transmission line of power system were studied and compared based on the simulation. According to on the basis of their simulation result they found that performance of installation of SVC is better control over power quality management at load end side as compared to source end.

Zahira et al., (2016) [44] examined Harmonic Reduction in Wind Power Generating System Using Shunt Active Filter with SPWM Technique. The proposed three-phase active power filter consists of a power converter, a DC-link capacitor and a filter inductor is connected at PCC. The simulation model of DFIG is constructed in the MATLAB/SIMULINK environment with the variable wind speed and connected to non-linear load. The SAF connected to the system will compensate the both the harmonic distortion and reactive power oscillation. The THD is measured with FFT analysis. These mitigations satisfied the international standards limit IEEE 519-1992.

Malathy et al., (2014) [45] investigated the mitigation of voltage sag and harmonics by providing proper reactive power support in grid connected wind energy system using STATCOM. They used fixed speed induction generator with pitch control model. STATCOM using IGBT was proposed to provide reactive power support to induction generator and nonlinear load connected in the grid. In the system, three phase faults are simulated using MATLAB and the voltage sag is detected by using the voltage and current controllers. Thus, with the presence of STATCOM the bus voltage level is maintained within the permissible limits and helps to overcome voltage sag during three phase faults. It was inferred that the reactive power compensation achieved by means of shunt connected FACTS device namely STATCOM aids the mitigation of voltage sag and harmonics in the system during three phase fault condition. The drawbacks in this work was using the fixed speed induction generator but the wind is intermittent and variable nature.

Dohare et al., (2017) [46] Performed power quality improvement by using STATCOM to grid connected wind energy system. They analyzed harmonics due to the grid connected nonlinear load by using Direct Control PWM technique of STATCOM. It is demonstrated that the THD after using STACOM has been improved considerably and is within the norms of the IEC standards.

Gupta et al., (2015) [47] analyzed the voltage sag at PCC of grid connected DFIG wind turbine during the three-phase fault occurred at the load side. A 3-level cascaded multilevel converter

based STATCOM was used to mitigate the grid voltage during the disturbance. A 3-phase fault was created for a transition time of 0.1secs to 0.2secs. Voltage sag was thus created for that interval, which is about 50% of the normal voltage. System during the voltage sag was analyzed and discussed by injecting the voltage needed for restoring the system to the normal operating condition.

Chourasia et al., (2013) [48] studied on the power quality of fixed speed induction generator grid connected wind turbine using BESS- STATCOM. Hysteresis current controller scheme was used to keep the control system variable between boundaries of hysteresis area and gives correct switching signals for STATCOM operation. The performance of STATCOM was tested under load variation condition. It has a capability to cancel out the harmonic parts of the load current thereby it maintained the source voltage and current in-phase and support the reactive power demand for the wind generator and load at PCC in the grid system, thus it gives an opportunity to enhance the utilization factor of transmission line.

Table 2-1: Comparative Analysis of Different Methods in Literature.

Authors	Methods	Controlling technique	Advantage	Limitation
Azad et al. [41]	SVC	FLC	Improves the voltage profile	SCIG not allow variation in the rotor speed
Kadam et al. [42]	STATCOM	Achieved by small variations in the switching angle of the semiconductor devices	Improves the voltage sag and swell	Squirrel Cage Induction Generator not control the wind speed variation
Sahu et al. [43]	SVC	PID	Improving the transmission line voltage stability & power quality	Less efficient
Zahira et al. [44]	Using Shunt Active Filter	SPWM Technique		Limitation to control both active and reactive power transfer
Dohare et al. [46]	STATCOM	Direct Control PWM	To mitigate harmonics as per IEC standard	Slow switching and less reliable

SVC cannot do its compensation task very well because of delays relevant to reactive power measurement and thyristor ignition. The DFIG can allow the rotor speed variation on average range -30-+30% of its synchronous speed and no need of the external capacitor bank to give the reactive power support. In this thesis DFIG is used to solve the problem related with SCIG. The DFIG active and reactive power can be control separately by using the vector control technique. This research aims to cover the above gaps in Table 2-1 by providing grid services offered by STATCOM due a high-performance candidate for SVC having better V-I operating characteristics chart in Figure 1-6. The response time of a STATCOM is shorter than that of an SVC, mostly by reason of the fast switching times provided by the IGBTs. STATCOM is based on high frequency switching voltage source converter while SVC performs as a controlled reactive admittance. STATCOM functions as a synchronous voltage source. STATCOM has better performance characteristics to mitigate harmonics and voltage variation than SVC.

2.2 Mathematical Modeling of DFIG Wind Turbine

As shown in Figure 2-1, the DFIG wind turbine consists of different main components such as wind turbine rotor, gearbox, generator, power electronic converters, and transformer for grid connection. The wind turbine is used to convert the wind kinetic energy into mechanical energy, where it is converted to electrical power via electrical generator [49].

The simulation model takes into account the dynamics of the wind turbine, the mechanical and electrical dynamics of the induction machine, and the electrical dynamics of the grid and rotor side inverters and DC bus. Taking the slower dynamics of blade pitch control into account, it is assumed that the blade pitch angle remains constant and the wind speed never exceeds the rated value of 12m/s [50].

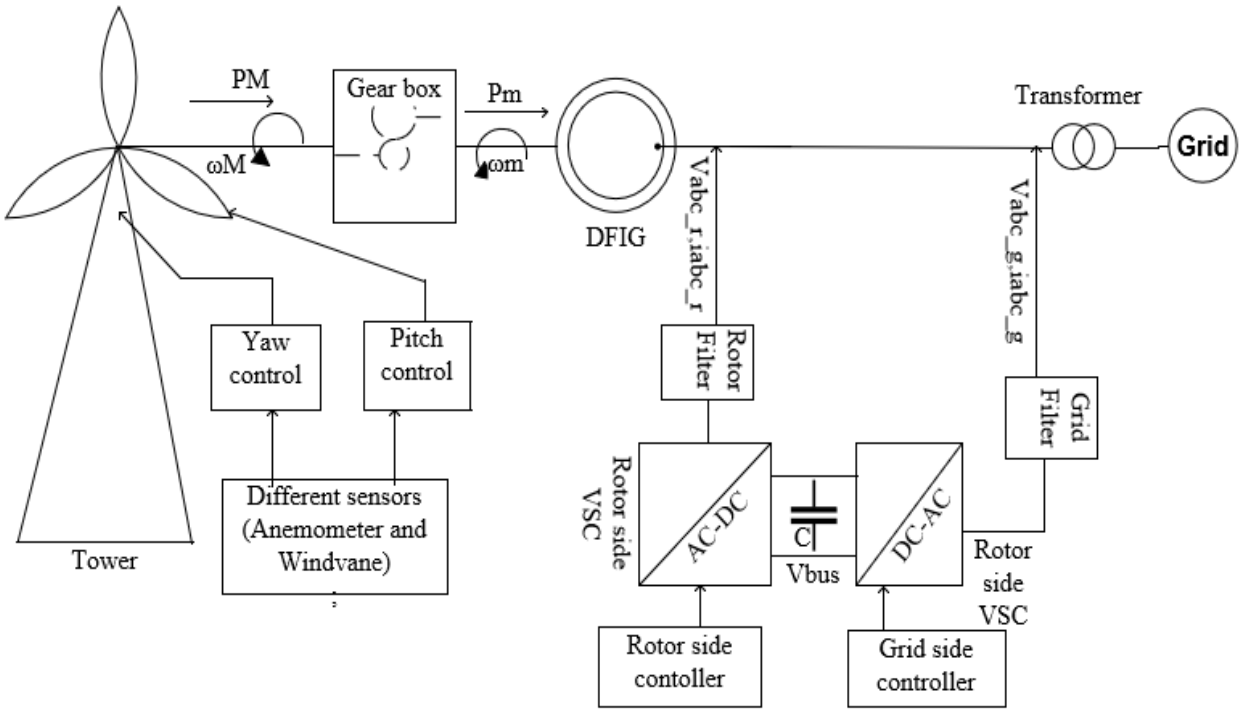

Figure 2-1: Block diagram of DFIG.

2.2.1 Reference Frame Transformation

The reference frame theory can be used to simplify the analysis of electric machines and also to facilitate the simulation and digital implementation of control schemes in wind energy conversion systems. A number of reference frames have been proposed over the years, of which the three-phase stationary frame (also known as abc frame), the two-phase stationary frame ($\alpha\beta$ frame), and the synchronous frame (dq rotating frame) are most commonly used [51].

I. abc/dq Reference Frame Transformation

The three-phase variables can be represented by a space vector $\vec{\chi}$ in a three-phase (abc) stationary reference frame (coordinate system). To transform variables in the abc stationary frame to the dq rotating frame, simple trigonometric functions can be derived from the orthogonal projection of the x_a, x_b, and $x_c$variables to the dq-axis.

$$x_d = x_a \cos\theta + x_b \cos(\theta - 2\pi/3) + x_c \cos(\theta - 4\pi/3)$$

$$x_q = -x_a \sin\theta - x_b \sin(\theta - 2\pi/3) - x_c \sin(\theta - 4\pi/3)$$

The transformation of the abc variables to the dq frames, referred to as abc/dq transformation, can be expressed in a matrix form:

$$\begin{bmatrix} x_d \\ x_q \end{bmatrix} = \frac{2}{3}\begin{bmatrix} cos\,\theta & cos(\theta - 2\pi/3) & cos(\theta - 4\pi/3) \\ -sin\,\theta & -sin(\theta - 2\pi/3) & -sin(\theta - 4\pi/3) \end{bmatrix}.\begin{bmatrix} x_a \\ x_b \\ x_c \end{bmatrix} \quad (2.1)$$

The Equations for an inverse transformation can be obtained through matrix operations, by which the dq variables in the rotating frame can be transformed back to the abc variables in the stationary frame. The transformation, referred to as dq/abc transformation, can be performed by

$$\begin{bmatrix} x_a \\ x_b \\ x_c \end{bmatrix} = \begin{bmatrix} cos\theta & -sin\theta \\ \cos(\theta - 2\pi/3) & -\sin(\theta - 2\pi/3) \\ \cos(\theta - 4\pi/3) & -\sin(\theta - 2\pi/3) \end{bmatrix}.\begin{bmatrix} x_d \\ x_q \end{bmatrix} \quad (2.2)$$

The resultant dq -axis components, x_d and x_q, are DC variables. This is one of the advantages of the abc/dq transformation, whereby three-phase AC variables can be effectively represented by two-phase DC variables. For the control of wind energy systems, the synchronous reference frame is often used.

II. abc/αβ Reference Frame Transformation

The transformation of three-phase variables in the stationary reference frame into the two-phase variables also in the stationary frame is often referred to as $abc/\alpha\beta$ transformation. Since the $\alpha\beta$ reference frame does not rotate in space, the transformation can be obtained by setting θ in Equation (2.1) to zero, from which

$$\begin{bmatrix} x_\alpha \\ x_\beta \end{bmatrix} = \frac{2}{3}\begin{bmatrix} 1 & -1/2 & -1/2 \\ 0 & \sqrt{3}/2 & -\sqrt{3}/2 \end{bmatrix}.\begin{bmatrix} x_a \\ x_b \\ x_c \end{bmatrix} \quad (2.3)$$

Similarly, the two-phase to three-phase transformation in the stationary reference frame, known as $\alpha\beta/abc$ transformation, can be performed by

$$\begin{bmatrix} x_a \\ x_b \\ x_c \end{bmatrix} = \begin{bmatrix} 1 & 0 \\ -1/2 & \sqrt{3}/2 \\ -1/2 & -\sqrt{3}/2 \end{bmatrix}.\begin{bmatrix} x_\alpha \\ x_\beta \end{bmatrix} \quad (2.4)$$

2.2.2 Steady State Modeling of DFIG

The relationships between the different frequencies of the machine are basics that must be known prior to the study of the electric Equations of the DFIG. Thus, the Equation that relates ω_s (frequency of stator voltages and currents), ω_r (frequency of rotor voltages and currents) and ω_m (rotor electrical speed) is as follows [52]:

$$\omega_s = \omega_r + \omega_m \tag{2.5}$$

The relation between the mechanical speed of the shaft Ω_m and the electrical speed ω_m depends on the pole pairs of the machine:

$$\omega_m = \rho\Omega_m \tag{2.6}$$

The units of these two Equations are given in rad/s. The slip s of the machine is defined as follows:

$$s = \frac{\omega_s - \omega_m}{\omega_s} = \frac{\omega_r}{\omega_s} \tag{2.7}$$

In DFIG, the stator windings are directly connected to the grid and thus, ω_s is constant. This frequency is also known as the synchronous frequency. However, ω_r obviously depends on the shaft's electrical speed ω_m, which leads to three operating modes of the machine dependent on the speed:

$$\omega_m < \omega_s \Rightarrow \omega_r > 0 \Rightarrow s > 0 \Rightarrow \text{Sub synchronous operation}$$

$$\omega_m > \omega_s \Rightarrow \omega_r < 0 \Rightarrow s < 0 \Rightarrow \text{Hyper synchronous operation}$$

$$\omega_m = \omega_s \Rightarrow \omega_r = 0 \Rightarrow s = 0 \Rightarrow \text{Synchronous operation}$$

Figure 2-2 shows the equivalent steady-state circuit of a DFIG. It is an idealized model in which only one phase of the stator and rotor is represented. Owing to the symmetry in the machine, the other two phases are modeled as essentially equal. It has been assumed that the machine is symmetrical and balanced in structure and that the magnetization is linear. As stated before, it is supposed that the stator windings are supplied by three-phase voltages directly from the grid, while the rotor is also supplied by three-phase voltages but independent of the stator voltages.

The electric Equations of this equivalent steady-state circuit, including the stator and rotor fluxes, are summarized as follows:

Voltage:
$$V_s = R_s I_S + j\omega_s L_{\sigma s} I_s + j\omega_s L_m (I_s + I_r) \tag{2.8}$$

$$\frac{V_r}{s} = \frac{R_r}{s} I_r + j\omega_s L_{\sigma r} I_r + j\omega_s L_m (I_s + I_r) \tag{2.9}$$

Fluxes
$$\psi_s = L_m (I_s + I_r) + L_{\sigma s} I_s = L_s I_s + L_m I_r \tag{2.10}$$

$$\psi_r = L_m (I_s + I_r) + L_{\sigma r} I_r = L_m I_s + L_r I_r \tag{2.11}$$

where $L_s = L_m + L_{\sigma s}$ being the stator inductance and $L_r = L_m + L_{\sigma s}$ being the rotor inductance.

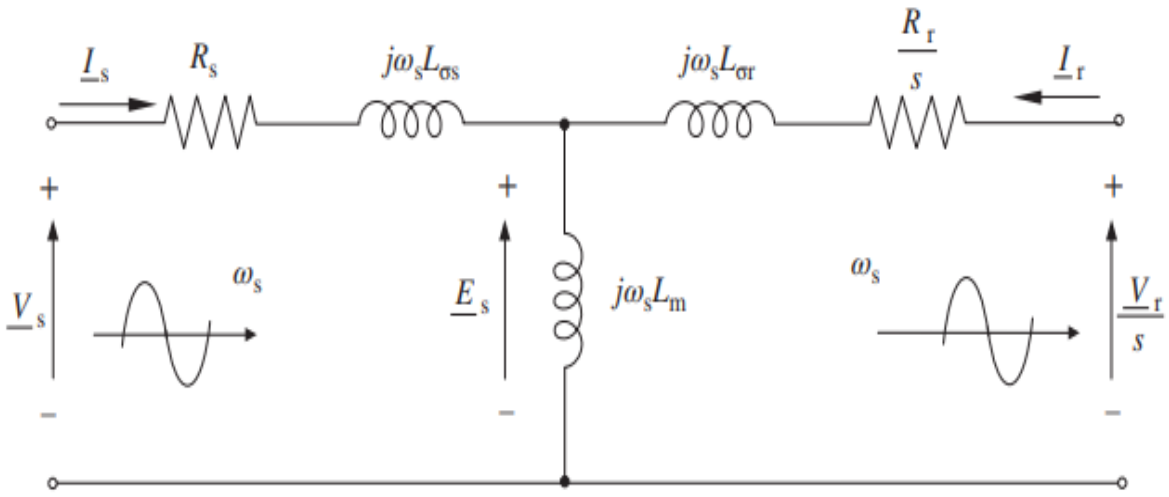

Figure 2-2: Steady-state equivalent circuit of the DFIG referred to the stator [51].

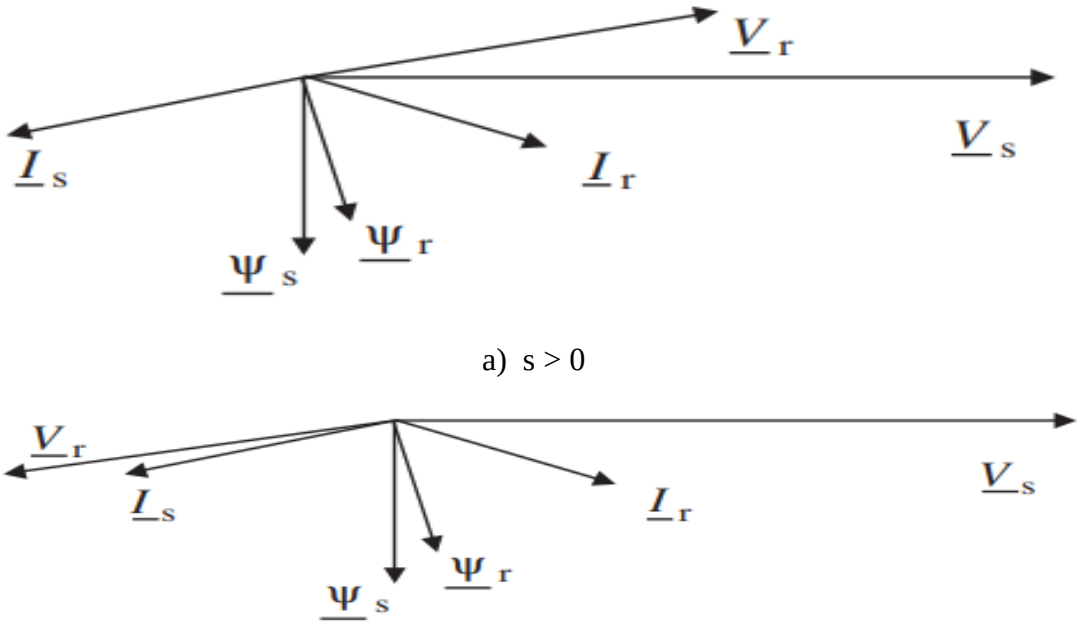

a) s > 0

b) s < 0

Figure 2-3: Phasor diagram in generator mode at Qs > 0 of a multi-megawatt DFIG [52].

2.2.3 Dynamic Modeling of DFIG

There are two commonly used dynamic models for the induction generator. One is based on space vector theory and the other is the dq-axis model derived from the space vector model. The space vector model features compact mathematical expressions and a single equivalent circuit but requires complex (real and imaginary part) variables, whereas the dq-frame model is composed of

two equivalent circuits, one for each axis. These models are closely related to each other and are equally valid for the analysis of transient and steady-state performance of the induction generator.

i. *dq* model

The stator and rotor voltages in the synchronous dq reference frame are given in Equations (2.12) - (2.15). The expressions of flux, voltages and currents are as in [53]

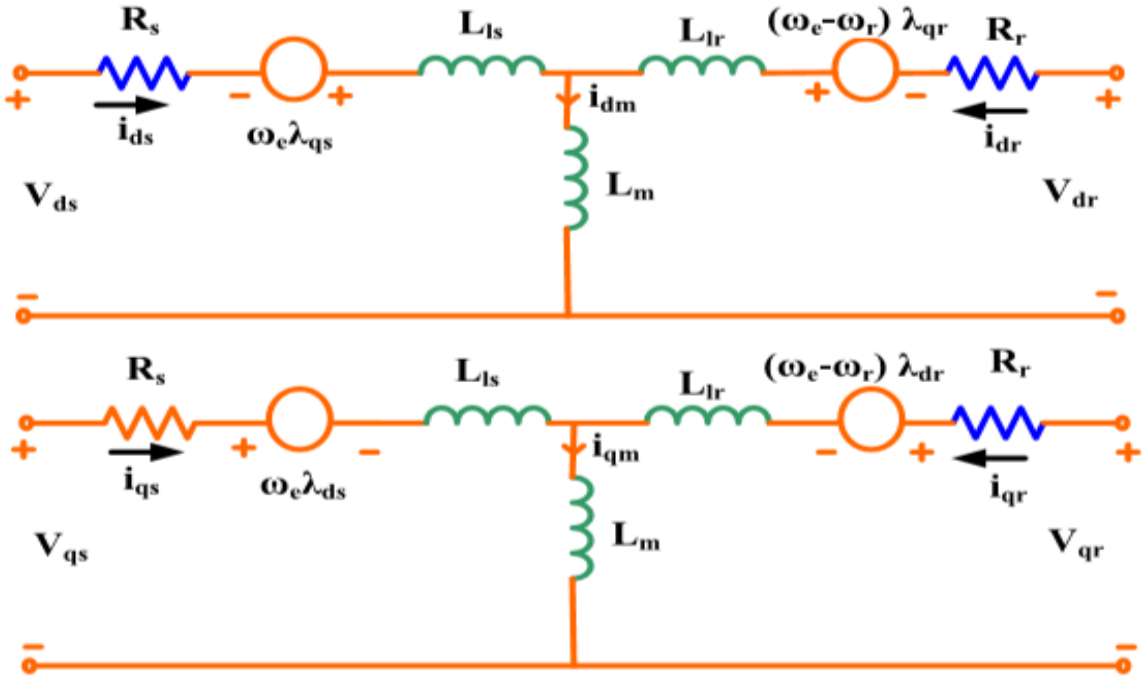

Figure 2-4: 'T-form' equivalent circuit of DFIG [53].

voltage Equations:

$$V_{ds} = R_s i_{ds} - \omega_e \lambda_{qs} + \frac{d\lambda_{ds}}{dt} \quad (2.12)$$

$$V_{qs} = R_s i_{qs} + \omega_e \lambda_{ds} + \frac{d\lambda_{qs}}{dt} \quad (2.13)$$

$$V_{dr} = R_r i_{dr} - (\omega_e - \omega_r)\lambda_{qr} + \frac{d\lambda_{dr}}{dt} \quad (2.14)$$

$$V_{qr} = R_r i_{qr} + (\omega_e - \omega_r)\lambda_{dr} + \frac{d\lambda_{qr}}{dt} \quad (2.15)$$

Here, V_{ds}, V_{qs} are dq stator voltages and V_{dr}, V_{qr} are dq rotor voltages. i_{ds}, i_{qs} are dq stator currents and i_{dr}, i_{qr} are dq rotor currents. ω_e is the supply angular frequency and ω_r is the rotor angular frequency, λ_{ds}, λ_{qs} are the dq stator flux linkages and λ_{dr}, λ_{qr} is the dq rotor flux linkages. R_s and R_r are the stator and rotor resistance respectively.

The L_s and L_r are the stator and rotor inductance respectively as given in Equations (2.16) & (2.17) and the flux linkages are given Equations (2.18) - (2.21).

$$L_s = L_m + L_{ls} \tag{2.16}$$

$$L_r = L_m + L_{lr} \tag{2.17}$$

L_{ls} and L_{lr} are the stator and rotor leakage inductance respectively and L_m is the magnetizing inductance.

Similarly, the fluxes yield:

$$\lambda_{ds} = L_s\, i_{ds} + L_m i_{dr} \tag{2.18}$$

$$\lambda_{qs} = L_s\, i_{qs} + L_m i_{qr} \tag{2.19}$$

$$\lambda_{dr} = L_m\, i_{ds} + L_r i_{dr} \tag{2.20}$$

$$\lambda_{qr} = L_m\, i_{qs} + L_r i_{qr} \tag{2.21}$$

In stator flux-oriented control, q-axis rotor current component controls the stator active power (Ps) and rotor d-axis current component controls the stator reactive power (Qs) respectively are given in Equations (2.22) & (2.23).

The torque and power expressions in the dq reference frame are equivalent to the $\alpha\beta$ Equations:

$$P_s = 3/2\,(v_{ds} i_{ds} + v_{qs} i_{qs}) \tag{2.22}$$

$$Q_s = 3/2\,(v_{qs} i_{ds} - v_{ds} i_{qs}) \tag{2.23}$$

2.2.4 Control of DFIG

I. Vector Control of DFIG

The operation of DFIG-based wind turbines completely depends on the control system used for the rotor and grid converters. The most common DFIG control algorithm is the vector control with proportional-integral controllers. Some of the advantages are less power ripple and lower converter switching frequency. However, it has some disadvantages such as transformation of the parameters to the reference frame, sensitive to varying machine parameters, high online computation owing to the PWM and regulation gains of PI controllers. In 1985, DTC method was introduced as an alternative for vector control method which reduces the complexity. Advantages of DTC method are fast dynamic response, robustness against variations of the machine parameters, simple implementation and low computation time. The disadvantages of this method are included significant torque/power ripple in steady state and variable switching frequency of converters. Based on the principles of the DTC, DPC strategy was proposed for direct control of the active

and reactive powers by selecting voltage vectors from a look up table. Like DTC method, it is not sensitive to the machine parameters variations and it creates oscillations in active and reactive power.

The CVDPC method is presented which is a combination of vector control and DPC. This method has the benefits of both methods including insensitive to changes of machine parameters, low computation time, simple implementation, less harmonic distortion. Generally, wind turbines are nonlinear systems. To overcome the nonlinearity of the system, nonlinear control methods can be used such as SMC. These methods usually have fast dynamic response and they are not sensitive to parameters variations. One concern for these methods is possibility of generating undesirable chattering in control output. In this thesis, the vector control method is used to control wind turbine. Two vector control schematics used for the rotor and grid converters are shown in Figures 2-5 and 2-6. The purpose of the vector control proposed for rotor side converter is extraction of maximum power from the wind and independent control of active and reactive power using the rotor current. The grid side converter is also controlled for keeping the DC link voltage and tuning the power factor [54].

II. Control of Rotor Side Convertor

The main purpose of RSC is to extract maximum power with independent control of active and reactive powers. Here, the RSC is controlled in stator flux-oriented reference frame. So, the active and reactive powers are controlled by controlling direct and quadrature axis rotor currents (i_{dr} and i_{qr}) respectively. Direct axis reference rotor current is selected such that maximum power is extracted for a particular wind speed. This can be achieved by running the DFIG at a rotor speed for a particular wind speed [55].

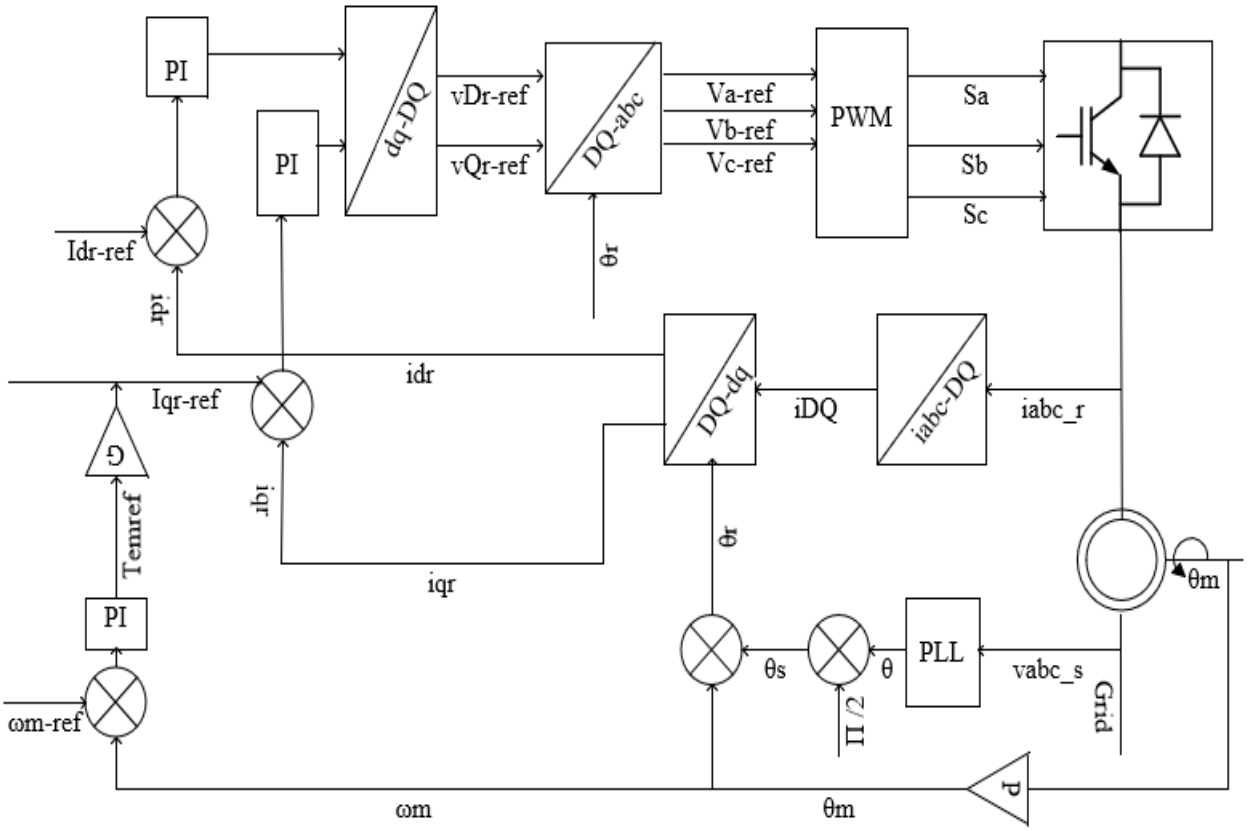

Figure 2-5: Complete vector control of the DFIG rotor side.

III. Control of Grid Side Convertor

The control block diagram of grid side converter is shown in Figure 2-6. The grid side converter is used to regulate the voltage of DC-link capacitor irrespective of magnitude & direction of the rotor power flow. We use Stator Voltage Oriented Control method for decoupled control of DC-link voltage and reactive power flow [56].

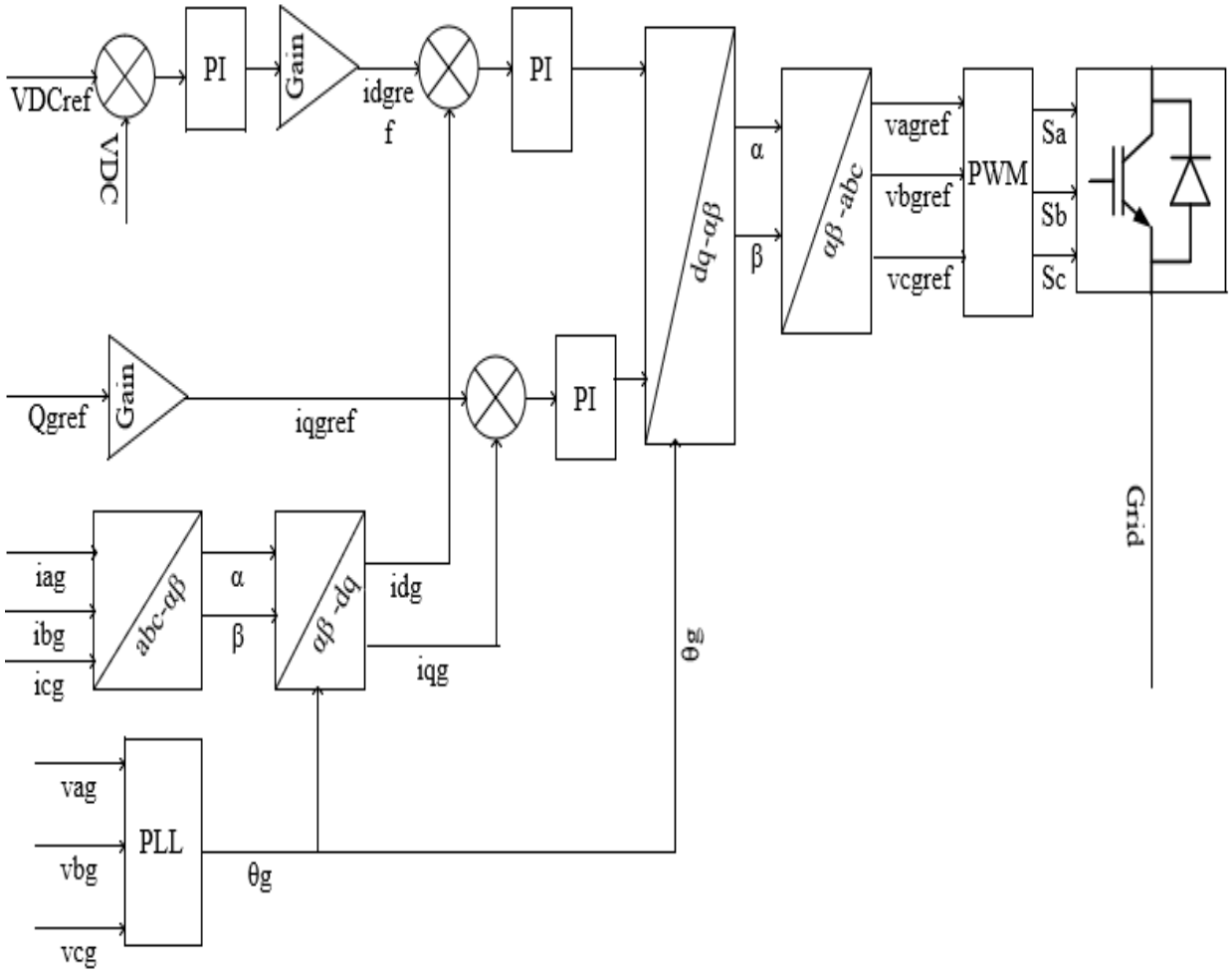

Figure 2-6: Grid voltage-oriented vector control block diagram of DFIG grid side.

2.2.5 PI Controller of Current Control Loop

However, Figure 2-7 shows that when choosing equal proportional-integral regulators for both loops, employing compensation of the cross terms, and neglecting the effect of the voltage source converter and the possible delays in computation or measurements, the equivalent closed-loop systems of both current loops are equal to a second-order system with two poles and a zero that can be placed by classic control theory choosing the appropriate gains of the PI regulators.

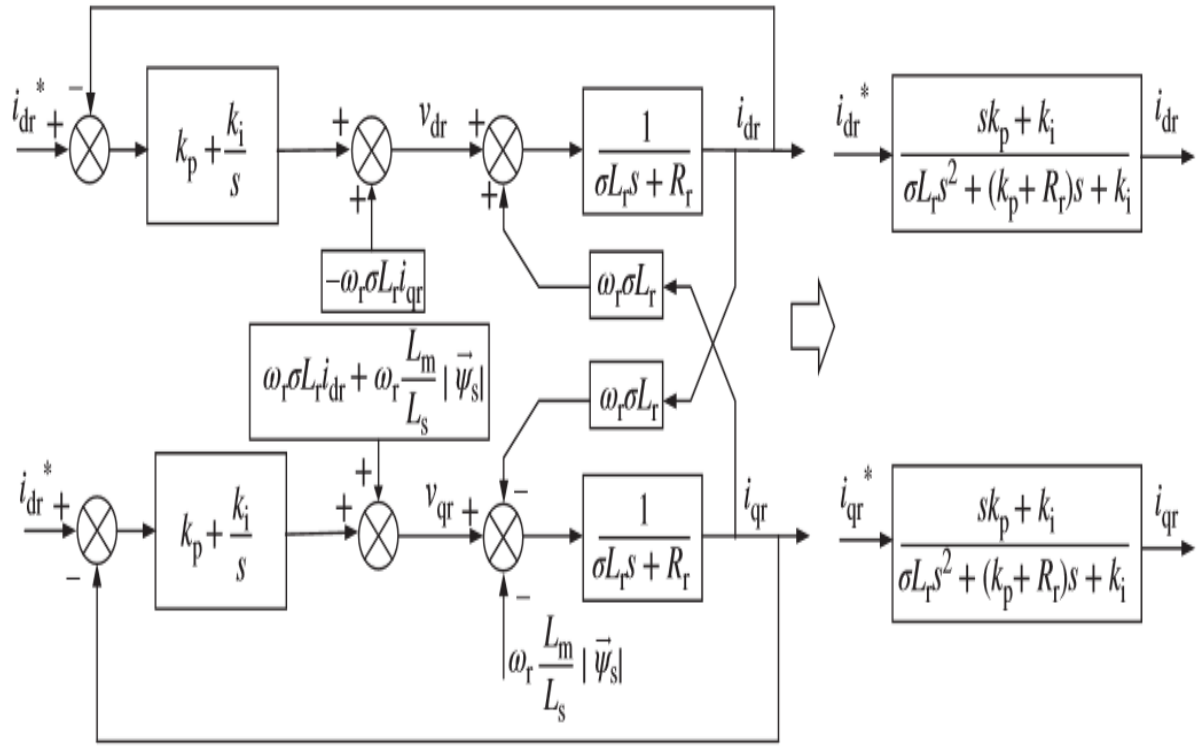

Figure 2-7: Second-order system of closed-loop current control with PI regulators [52].

By using the transfer function of Figure 2-7, K_P and K_i of PI controller can be analytically calculated as:

$$K_{Pr} = 2\omega_{ni}\sigma Lr - Rr \tag{2.24}$$

$$K_{ir} = {\omega_{ni}}^2 \sigma L_r \tag{2.25}$$

2.2.6 Power and Speed Control Loops

Figure 2-8 shows the equivalent closed-loop systems of the Qs and ω_m loops, assuming that the current loops have been tuned much faster than the external loops and neglecting converter dynamics or measurement and computing delays. It can be seen that the simplified closed-loop systems yield into a first- and second-order system that can be tuned by choosing the appropriate gains of the PI regulators. Alternatively, if the application allows it, it is typical to set the rotor i_{dr} current to zero (eliminating the Qs loop), minimizing the necessary rotor current and saving the dimensioning of the rotor windings design and the rotor-side converter. Obviously, this is achieved by the means of increasing the stator winding dimensioning.

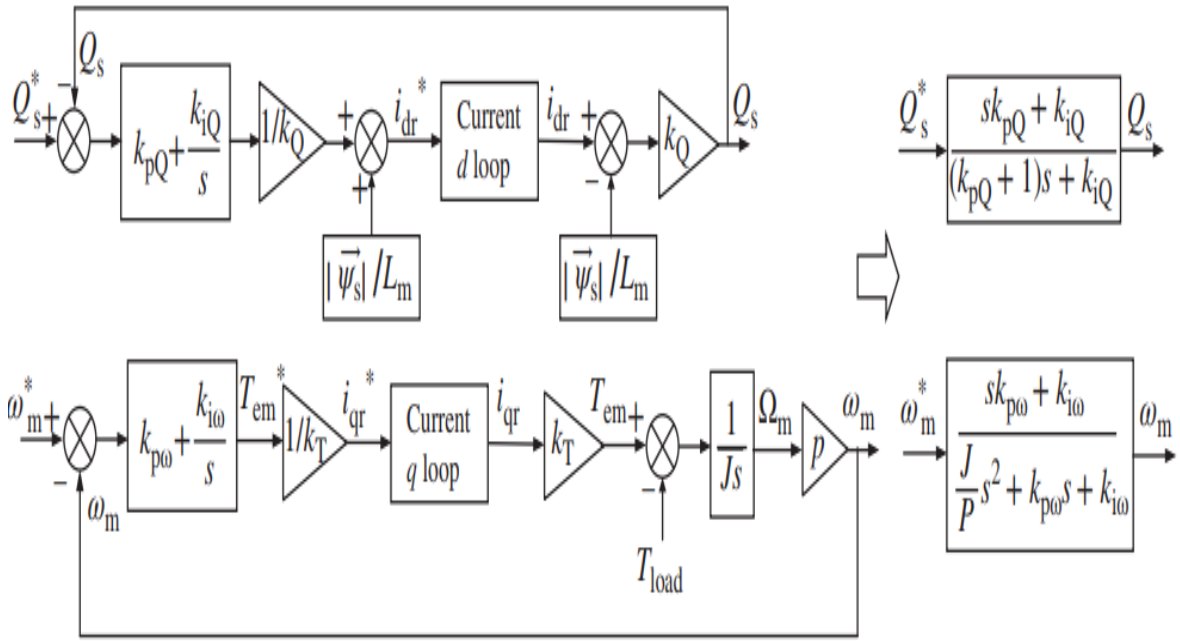

Figure 2-8: Closed-loop system of Qs and ω_m loops (T_{load} considered equal to zero) [52].

$$K_{P\omega} = (2\omega_{nn}\sigma J)/P \tag{2.26}$$

$$K_{i\omega} = (\omega_{nn} J)/P \tag{2.27}$$

CHAPTER THREE

METHODOLOGY

Figure 3-1 presented the flowchart for the developed work. As shown in the Figure 3-1, before the beginning of the thesis, numerous literature reviews have been conducted to gain the methods and techniques that have been worked by other scholars in mitigation of harmonics and voltage variation of grid connected wind power. The tasks of data collection and analysis are performed in the next step. Based on the data analysis, mathematical and Simulink models of DFIG, SVC and STATCOM incorporating with their control scheme are introduced in the next step. Determining the proper design parameters of models are followed. Then mitigation of harmonics and voltage dip analysis are performed due to both VSC/no linear load and linear/nonlinear loads that are connected at PCC respectively, in the case of existing the SVC and the proposed STATCOM scheme. Results obtained in both cases are compared and analyzed.

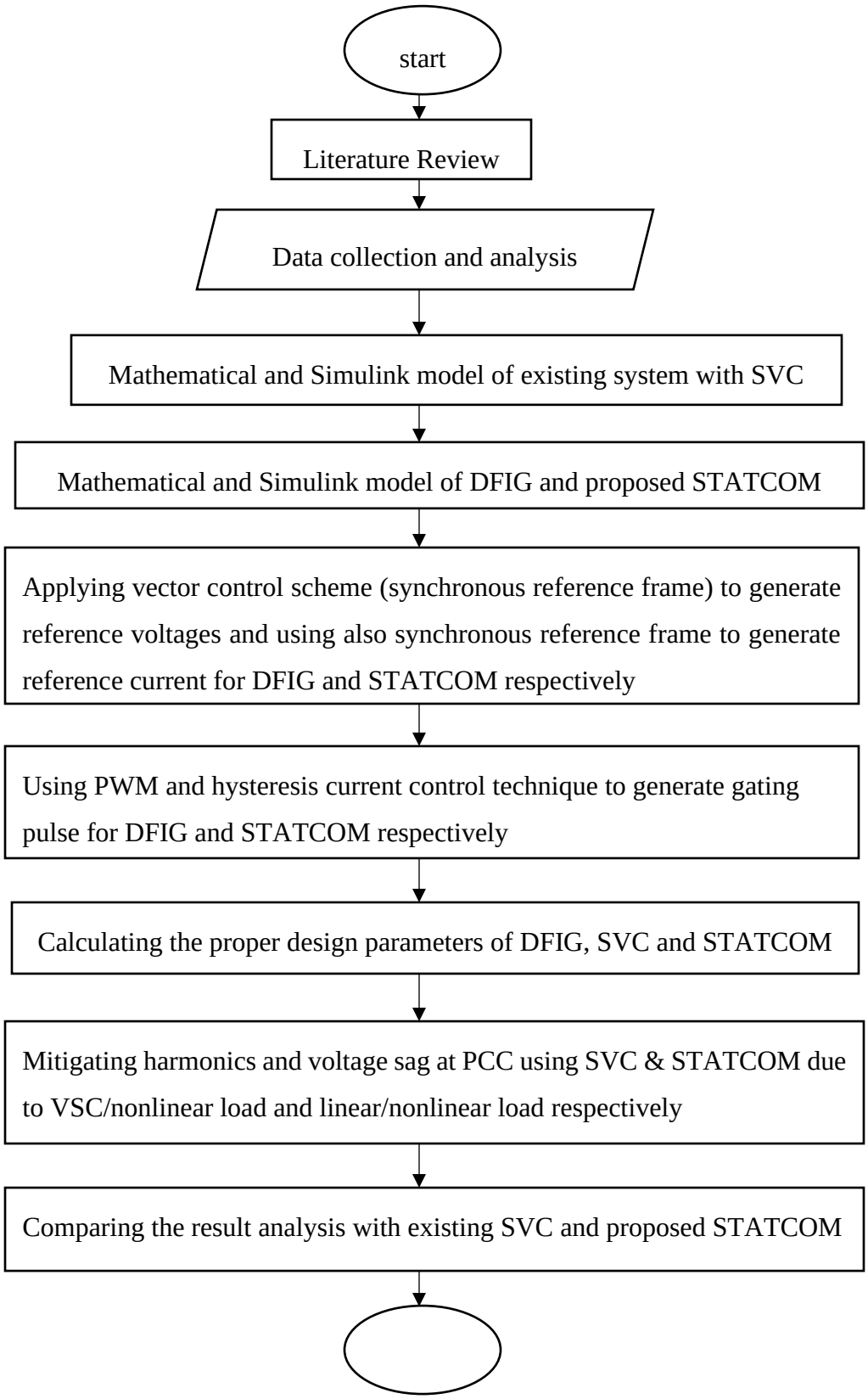

Figure 3-1: Flowchart of the performed work.

3.1 Data Collection and Analysis

The recorded data of both mechanical and electrical quantities such as; average, maximum and minimum wind speeds, total electricity production time in hours, system normal time in hours, average, maximum and minimum wind powers, average, maximum and minimum reactive powers, electricity consumption in (kwh), three-phase grid voltages, three-phase grid-currents and Wind Turbine Availability (%) are collected.

I. Analyzing Wind Speed Characteristics

Cut-In Speed: The wind speed at which a wind turbine begins to produce power. Cut-in speed of Adama-II wind power is 3.5m/s.

Rated Speed: The "rated wind speed" is the wind speed at which the "rated power" is achieved and generally corresponds to the point at which the conversion efficiency is near its maximum. Rated speed of the Adama-II wind power plant is 11.25m/s. In most cases, the power output above the rated wind speed is maintained at a constant level. Rated Power output is the power output at, or above, the rated speed.

Cut-Out Speed: The cut-out speed (25m/s) is the wind speed at which the turbine may be shut down to protect the rotor and drive train machinery from damage, or high wind stalling characteristics.

Figure 3-2 shows the average wind speed variation with time. The variation in wind speed is 5-14 m/s with average value of 10 m/s. When these wind speed variations are happening to wind turbine, it causes power fluctuations. These power fluctuation results voltage variation.

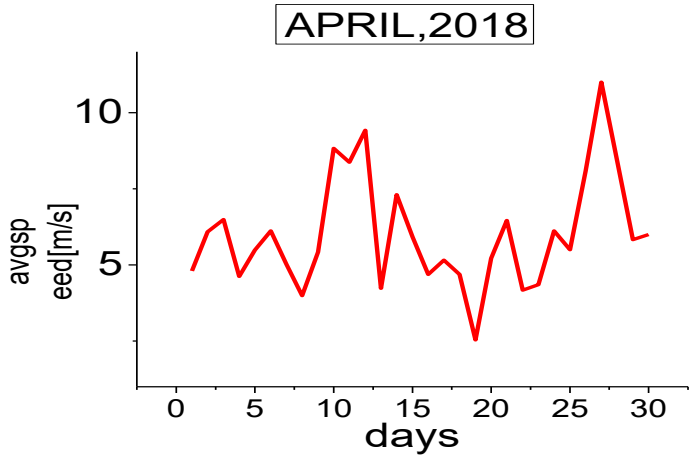

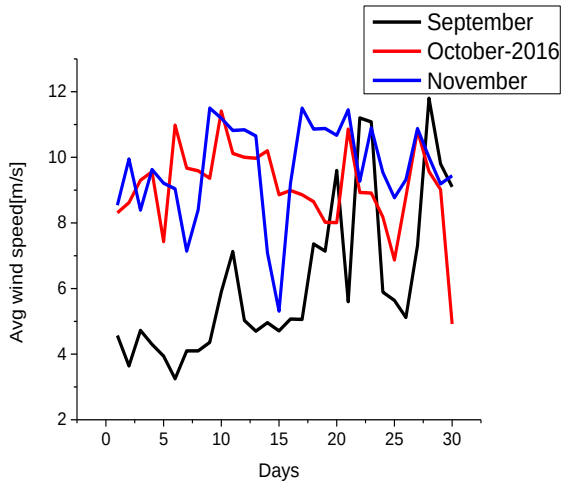
September
October-2016
November
Avg wind speed[m/s]
Days

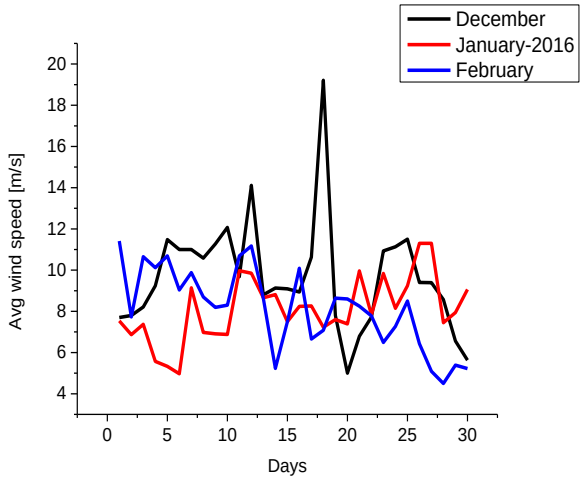
December
January-2016
February
Avg wind speed [m/s]
Days

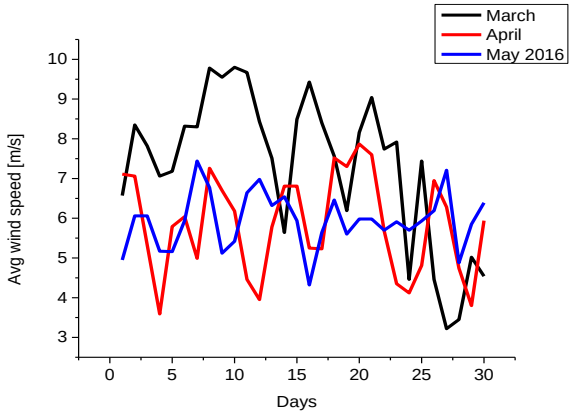
March
April
May 2016
Avg wind speed [m/s]
Days

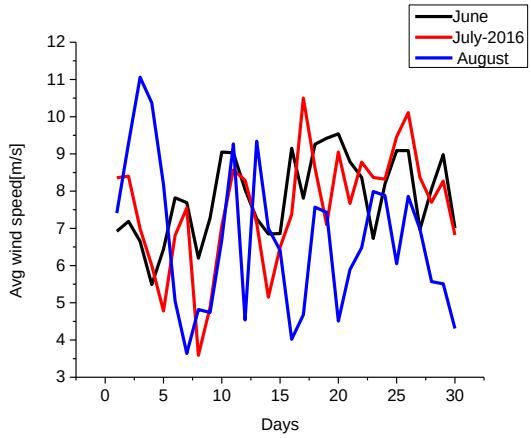
June
July-2016
August
Avg wind speed[m/s]
Days

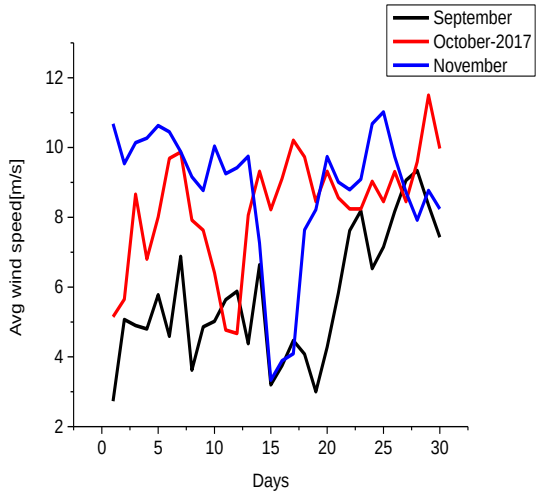
September
October-2017
November
Avg wind speed[m/s]
Days

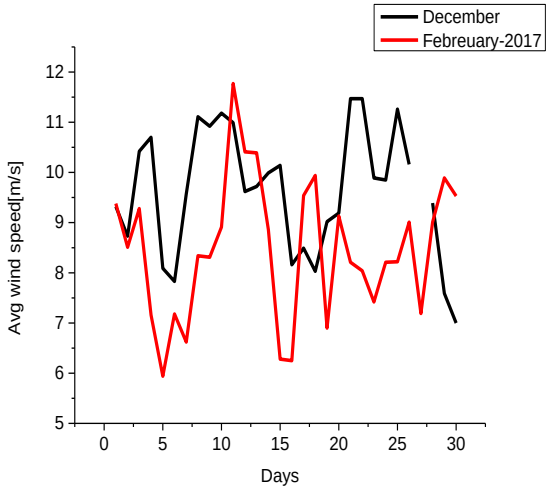
December
Febreuary-2017
Avg wind speed[m/s]
Days

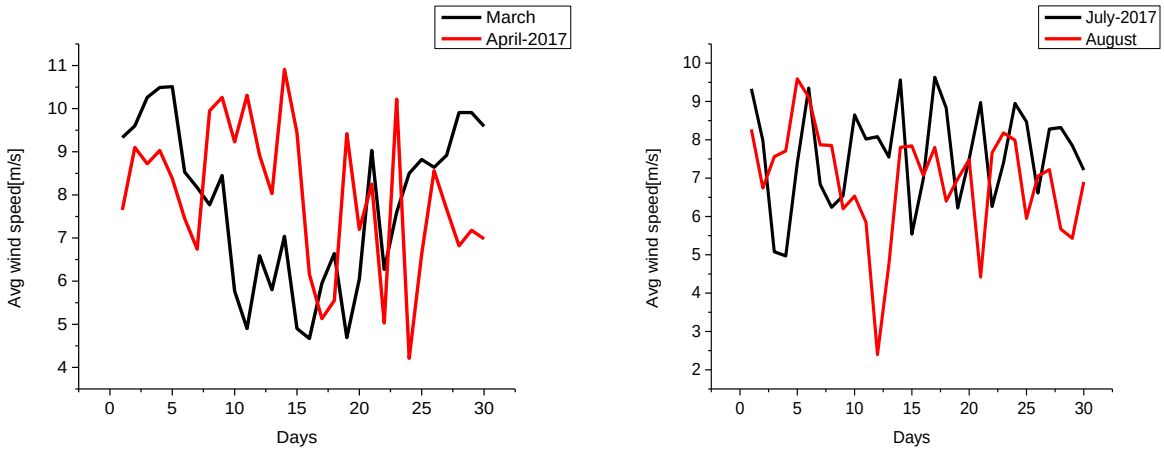

Figure 3-2: Wind speed variation of Adama II wind farm from 2016-2018.

3.2 Description of Existing Grid-connected Wind Farm

The existing system of Adama II wind farm includes:102 turbines with 153MW total installed capacity wind turbines, 90MVA main power transforme,30MVar MCR,15MVar third and fifth harmonic filters, 1600kVA unit transformer,30KW non-linear loads and 10Km 230KV single circuit overhead transmission line which fed to the grid of Koka hydropower switching substation.

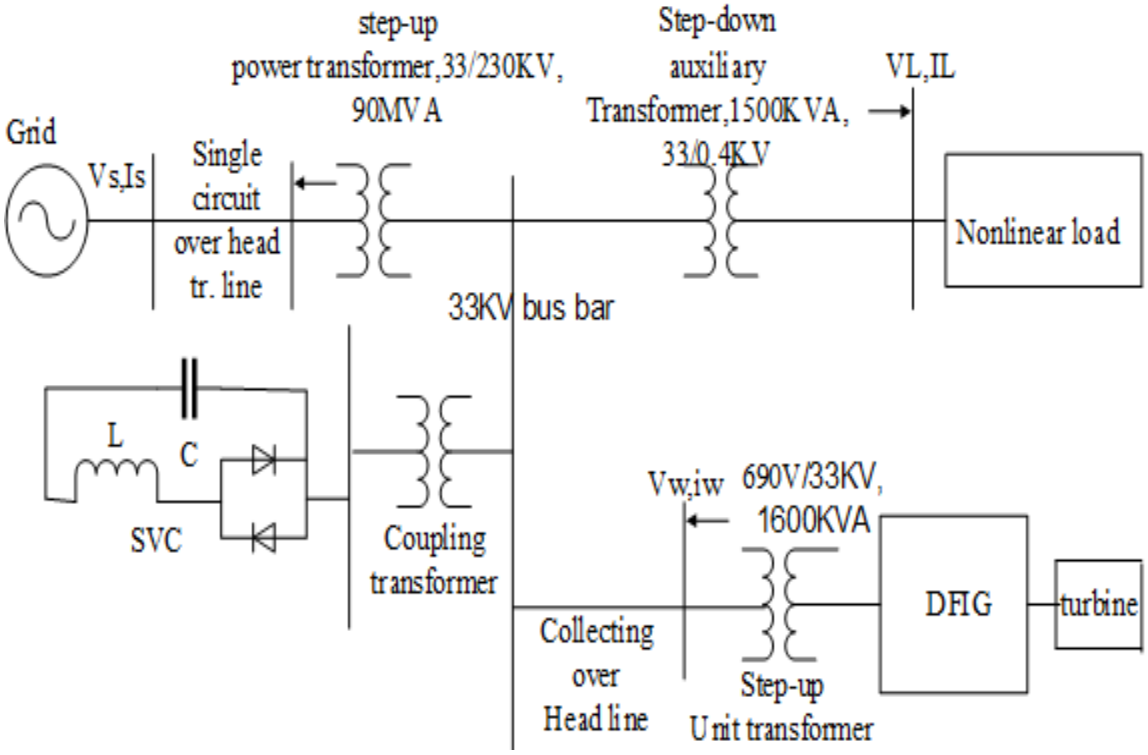

Figure 3-3: Existing model Adama II wind farm.

3.2.1 General Arrangement of the Adama II wind power Project

Considering the maximum wind speed, average wind speed and turbulence intensity, the project is suitable for the IEC II wind turbines. Seven types of wind turbines with the capacity of 1500KW each are compared with each other in the feasibility study, including Sinovel SL1500/77, Goldwind GW77/1500, Sany Electric SE77/15 and UP77/1500. Through comparison of their technical and economics indexes, the Sany Electric SE7715 1500KW is selected as the proposed turbine for this in the feasibility study.

The Sany SE77/1500KW WTGs adopt the design proposal with horizontal shaft, lamina, upwind, variable blade pitch and double-fed generator. The range of the survival temperature is -40^{0}C~+50 ^{0}C, the range of operation temperature is -30^{0}C~+50 ^{0}C, the design standard for the extreme wind speed is 59.5m/s (IEC II standard). the above factors can meet the requirements of the local site condition.

i. Lay out of the project site

Adama II wind power project is located in a mountainous hilly terrain and the area is small, and layout area are three mountain ridges. An optimized arrangement scheme calculated through wind farm software is recommended as:

The installed capacity of the area is 153 MW, with 102 sets of wind turbines of 1500 KW. Due to the restriction of the area and in order to place the turbines along the mountain ridges in lines as many as possible, the distance between the two at vertical prevailing wind direction shall be limited to 4 times the rotor diameter and 6 times at prevailing the wind direction.

ii. Electricity production estimation

102 sets of Sany SE77/1500 KW wind power units are installed in this project and the total installed capacity is 153 MW. According to the wind resource map of the wind power project calculated through Metedoyn-WT software with the effect of air density, wake flow, control, turbulence reduction, rotor surface pollution etc., the annual generation of the wind power of the wind power project, the full hour per year and the capacity factor are 476.665 GWh, 3,115 h and 0.35 respectively [57].

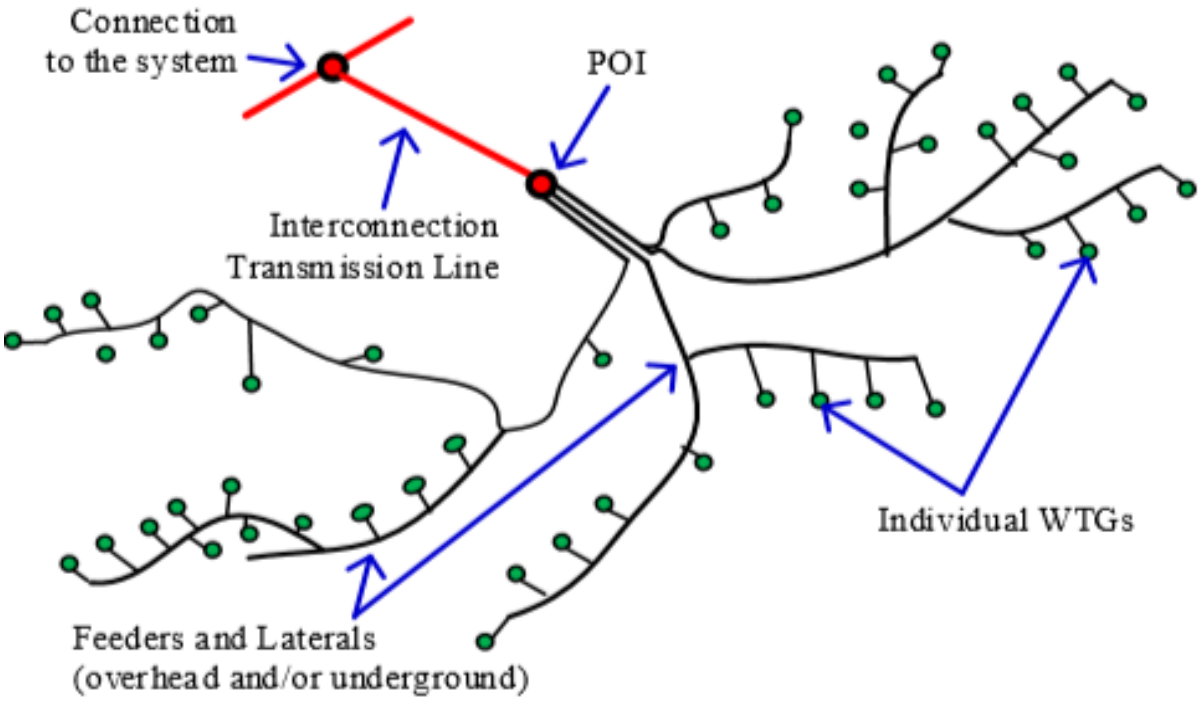

Figure 3-4: Physical diagram of a typical WPP [58].

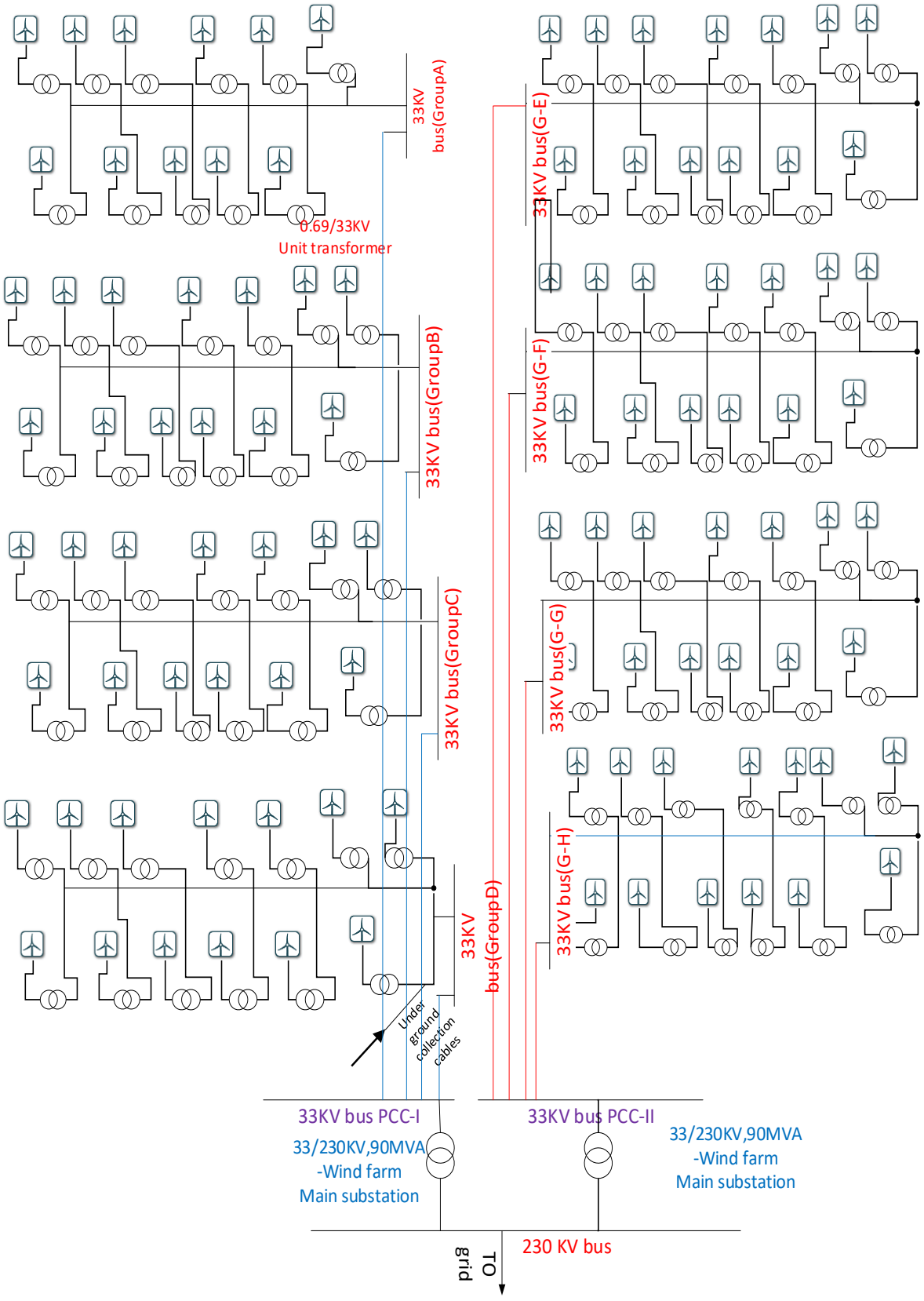

Figure 3-5: General layout of grid connected Adama II wind farms.

3.2.2 System Access Program

According to the conditions of national grid suggested that Adama II wind power project is connected to Koka 230 KV switch substation by a single 230 KV transmission line. This scheme will not only accomplish the electricity transmission for Adama wind power project, but also minimizes the land use and influences in the local residents, reduces the cost of Adama II. According to preliminary calculation, the 230 KV transmission line is 10 Km overhead lines.

I. Connection for collector circuit of the project

The unit capacity of the power unit in the project is 1500KW, and its export voltage is 690V.The energy generated is firstly conveyed to the low voltage side of the unit substation via cables. Through the unit substation, the voltage is boosted to 33KV. It then is carried to the 33KV bus bar of the boosting substation of the 230KV wind power project through 33KV cables. And finally, it reaches the power grid at voltage 230KV through the main transformer, and then via 230KV overhead conductor.

II. Main electrical connection and main equipment in 230KV boosting substation

- **230KV connection**

230KV connection is the single bus mode. Its characteristics are: wiring simple and clear, less investment, flexible configuration and easy to achieve automation remote automation and relay protection. There are 2 main transformers installed in the 230KV step-up substation. The capacity of each transformer is 90MVA. The type of main transformer is 230/33KV three-phase oil immersed air cooled OLTC (on load tap changer).

- **33KV connection**

The low-voltage side's voltage level of main transformer is 33KV and it is connected by single - bus wiring with 2 sections. WTGs-unit transformers are divided into 9 to connect with bus-bar at 33KV side of 230KV step-up substation. 33KV HV switchgear is adopted for 33KV distribution system, including 9 incoming line cubicles for 33KV bus-bar, 2PT and lightening arrestor, 4 reactive power compensation device cubicles (SF6 circuit breaker),one 33KV in door HV switchgear cubicles (for aux-transformer), 2 outgoing line cubicles, 2 earthing transformer, 2 bus-tie circuit breaker cabinet, 22 HV switch cabinets in total.

3.3 Design of Developed Model

3.3.1 Description of Studied Grid-Connected Wind Farm

The developed system consists of three-phase balanced and symmetrical grid, shunt connected STATCOM, DFIG type wind turbine and nonlinear load connected at PCC of gird connected wind power system. The Figure 3-6 represents overall system model of the study.

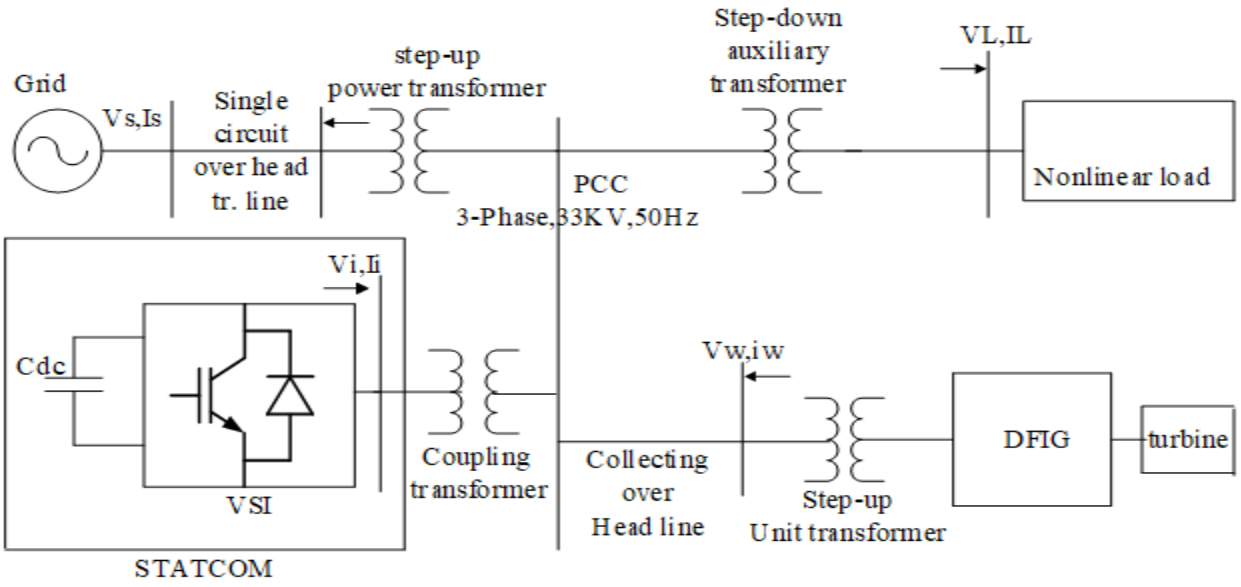

Figure 3-6: Complete developed model of Adama II wind farm.

In this thesis we are taking the study on only one section of 33KV switchgear from two due to their similarity of each other. The low-voltage side's voltage level of main transformer is 33KV and it is connected by single-bus wiring. In this study we are also selecting WTGs-unit transformers which are divided into 4 groups of section two connected with bus-bar at 33KV side of 230KV step-up substation. The layout diagram of the variable speed induction generators (VSIGs) wind farm is shown in Figure 3-7. The studied wind farm represents a part of an existing system in Adama-II with typical manufacturer turbines technical data and the associated feeders and lines electrical parameters. The medium voltage grid of wind farm consists of four 33kV feeders, and each feeder has 13 wind turbine generators. Wind turbine has a step-up unit transformer with 1600 KVA rating capacity and voltage ratio of 0.69 /33kV. The average wind speed is 11.25 m/s at 70 m above ground level. The turbines are coupled to induction generators with fixed capacitors. The wind farm is connected to the grid at the PCC, which is coupled to 90 MVA and voltages 33/230 kV substation.

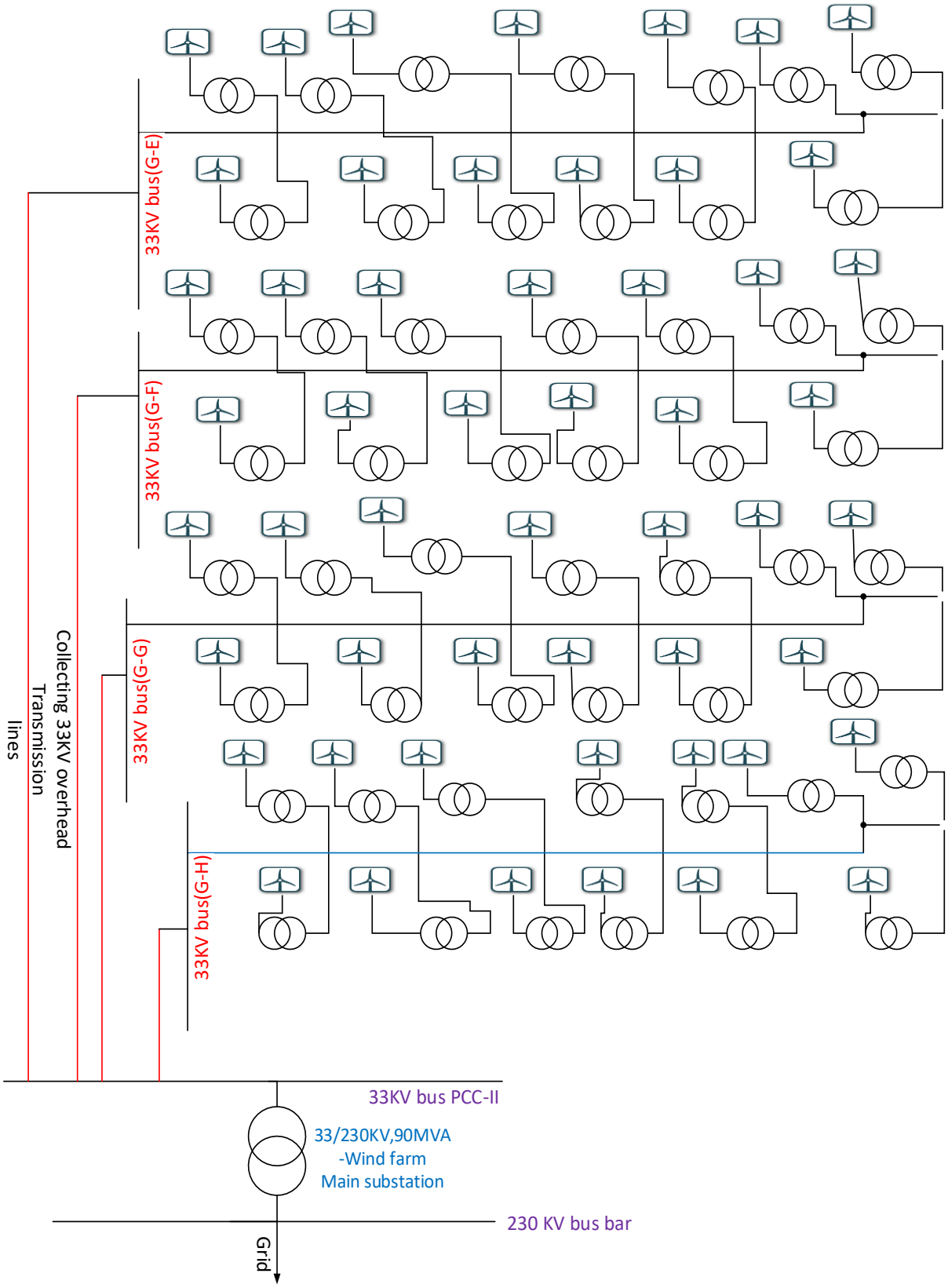

Figure 3-7: Layout of studied grid connected Adama II wind farms.

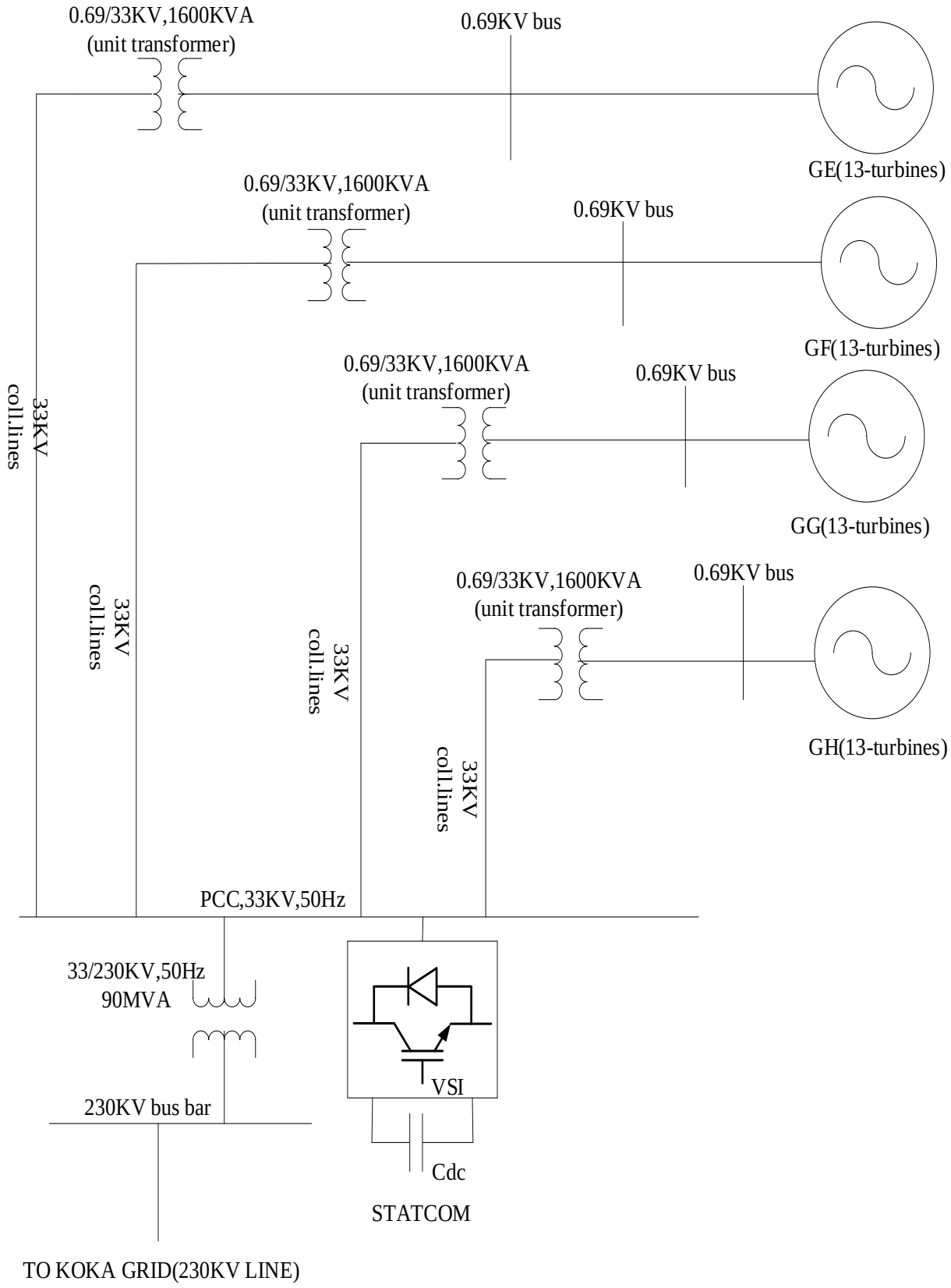

Figure 3-8: Single line diagram of developed model.

3.3.2 Single-Machine Equivalent Representation

According to the WPP modeling guide from the International Electrotechnical Commission (IEC) and the Western Electricity Coordinating Council (WECC), a WPP can be aggregated into one rescaled single-machine model with an equivalent wind speed. A typical WPP topology and its single-machine equivalent model proposed by WECC are shown in Figure 3-9 [59].

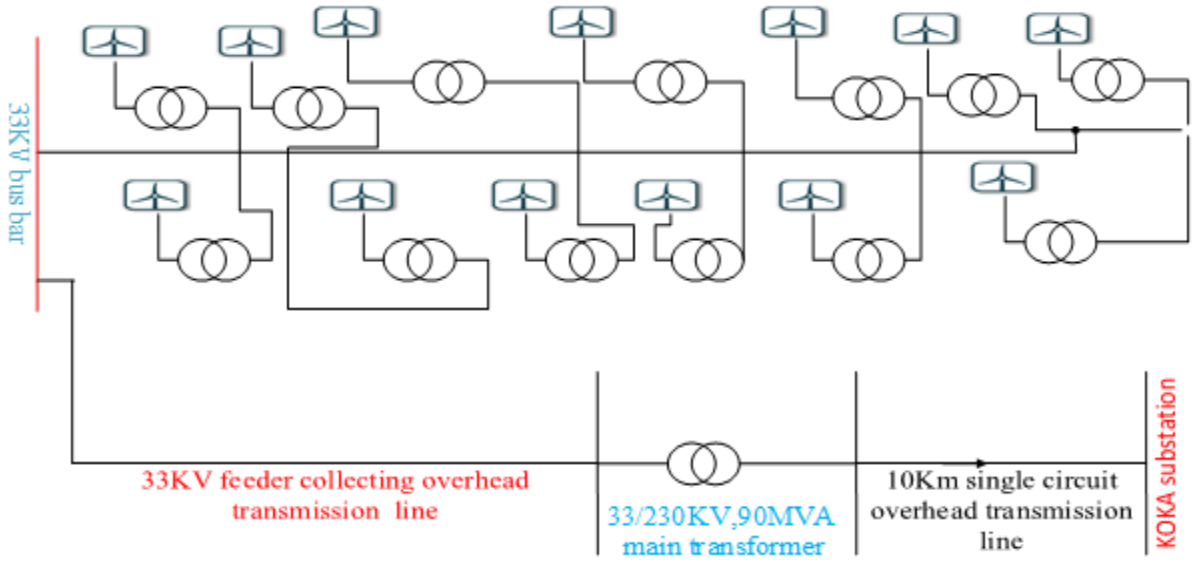

Figure 3-9: Single line representation of single feeder.

i. Aggregation of wind turbine

In order to avoid the necessity of developing a detailed model of a wind farm with tens or hundreds of wind turbines and their interconnections, aggregated wind farm models are needed .The main objective of the thesis is dealing with the system level voltage variation so that the aggregation of number of turbine unit as per equivalent wind turbines . The study is carrying on one of the selected wind turbine feeders and by assuming all the 13 turbine units are assumed closely same for the sake of aggregation of wind turbines.

ii. Aggregation of drive train

Since a large number of wind turbines are connected to a common bus, it is assumed that the disturbance originating in the bus affects the performance of all of the individual machines identically, and the individual rotor oscillations lie in phase with each other. All of the wind turbines are therefore considered to be connected in parallel, mechanically [60].

Considering number of turbines, the equivalent model variables of a wind farm are expressed as:

$$H_t = \sum_{k=1}^{N} H_{tk} \quad (3.1)$$

$$H_g = \sum_{k=1}^{N} H_{gk} \quad (3.2)$$

$$K_{tg} = \sum_{k=1}^{N} K_{gk} \quad (3.3)$$

$$D_{tg} = \sum_{k=1}^{N} D_{tgk} \quad (3.4)$$

Where,

H_t Inertia constant of wind turbine (s)

H_g Inertia constant of generator (s)

D_t Damping coefficient of wind turbine (pu)

D_g Damping coefficient of generator (pu)

D_{tg} Damping coefficient between wind turbine and generator (pu)

K_{tg} Shaft stiffness between wind turbine and generator (pu)

iii. Aggregation of Induction Generators

Aggregation of wind turbines is an important issue during the planning of grid integration of large-scale wind farms and stability studies. One of the important considerations for the aggregation is to understand the potential for mutual interaction between the various wind turbines in a wind farm. Reactive power compensation and stability study of wind farms are typically done considering the aggregated model of wind turbine generators. Aggregation of wind turbine generators is somewhat different from the aggregation of simple induction machines for motor application. The oscillation in the power output of the induction generator is dominated by the dynamics of the mechanical drive train due to the fact that the inertia constant of the wind turbine is much higher than that of induction generator. Representing large number of induction generators like Adama II DFIG by a single equivalent induction generator under certain consideration which are as follows: In this thesis, the aggregation of the wind turbines has been performed for the mitigation of voltage variation and harmonics at PCC.

i. If different wind turbines are subjected to different wind speeds due to being located over a wide geographical region, or subjected to different types of disturbances.

ii. If different sizes of same type of induction generator-based wind turbines (having different drive trains, blades structure, etc.) are aggregated together by one equivalent IG based wind turbine.

In this thesis, the aggregation of the wind turbines has been performed for the investigation of voltage and harmonic mitigation. The rating of an aggregated wind farm can be expressed as the summation of the rating of each machine:

$$S_{eq} = \sum_{k=1}^{N} S_k \tag{3.5}$$

where, S_k is the kVA rating of single machine and S_{eq} is the rating of the equivalent machine. This is known as the kVA weighted averaging, one of the most commonly used methods of aggregating induction machines for power system stability studies. In a wind farm, if all the induction machines are not identical then aggregated parameters are calculated as the weighted average of the respective parameter of individual machines. The generalized method for the calculation of the aggregated parameters (x_{egg}) of the generator is as follows:

$$x_{egg} = \sum_{k=1}^{N} \alpha_k \, x_k \tag{3.6}$$

where, x_k is the parameter of k-th generator and ak is a factor, which is calculated as

$$\alpha_k = \frac{S_k}{\sum_{k=1}^{N} S_k} \tag{3.7}$$

The aggregation of shunt capacitors C_{gk} at the terminal of an induction generator can be done as,

$$C_g = \sum_{k=1}^{N} C_{gk} \tag{3.8}$$

where, C_{gk} is the shunt capacitance at the k-th generator terminal.

3.4 Modeling of Static Synchronous Compensator

A STATCOM is shunt-connected reactive power compensation device that is capable of generating and/or absorbing reactive power and in which the output can be varied to control the specific parameters of an electric power system. The STATCOM is a static compensator and is used to regulate voltage in order to improve dynamic stability. In this thesis, STATCOM comprises three basic components that are: two-level based six-pulse IGBT VSI, DC- link capacitor and an inductor with coupling transformer. To achieve a good performance of STATCOM, these three basic components should be selected properly. This device is similar to a synchronous condenser,

and as it is an electronic device, it has no mechanical inertia while having improved better characteristics such as its fast dynamics and low cost of installation and its maintenance to synchronous condensers. Figure 3-10 shows the basic STATCOM model which is connected to the AC system bus through a coupling transformer. In a STATCOM, the maximum compensating current is independent of system voltage, so it operates at full capacity even at low voltages. The advantages of STATCOM includes: flexible voltage control for power quality improvement, fast response, and applicability for use with high fluctuating loads. The main function of STATCOM is to provide controllable three-phase AC voltage which is free from harmonics at the PCC by providing with controllable reactive power [61].

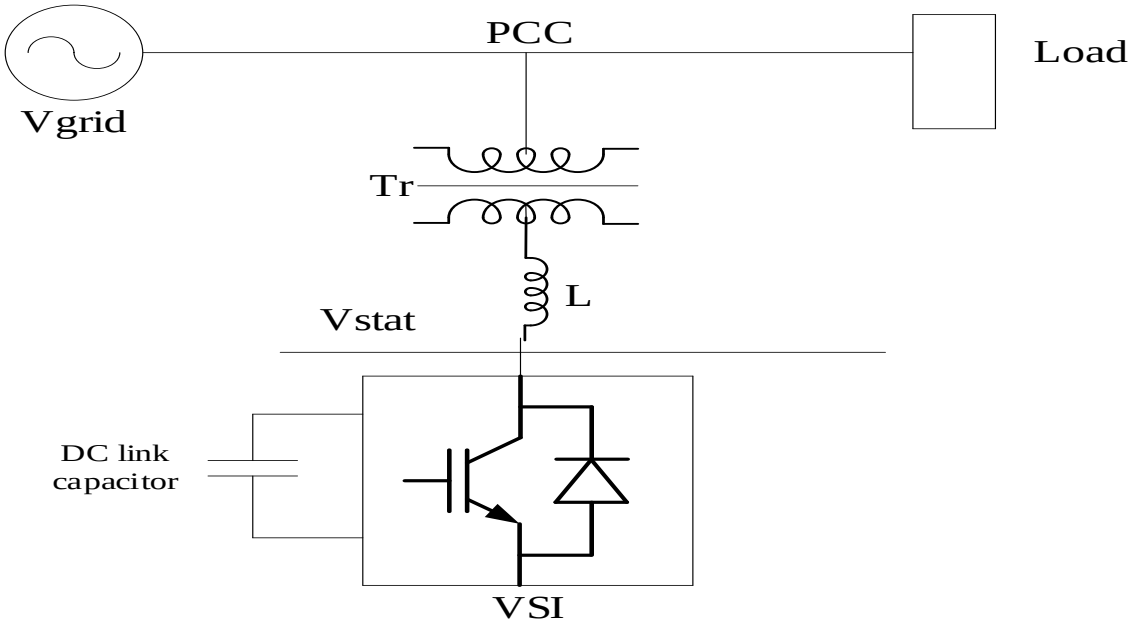

Figure 3-10: Schematic diagram of STATCOM.

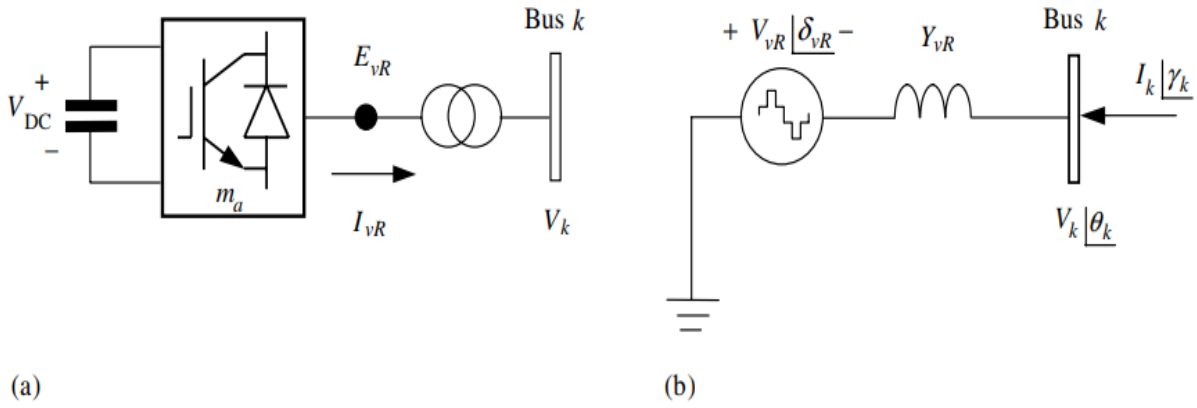

Figure 3-11: Equivalent circuit of STATCOM [62].

3.4.1 Reasons for Choosing STATCOM

A STATCOM is a better option to provide reactive power to a power system, with low voltage problems, while the SVC can generally make more than the STATCOM to limit the dynamic over-voltages.

The slope and the reactance, along with the output voltage in the VSI can be set to I_{ST} to control the scheme of the STATCOM, a set of characteristic slopes of voltage-current in the device for several voltage ranges. The STATCOM performance for voltage regulation is quite similar to the SVC, but in a more robust way, because the STATCOM operation is not related to low voltage conditions. Under reduced voltage levels STATCOM can keep working in a leading or lagging way, in contrast to that, the current limits established for a conventional SVC are proportional to the voltage.

Capacitors are usually connected to fixed wind speed turbines to enhance the system voltage because they are a source of reactive power. Mechanically switched fixed shunt capacitors can enhance the system's voltage stability limit, but is not very sensitive to voltage changes. Also, voltage regulated by the wind generators equipped with only fixed capacitors can become higher than the voltage limit of 1.05 p.u. Hence, a fixed capacitor cannot serve as the only source of reactive power compensation.

One of the most important advantages of using STATCOM over a Thyristor based SVC is that its compensating current is not dependent on the voltage level at the connection point which means that the compensating current is not lowered as the voltage drops [63].

3.4.2 Selection of the Semi-conductor Device

Power semiconductor switches are basically switching that convert electrical energy. They can be categorized depending on how controllable they are. There are three main categories [64]:

i. Diodes (two-layer semiconductor devices), where both turn on and off states are dictated by the power circuit. Fast-recovery diodes with small recovery time are of interest here since they are designed to be used in high frequency circuits in parallel with controllable switches.
ii. Thyristor (four-layer semiconductor devices), where turn on state is controlled by a control signal and turn off state by the power circuit.

iii. Controllable switches, where both states are controlled by control signals, such as IGBTs, integrated gate commutated Thyristor or IGCTs, injection enhanced gate Thyristor or IEGTs, gate turn-off Thyristor or GTOs, bipolar junction transistors or BJTs, metal oxide semiconductor field effect transistors or MOSFETs and MOS controlled Thyristor or MCTs.

3.4.3 Voltage Source Inverter Model

Voltage source converter consists of the DC link capacitor at DC side and three phase–three wire configured IGBT inverter at the ac side. A VSI is DC-to-AC converter that in most cases uses IGBT technology. Figure 3-12 shows how a VSI is connected to the grid. Its basic operational principle is that it creates a desired AC voltage using the pulse width modulation method. Figure 3-13 shows a simplified transmission line representation.

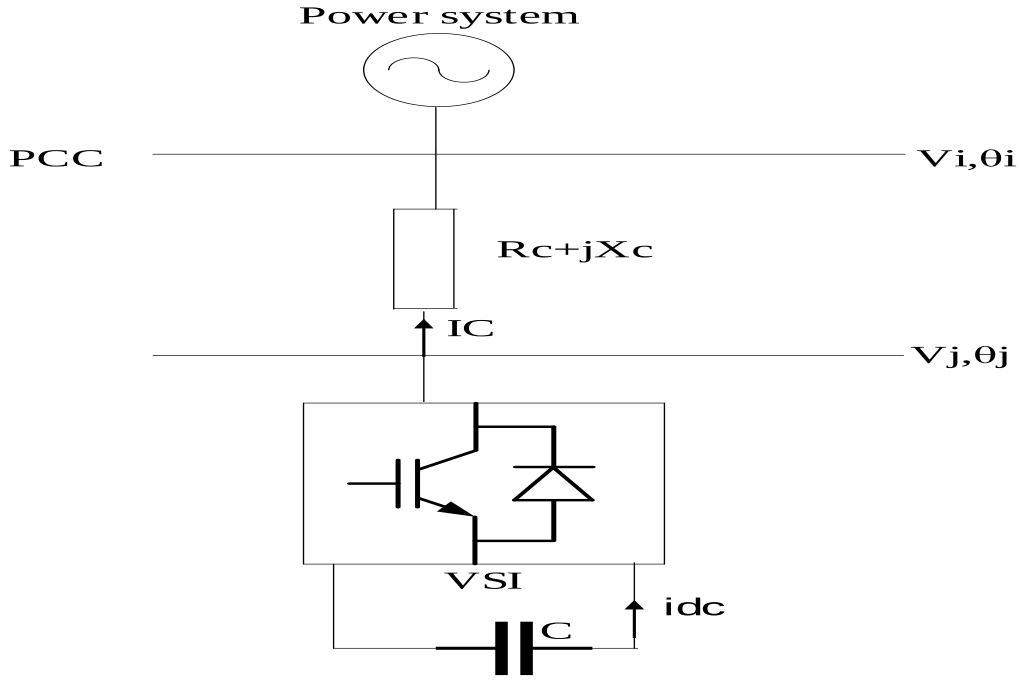

Figure 3-12: STATCOM grid connection.

Assuming that V_i is the system's AC voltage V_j is STATCOM's AC output voltage $\Theta_{ij} = \Theta_i - \Theta_j$ is the electrical angle between nodes *i* and *j* and X_L is the line reactance, the apparent power S flow will be:

$$S = 3.\frac{V_i V_j}{X_L}.sin\Theta_{ij} - j.3.(\frac{V_i V_j}{X_L}.cos\Theta_{ij} - \frac{{V_i}^2}{X_L}) \quad (3.9)$$

$$S = P - j.Q$$

Where P is active power flow and Q is the reactive power flow. Equation (3.9) shows that active power flow is affected by variations of the electric angle whereas the reactive power flow by the magnitude of voltage difference between V_i andV_j. If $\Theta_{ij}$is leading then active power flows from the system to the STATCOM, if Θ_{ij} is lagging then active power flows from the STATCOM to the system. If $\Theta_{ij} = 0$, then the active power is zero and the reactive power is:

$$Q = \frac{V_i}{X_L}(V_j - V_i)$$

When $V_j > V_i$, the STATCOM provides the system with capacitive compensation since it injects current to the system. When $V_j < V_i$, the STATCOM provides the system with inductive compensation and when $V_j = V_i$, there is no reactive compensation.

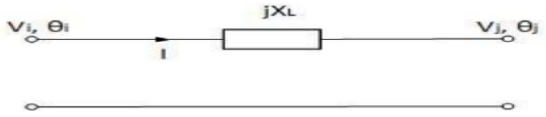

Figure 3-13: Simplified model of the transmission line [64].

I. Model of Three Phase Six-pulse Two-level IGBT Based Inverter

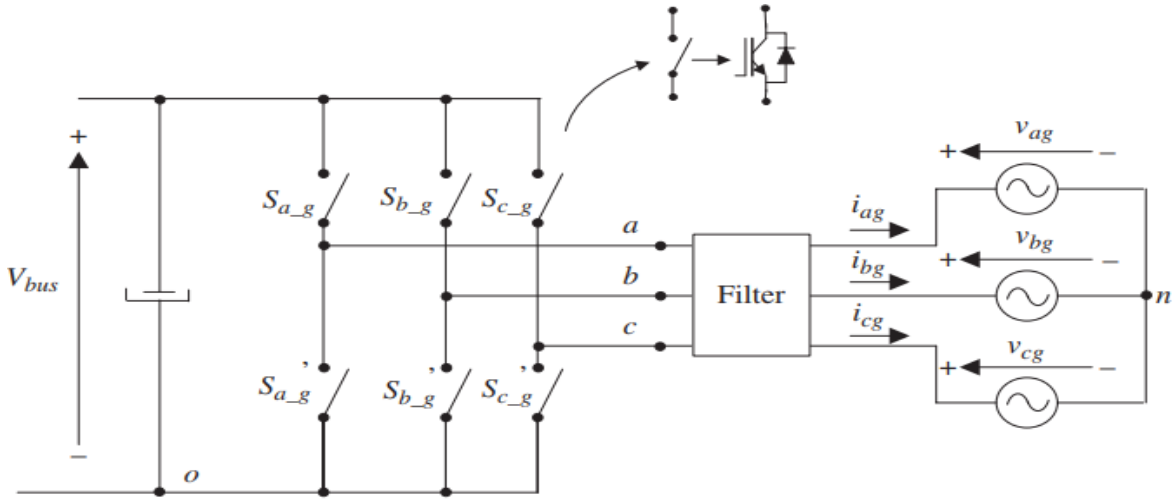

Figure 3-14: Grid-connected VSI power circuit [65].

It contains six switches $S_1 - S_6$. The switches of each leg are complementary. The inverter is supplied by two equal DC sources, the neutral point of which is denoted by N. A three-phase load is connected at the output of the inverter. The load neutral is denoted by n.

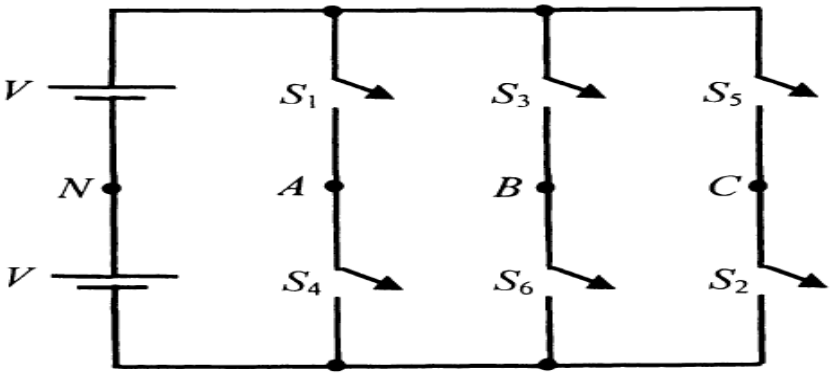

Figure 3-15: Schematic diagram of a three-phase inverter.

- ✓ Definition of three-phase switching function

$S_A = 1$, If A-phase top switch is ON

$S_A = o$, If A-phase bottom switch is OFF

$S_B = 1$, If B-phase top switch is ON

$S_B = 0$, If B-phase bottom switch is OFF

$S_C = 1$, If C-phase top switch is ON

$S_C = 0$, If C-phase bottom switch is OFF

- ✓ Switching function, pole voltage and line voltages are expressed as:

$$V_{AO} = (S_A - 0.5)VDC \tag{3.10}$$

$$V_{BO} = (S_B - 0.5)VDC \tag{3.11}$$

$$V_{CO} = (S_C - 0.5)VDC \tag{3.12}$$

$$V_{AB} = (\ V_{AO} - V_{BO}) \tag{3.13}$$

$$V_{BC} = (\ V_{BO} - V_{CO}) \tag{3.14}$$

$$V_{CA} = (\ V_{CO} - V_{AO}) \tag{3.15}$$

- ✓ Three phase balanced load voltage with unconnected neutral-n is given as:

$$V_{An} = \frac{(V_{AB} + V_{CA})}{3} \tag{3.16}$$

$$V_{Bn} = \frac{(V_{BC} + V_{AB})}{3} \tag{3.17}$$

$$V_{Cn} = \frac{(V_{CA}+V_{BC})}{3} \quad (3.18)$$

Where V_{AO}, V_{BO}, V_{CO} are pole voltages V_{AB}, V_{BC}, V_{CA}, are line voltages, V_{An}, V_{Bn} and V_{Cn} phase voltages.

This thesis considers an idealized behavior of IGBTs and diodes, and does not take into account phenomena such as voltage drop in the semiconductors or switching times.

II. DC-Link Model

The reference value of the capacitor voltage V_{dcref} is selected mainly on the basis of ac output voltage. For satisfactory operation the magnitude of V_{dcref} should be higher than the magnitude of the source voltage V_s by suitable operation of switches a voltage V_s having fundamental component V_{C1} is generated at the AC side of the inverter. This results in flow of fundamental frequency component I_{S1}, as shown in Figure 3-16. The phasor diagram for $V_{C1} > V_s$ representing the reactive power flow is also shown in the Figure 3-16. In this I_{S1} represent fundamental component [66] .

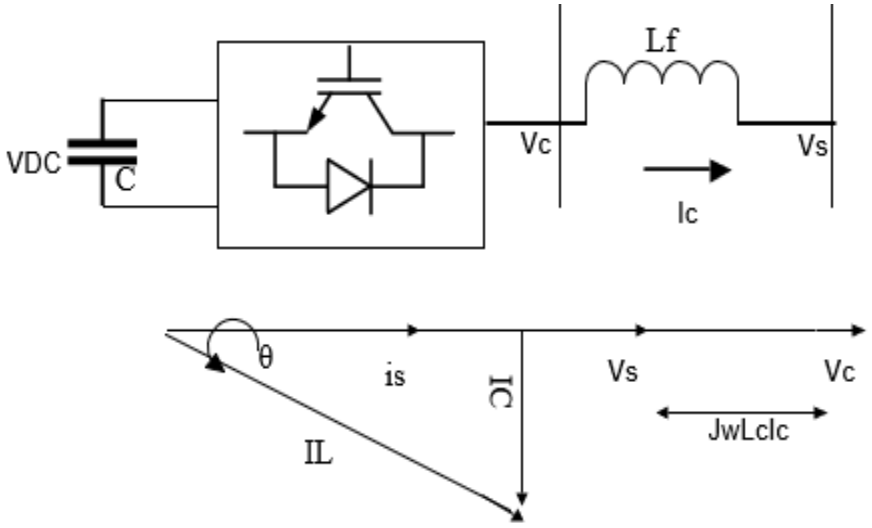

Figure 3-16: Single line and vector diagrams for STATCOM.

$$I_{C1} = \frac{V_{C1} - V_s}{\omega Lf} = \frac{V_{C1}}{\omega Lf}\left(1 - \frac{V_s}{V_{C1}}\right) \quad (3.19)$$

$$Q_{C1} = Q_{L1} = 3V_s I_{C1} \quad (3.20)$$

$$Q_{C1} = Q_{L1} = 3V_s * \frac{V_{C1}}{\omega Lf}\left(1 - \frac{V_s}{V_{C1}}\right) \quad (3.21)$$

In this project the ceramic type of capacitor with appropriate rating is used to withstand high heating effect.

III. Non-Linear Load Model

A three-phase diode rectifier with input impedance and R load is considered as a nonlinear load. Due to the presence of source inductance, six overlapping and six non overlapping conduction intervals occur in a cycle. During a non-overlapping interval only two diodes will conduct while during an overlapping interval three diodes of the bridge will conduct simultaneously. The dynamic Equations during non-overlap and overlap intervals are given in (3.22)and (3.23) respectively [67]:

$$\frac{di_d}{dt} = \frac{(V_{Sl} - (2R_s + R_L)\, i_d - 2V_d)}{2L_s} \tag{3.22}$$

$$\frac{di_d}{dt} = \frac{(V_{Sl} - (1.5R_s + R_L)\, i_d - 2V_d)}{1.5L_s} \tag{3.23}$$

Where R_s and L_s are the elements of the source inductance, V_d is the voltage drop across each device, R_L is the element of load impedance, i_d is the load current flowing through the diode pairs. V_{Sl} is the AC side line voltage segment ($V_{ac}, V_{bc}, V_{ba}, V_{ca}, V_{cb}, V_{ab}$ during non-overlap, and $V_{bc}+\frac{V_{ac}}{2}, V_{ba}+\frac{V_{bc}}{2}, V_{ca}+\frac{V_{ba}}{2}, V_{cb}+\frac{V_{ca}}{2}, V_{ab}+\frac{V_{cb}}{2}, V_{ac}+\frac{V_{ab}}{2}$ during overlap intervals) based on diode pair conduction. The phase currents i_{sa},i_{sb} and i_{sc} are obtained by i_d , considering the respective diode pair conduction.

3.4.4 Control Scheme of STATCOM

The control scheme approach is based on injecting the currents into the grid using "bang-bang controller." The controller uses a hysteresis current controlled technique. Using such technique, the controller keeps the control system variable between boundaries of hysteresis band area and gives correct switching signals for STATCOM operation. The control scheme for generating the switching signals to the STATCOM is shown in Figure 3-17. Control algorithm needs the measurements of variables such as: three-phase source current, voltage, DC voltage, inverter current with the help of sensor [68].

The basic control system block diagram of a STATCOM is shown in Figure 3-17. Main objective of the STATCOM controller is to regulate the voltage at the PCC rapidly in the desired range and

keep its DC-link voltage constant. By controlling the phase and magnitude of the STATCOM output voltage, the power exchange between the ac system and the STATCOM can be controlled effectively. The STATCOM is controlled in a synchronously rotating reference frame using the dq transformation.

The actual signals of the DC-link voltage and the PCC voltage (V_{DC} and V_{PCC}) are compared with their reference values(V_{DCref} and V_{PCCref}) to form the error signals, which are passed through the PI controllers to generate the reference signals for the d-axis and q-axis current components (I_{dref} , I_{qref}) respectively. The current quantities are transformed to a special reference frame that rotates at the same speed as the supply voltage space phasor with the real axis (x-axis) of the reference frame aligned to the supply voltage vector.

At steady state, the reference frame speed equals the synchronous speed. These reference currents I_{aref}, I_{bref}, I_{cref} are compared with the actual currents I_a, I_b, I_c (ac current obtained from the PCC terminal) to get the error signal. The error signals are used to generate the control signal to drive the PWM converter. Here Hysteresis current control technique is used to generate the switching pulses. The control variables are the current injected by the STATCOM and the reactive power injected into the system [69].

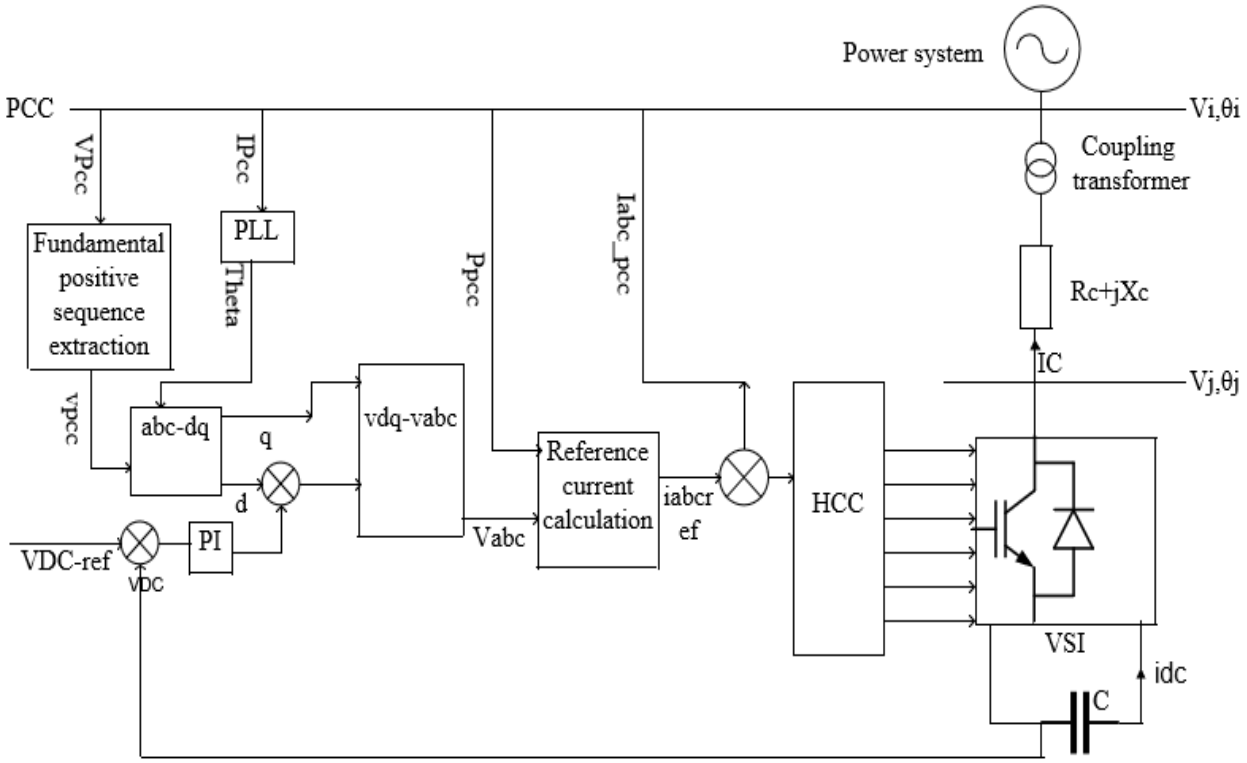

Figure 3-17: Synchronous reference frame control block diagram of a STATCOM.

- **Determination of switching frequency (f_s) and hysteresis bandwidth (HB)**

CASE I: Hysteresis Band Current Control

Hysteresis band current control method is used for its improved stability, fast transient response, simple implementation & higher accuracy in current tracking.

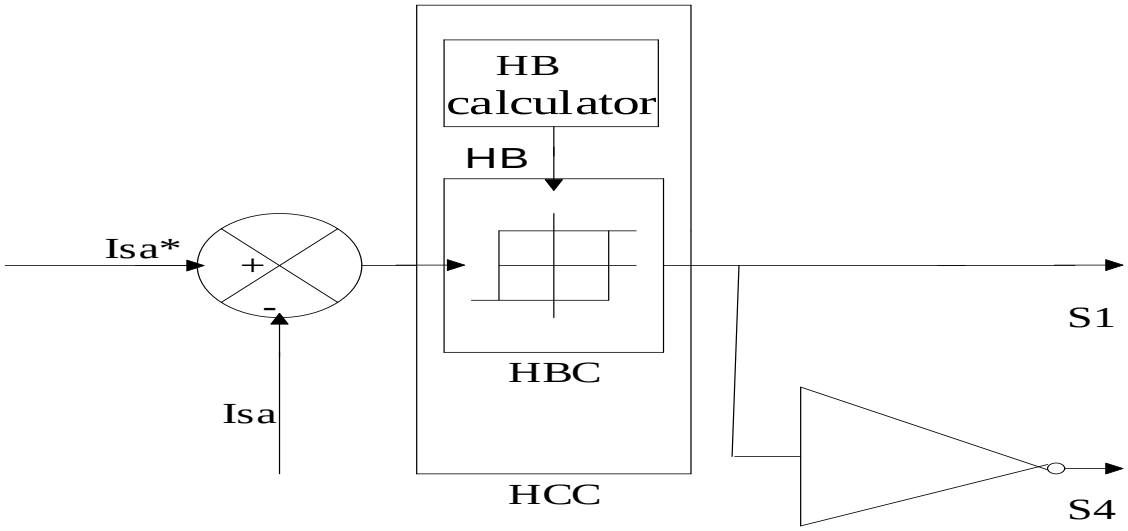

Figure 3-18: Hysteresis band current controller loop.

The switching signals are produced directly when the error exceeds an assigned tolerance band as shown in Figure 3-19.

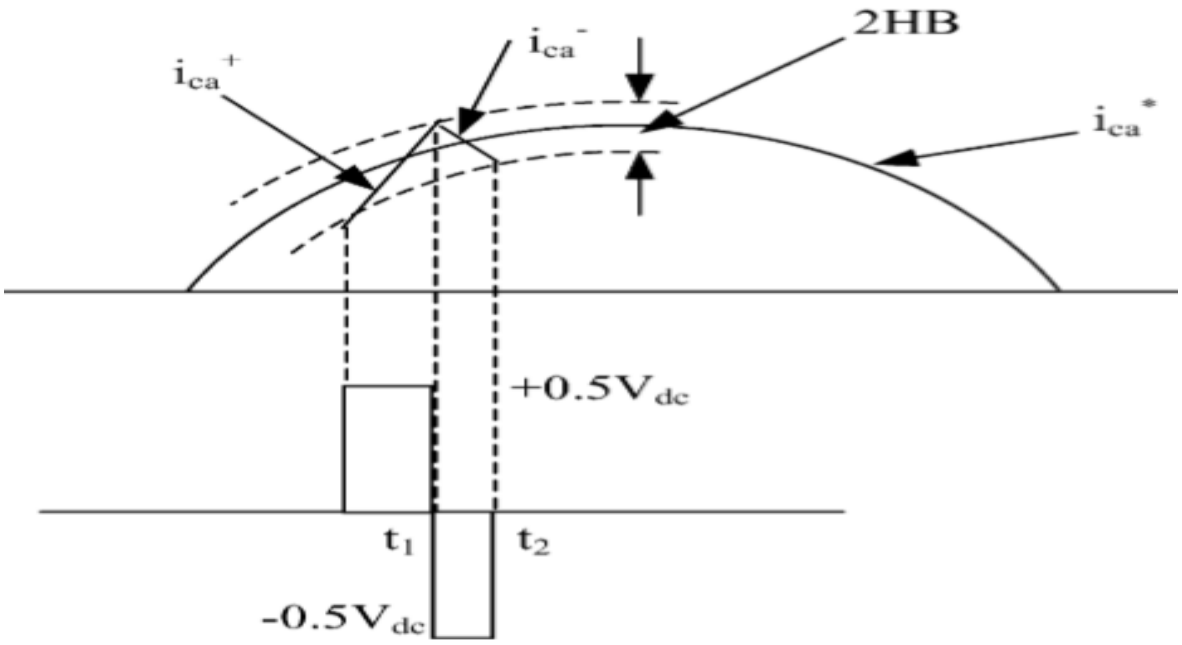

Figure 3-19: The upper and lower bands of the reference compensation current [70].

The algorithm of the hysteresis blocks, for phase-a

Working principle

$$I_{sa} > (isa^* + HB) \rightarrow S_A = 0 \quad (3.24)$$

$$I_{sa} > (isa^* - HB) \rightarrow S_A = 1 \quad (3.25)$$

Where, S_A is switch of leg phase A

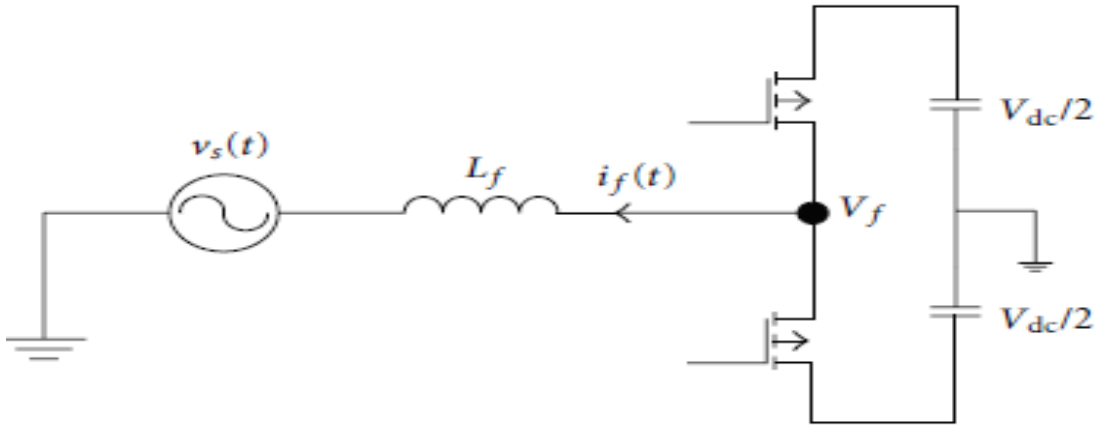

Figure 3-20: Single-phase diagram of a power system with VSI [71].

- **Calculations of switching frequency (f_s) and hysteresis band (HB)**

The following Equations can be written in the respective switching intervals(t_1) and(t_2) from Figure 3-20.

Positive sign indicates that switch S_1 is ON state at rising time whereas negative sign indicates

S_1 Is OFF state at falling time

By using KVL for phase A

$$\frac{di_{sa}^+}{dt} = \left(\frac{\frac{V_{DC}}{2} - V_{Sa}}{L}\right) \quad (3.26)$$

$$\frac{di_{sa}^-}{dt} = -\left(\frac{\frac{V_{DC}}{2} + V_{Sa}}{L}\right) \quad (3.27)$$

Let t_1 is the switch ON period whereas t_2 is switch OFF period

$$\frac{di_{sa}^{+}}{dt}t_1 - \frac{di_{sa}^{*}}{dt}t_1 = 2HB \tag{3.28}$$

$$\frac{di_{sa}^{-}}{dt}t_2 - \frac{di_{sa}^{*}}{dt}t_2 = -2HB \tag{3.29}$$

Adding Equation (3.28) and Equation (3.29),

$$\frac{di_{sa}^{+}}{dt}t_1 - \frac{di_{sa}^{*}}{dt}t_1 + \frac{di_{sa}^{-}}{dt}t_2 - \frac{di_{sa}^{*}}{dt}t_2 = 2HB + (-2HB) \tag{3.30}$$

$$\frac{di_{sa}^{+}}{dt}t_1 - \frac{di_{sa}^{*}}{dt}t_1 + \frac{di_{sa}^{-}}{dt}t_2 - \frac{di_{sa}^{*}}{dt}t_2 = 0$$

$$\frac{di_{sa}^{+}}{dt}t_1 + \frac{di_{sa}^{-}}{dt}t_2 - \frac{di_{sa}^{*}}{dt}(t_2 + t_1) = 0 \tag{3.31}$$

$$T_C = t_2 + t_1 = \frac{1}{f_C} \tag{3.32}$$

Where, f_C is the switching frequency and i_{sa}^{*} is the desired reference source current

Substituting Equation (3.32) into Equation (3.31.) yields,

$$\frac{di_{sa}^{+}}{dt}t_1 + \frac{di_{sa}^{-}}{dt}t_2 - \frac{di_{sa}^{*}}{dt}\left(\frac{1}{f_C}\right) = 0 \tag{3.33}$$

Subtracting Equation (3.29) from Equation (3.28) gives,

$$\frac{di_{sa}^{+}}{dt}t_1 - \frac{di_{sa}^{*}}{dt}t_1 - \left(\frac{di_{sa}^{-}}{dt}t_2 - \frac{di_{sa}^{*}}{dt}t_2\right) = 2HB - (-2HB) \tag{3.34}$$

$$\frac{di_{sa}^{+}}{dt}t_1 - \frac{di_{sa}^{*}}{dt}t_1 - \left(\frac{di_{sa}^{-}}{dt}t_2 - \frac{di_{sa}^{*}}{dt}t_2\right) = 4HB$$

Substituting Equations (3.24) and (3.25) into Equation (3.33)

$$\left(\frac{\frac{V_{DC}}{2} - V_{Sa}}{L}\right)t_1 - \left(\frac{\frac{V_{DC}}{2} + V_{Sa}}{L}\right)t_2 - \frac{di_{sa}^{*}}{dt}\left(\frac{1}{f_C}\right) = 0$$

$$(t_2 - t_1) = -\frac{2L}{V_{DC}f_C}\left(\frac{V_S}{L} + \frac{di_{sa}^{*}}{dt}\right) \tag{3.35}$$

Substituting Equations (3.29) and (3.28) into Equation (3.34) gives,

$$4HB = \frac{0.5V_{DC}}{f_C L} - (t_1 - t_2)\left(\frac{V_S}{L} + \frac{di_{sa}^{*}}{dt}\right) \tag{3.36}$$

Substituting Equations (3.35) into Equation (3.336) and simplifying gives,

$$HB = 0.125 * \frac{V_{DC}}{f_C L}[1 - \frac{4L^2}{{V_{DC}}^2}\left((\frac{V_S}{L} + m)^2\right)] \quad (3.37)$$

Where, $m = \frac{di_{sa}^*}{dt}$ is the slope of desired reference source current wave form. In hysteresis current control scheme, Hysteresis band (HB) calculated in (3.37) is modulated at different points of fundamental frequency cycle to maintain the switching frequency of the inverter constant. The calculated variable bandwidth HB is applied to the hysteresis band current controller. In this work the required gating signal for STATCOM is produced by HCC.

3.4.5 Static Var Compensator

They could be broadly classified as under:

i. TSC (Thyristor Switched Capacitors)
ii. FC-TCR (Fixed Capacitor Thyristor Controlled Reactor)
iii. TCR (Thyristor Controlled Reactor)
iv. TSR and TCR (Combination of Both)

FC-TCR (Fixed Capacitor Thyristor Controlled Reactor)

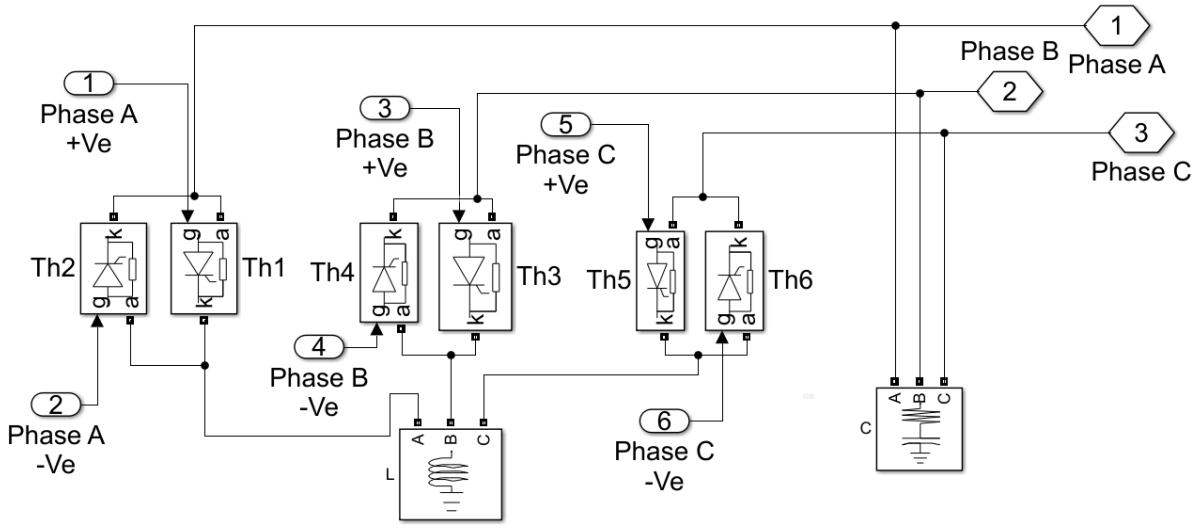

Figure 3-21:FC-TCR of SVC.

TCR Inductor is the design parameter and needs to be fixed for maximum VAR absorbing capability. TCR is connected in delta fashion in order to reduce harmonics. Inductance of each branch in delta can be computed using Equation (3.38) [72].

And substituting V =33KV, KVAr(L) = 30000

$$\mathrm{L} = \frac{\mathrm{V}^2}{2(1000 * 2\pi \mathrm{f} * \mathrm{KVAr(L)}} \tag{3.38}$$

$$\mathrm{L} = \frac{(33000)^2}{2(1000 * 2\pi(50) * 30000)}$$

$$\mathrm{L} = 0.05777\mathrm{H}$$

Here, f is the system frequency, V is system line voltage L, represent total Inductance needed for maximum reactive VAR absorption, KVAr(L), represent maximum inductive VARs to be provided. This value of L is fixed for each branch so as to absorb maximum vars. The thyristor valve controls the VAR injection to bring in controllability and to exactly meet the demand.

Thus, by fixing the value of C, the design parameter is limited to provide the maximum VAR's required by each TSC branch. Thus, by fixing the value of C, the design parameter is limited to provide the maximum VAR's required by each TSC branch.

And substituting V = 33KV, KVAr(C) = 15000

$$\mathrm{C} = \frac{1000 * \mathrm{KVAr}(C)}{2\pi \mathrm{f} * \mathrm{V}^2} \tag{3.39}$$

$$\mathrm{C} = \frac{1000 * 15000}{2\pi \mathrm{f} * (33000)^2}$$

$$\mathrm{C} = \ 0.43844\mu F$$

Here, f is the system frequency, C represent the total capacitance required for maximum VARs injection, kVAR(C), represent maximum capacitive VARs to be provided.

Thyristor controlled reactor is as if variable admittance and is function of delay angle α.

$$B_L(\alpha) = \frac{1}{\omega L}\left(1 - \frac{2\alpha}{\pi} - \frac{sin2\alpha}{\pi}\right) \tag{3.40}$$

The current in the reactor can be controlled by the method of firing delay angle control. The closure of the thyristor valve is delayed w.r.t the peak of applied voltage in each half cycle. Let the firing delay angle is α, applied voltage is v.

$$\mathrm{v(t)} = \ v_m cos\omega t$$

$$i_L(t) = \frac{v_m}{\omega L}(sin\omega t - sin\alpha)$$

The amplitude $I_{LF}(\alpha)$ of the fundamental reactor current $i_{LF}(\alpha)$ can be expressed as:

$$I_{LF}(\alpha) = \frac{v_m}{\omega L}\left(1 - \frac{2\alpha}{\pi} - \frac{sin2\alpha}{\pi}\right) \tag{3.41}$$

The control range of the TCR firing angle 'α' extends from 90^0 to 180^0.

Control of SVC

Figure 3-22 shows the static Var compensator controller with different controller blocks.

Voltage Measurement System: measures the positive-sequence voltage to be controlled (HV).

Voltage Regulator: uses the voltage error bet ween V_m and V_{ref} to determine the SVC susceptance B needed to keep the system voltage constant.

Distribution Unit: determines the capacity of current and the number of TSC_s be switched in and out and inductive current (to cancel surplus capacitive current) of TCR, hence required firing angle α of TCR_s.

Synchronizing system: using a phase locked loop (PLL) synchronizes secondary voltage a pulse generator that send appropriate pulses to the thyristor.

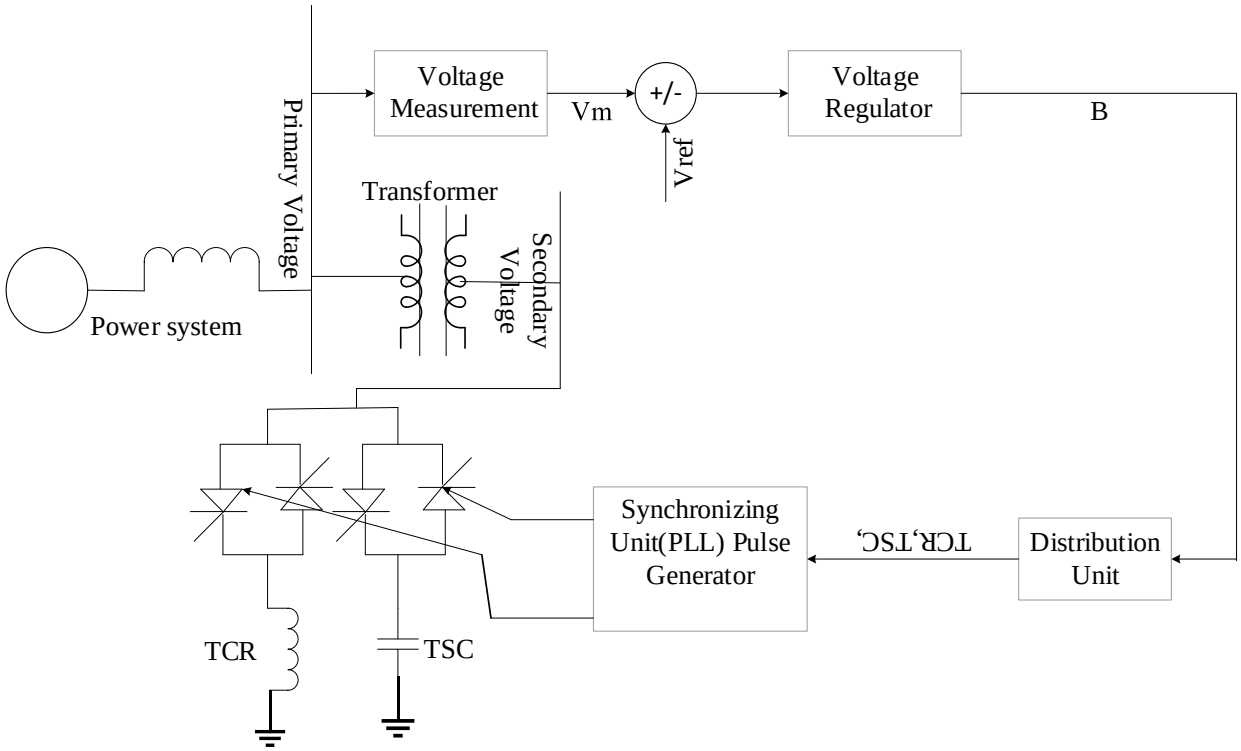

Figure 3-22: General Controller of SVC.

3.4.6 Design of STATCOM Components

STATCOM consists of the following component:

i. Voltage source converter
ii. Coupling element
iii. DC energy storage device
iv. DC bus Controller

I. Estimation of STATCOM Capacity

In order to evaluate the required STATCOM size for the power system under study, the wind farm model is represented by the aggregated equivalent circuit as shown in Figure 3-9. The wind turbines and generators are lumped into a single equivalent machine whose rating is equal to the sum of individual unit ratings [73].

II. Selection of Nominal DC Bus Voltage

Selection of reference voltage of DC side capacitor V_{DCref} is one of the important parameters. The peak capacitor voltage is the maximum voltage to be supported by the switches, while the lower capacitor voltage will determine the STATCOM capability to force its current to follow the intended reference wave form. If the capacitor voltage falls below the reference voltage, STATCOM will not be able to shape its current as intended, and hence mal operation may occur.

Normally, the DC link voltage of VSC must be greater than twice the peak of maximum phase voltage. The design criteria for the selection of reference DC bus voltage can be achieved by considering ac output voltage. Therefore, from the ac line voltage ab is 690V so, the DC link voltage is estimated as [74]:

$$V_{DC} \geq \frac{2*\sqrt{2}}{m*\sqrt{3}} * V_{ab} \tag{3.42}$$

Where V_{ab} is ac three phase line voltage, m modulation Index i.e. assuming the modulation index is 1 the equivalent input DC source voltage is calculated as:

$$V_{DC} \geq \frac{2 * \sqrt{2}}{m * \sqrt{3}} * V_{ab}, \qquad V_{DC} \geq \frac{2 * \sqrt{2}}{1 * \sqrt{3}} * 690, \qquad V_{DC} \geq 1{,}126.765V$$

$$V_{DCmin} = 1{,}126.765V$$

Considering nominal AC voltage variation constant, filter voltage drops and dead band in PWM output:

$$V_{DC} = \frac{1.05 * 1.05 * 1.1 * \frac{2 * \sqrt{2}}{1 * \sqrt{3}} * 690}{d} = 1{,}366.48V$$

$$V_{DCmax} = 1{,}366.48V$$

Where 1.05 is dead band factor due to PWM switch,1.05 is nominal ac voltage variation factor and 1.1 is filter voltage drop factor and d is duty cycle which is 1.

Therefore, input DC bus voltage can be calculated $1{,}126.765V \leq V_{DC} \leq 1{,}366.48V$ and in this thesis 1,150V DC is used to get the equivalent three phase ac voltage of 690V from VSC of STATCOM.

III. Selection of DC Bus Capacitor

The DC side capacitor serves two main purposes: (i) it maintains a DC voltage with small ripple in steady state, and (ii) serves as an energy storage element to supply real power difference between load and source during the transient period. In the steady state, the real power supplied by the source should be equal to the real power demand of the load plus a small power to compensate the losses in the STATCOM. Thus, the DC capacitor voltage can be maintained at a reference value.

However, when the load condition changes the real power balance between the mains and the load will be disturbed. This real power difference is to be compensated by the DC capacitor. This changes the DC capacitor voltage away from the reference voltage.

In order to keep satisfactory operation of the STATCOM, the peak value of the reference current must be adjusted to proportionally change the real power drawn from the source. This real power charged/discharged by the capacitor compensates the real power consumed by the load. If the DC capacitor voltage is recovered and attains the reference voltage, the real power supplied by the source is supposed to be equal to that consumed by the load again.

Thus, in this fashion the peak value or the reference source current can be obtained by regulating the average voltage of the DC capacitor. A smaller DC capacitor voltage than the reference voltage means that the real power supplied by the source is not enough to supply the load demand. Therefore, the source current (i.e. the real power drawn from the source) needs to be increased,

while a larger DC capacitor voltage than the reference voltage tries to decrease the reference source current.

A small value of dc capacitor may lead to a large ripple in the steady state and wide fluctuation in the DC bus voltage under transient conditions. Whereas a higher value of capacitor reduces fluctuations and ripple in the DC bus voltage, but the overall cost and size of the system will increase [75]

$V_{DC} = 2\sqrt{2}V_{C1}$

For $V_{DC} = 1150v$

$$V_{C1} = \frac{V_{DC}}{2\sqrt{2}} = \frac{1150}{2\sqrt{2}} = 406.5863Vac$$

For three –phase $V_{C1} = \sqrt{3} * 406.59$

$V_{C1} = 704.2283v$

For $V_s = 690V$ and $L = 11mH$

$$I_{C1} = \frac{V_{C1} - V_s}{\omega Lf} = \frac{V_{C1}}{\omega Lf}\left(1 - \frac{V_s}{V_{C1}}\right)$$

$$I_{C1} = \frac{704.2283 - 690}{2 * pi * 50 * 0.011}$$

Therefore,

$Q_{C1} = Q_{L1} = 3V_s I_{C1}$

$$Q_{C1} = Q_{L1} = \frac{V_{rms}^2}{X_C}$$

$$X_C = \frac{V_{rms}^2}{Q_{L1}}$$

$$X_C = \frac{1}{\omega fC}$$

$$C = \frac{1}{X_C * \omega f}$$

In this project the ceramic type of capacitor with appropriate rating is used to withstand high heating effect.

IV. Selection of Interfacing Inductor

An inductor is used between voltage source inverter and the supply terminal voltage to filter out the switching harmonic. The selection of inductor value is very crucial. If inductor value is small, large switching ripple are injected into the current. Whereas a large value of inductor will reduce the current ripple but at the same it will not allow the proper tracking of the compensating current because of their lagging nature. So, to obtain satisfactory performance an optimum selection of the inductor used between voltage source inverter and the supply terminal voltage is essential [76].

The inductance of the coupling reactor (L_r) depends on the value of the VSC switching frequency f_s , and the line ripple current $I_{cr,pp}$ and DC bus voltage V_{DC} as follows [77]:

$$L_r = \frac{\sqrt{3} * m * V_{DC}}{12 * \alpha * f_s * I_{cr,pp}}$$

Where the m is the modulation index, α is the overloading factor and,

the line ripple current is calculated as: $I_{cr,pp} = 0.05 * \sqrt{2} * I_{rms}$

3.4.7 Design of PI Controller for STATCOM DC-Bus Voltage Control

In this thesis the PI controller is used to control the capacitor voltage of DC bus input source. Capacitor bank is used as energy storage system for DC voltage input of STATCOM. Figure 3-23 with an L and C filters at the output of the SATCTOM is the source current, i_L is the load current, i_C is the output current of the SATCTOM while i_{ref} is its reference value. R_s and L_s are the equivalent resistance and inductance of the source and line. The output filter of STATCOM includes L_1, R1, C and R_d that can easily eliminate the higher ordered harmonics of the VSC. Ziegler-Nichols method is used for tuning of PID controllers.

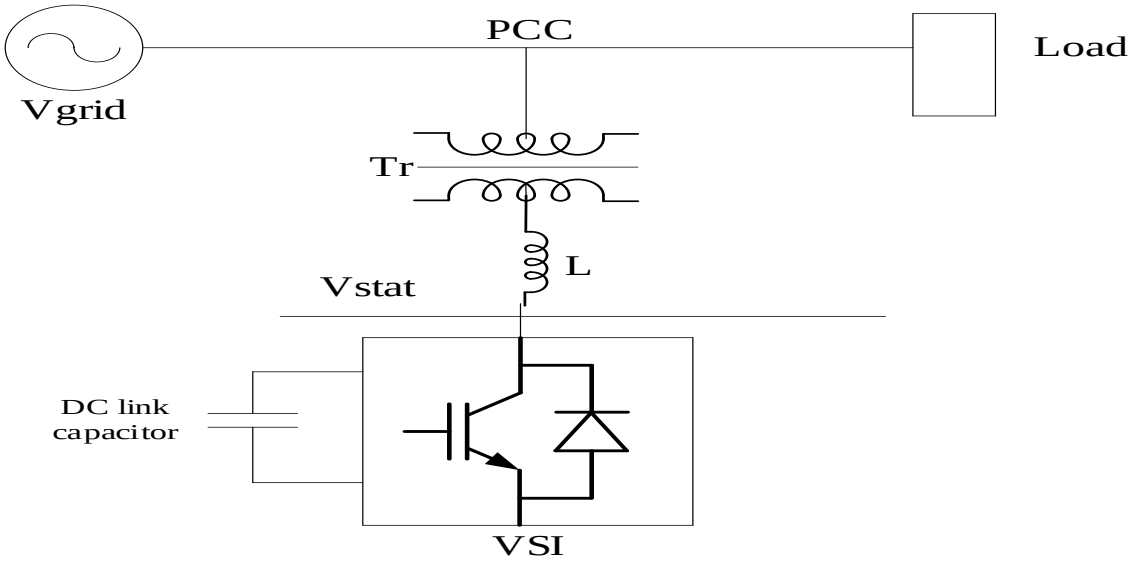

Figure 3-23: STATCOM with passive output LC filter.

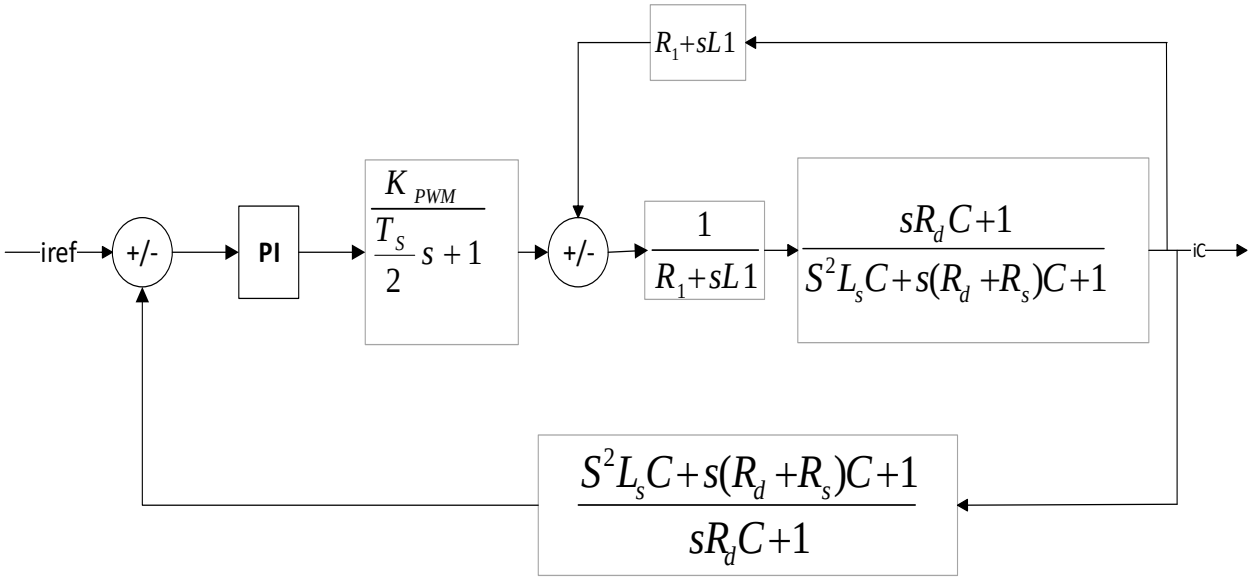

Figure 3-24: Block diagram of control circuit.

$$T(s)=\frac{K_pK_{PWM}}{(s\frac{T_s}{2}+1)}\cdot\frac{s^2L_sC+s(R_d+R_s)C+1}{(sL_1+R_1)[s^2L_sC+s(R_d+R_s)C+1]+s(R_dC+1)(sL_s+R_s)}$$

Using the Ziegler-Nichols method with the equation:

$$K_{P\omega}=(2\omega_{nn}\sigma J)/P \tag{3.43}$$

$$K_{i\omega}=(\omega_{nn}J)/P \tag{3.44}$$

3.4.8 Voltage Variation Analysis

Variation of voltage has several impacts on reactive and active power of grid connected wind farms. In low-voltage situation, most of the current will flow through the generator, power equipment and the line which leads to increase the losses. On the other side low voltage also affects power factor. This effect occurs when capacitive Var generated by installing capacitor, decreased by reduction of voltage. Voltage increment also affects systems operation; higher voltage will increase the stress on the insulation which leads to reduce the life of them and the magnetization Var of transformer.

3.4.9 Harmonic Distortion Analysis

The harmonic results due to the operation of power electronic converters. The harmonic voltage and current should be limited to the acceptable level at the point of wind turbine connection to the network. To ensure the harmonic voltage within limit, each source of harmonic current can allow only a limited contribution, as per the IEC-61400-36 guideline. The rapid switching gives a large reduction in lower order harmonic current compared to the line commutated converter, but the output current will have high frequency current and can be easily filtered.

To limit both voltage and current harmonic distortion, IEEE Standard 519-1992 proposes to limit harmonic current injection from end users so that harmonic voltage levels on the overall power system will be acceptable if the power system does not inordinately accentuate the harmonic currents.

IEEE519:" recommended practices and requirements for harmonic control in electrical power systems"

i. Point of Common Coupling

Is a point of metering, or any point as long as both the utility and the customer can either access the point for direct measurement for the harmonic's indices meaningful to both, and estimate the harmonic indices at the point of interference through mutually agreeable method. Within an industries load, the point of coupling is the point between the nonlinear and other loads.

ii. Total Harmonic Distortion

It is the measure of closeness of wave form with respect to its fundamental component.it is an important measure of performance in electrical system.

Mathematically it is expressed as:

$$THDi = \frac{\sqrt{\sum_{h=2}^{hmax} Mh^2}}{M1} \quad (3.45)$$

Where, Mh is the rms value of harmonic component h of the quantity M. The THD is a very useful quantity for many applications. It is the most commonly used harmonic index. However, it has the limitation that it is not a good indicator of voltage stress within a capacitor because that is related to the peak value of voltage waveform.

Fourier series is the mathematical tool used to extract the fundamental and harmonic components from a distorted waveform.

iii. Total Demand Distortion

Current distortion level expressed by THD can be sometimes misleading because a small current may have a high THD but not a significant threat to the system. Many adjustable-speed drives exhibit high THD but because of small magnitude of current they are harmless. Therefore, IEEE has recommended use of another harmonic measurement by referring THD to fundamental of peak demand load current. It is called total demand distortion and given by:

$$THDi = \frac{\sqrt{\sum_{h=2}^{hmax} Ih^2}}{IL} \quad (3.46)$$

Where, IL is the peak or maximum demand load current at the fundamental frequency component measured at the PCC.

3.5 Economic cost Analysis

In DAMA II wind farm main substation, SVC comprises a TCR rated at 30 MVAr at nominal voltage (34.5 kV), a 3rd harmonic filter rated at 15Mvar, a 5th harmonic filter rated at 15Mvar. The overall dynamic control range of the SVC is 0 – 60 MVAr at each of two 33KV busbar. In this thesis only one 33KV busbar which contains 13 wind turbines of 4 feeder i.e. 13*4*1.5=78MW and 33/230KV with 90MVA main transformer is selected.

i. Cost of SVC

Generally, the cost of an SVC system has two components: the installation costs and operating expenses. The total cost of the entire installed systems comprises the equipment price and the delivery and installation of the device and service. Specifically, the operating cost of the devices is approximately 5% to 10% of the total installation cost.

Therefore, the cost functions for the SVC and STATCOM are developed as follows:

$$C_{SVC} = 0.0004S^2 - 0.262S + 81.5\$perKvar \quad (3.47)$$

$$C_{SVC} = 0.0003S^2 - 0.305S + 127.38\$perKvar$$

$$C_{STATCOM} = 0.0004S^2 - 0.3225S + 128.75\$perKvar \quad (3.48)$$

$$C_{STATCOM} = -0.0008S^2 - 0.155S + 120\$perKvar$$

Using the above eqution (3.47) with 60MVAr rating of SVC,

$$C_{SVC} = 0.0004S^2 - 0.262S + 81.5\$perKvar$$

$$C_{SVC} = 0.0004(60)^2 - 0.262(60) + 81.5\$perKvar$$

$$C_{SVC} = 1.44 - 15.72 + 81.5\$perKvar$$

$$C_{SVC} = 67.22\$perKvar$$

$$C_{SVC} = 0.0003S^2 - 0.305S + 127.38\$perKvar$$

$$C_{SVC} = 0.0003(60)^2 - 0.305(60) + 127.38\$perKvar$$

$$C_{SVC} = 1.08 - 18.3 + 127.38\$perKvar$$

$$C_{SVC} = 110.16\$perKvar$$

An overall cost for reactive power 60MVAr, SVC ranges from $67 to $110 per kVAr.

i. Cost of STATCOM

The STATCOM rating estimated in this thesis is 4*13*1.5*0.368=28.704MVAr.

Using the above eqution (3.48) with 28.704 MVAr rating of STATCOM,

$$C_{STATCOM} = 0.0004S^2 - 0.3225S + 128.75\$perKvar$$

$$C_{STATCOM} = 0.0004(28.7)^2 - 0.3225(28.7) + 128.75\$perKvar$$

$$C_{STATCOM} = 0.33 - 9.257 + 128.75\$perKvar$$

$$C_{STATCOM} = 120\$perKvar$$

$$C_{STATCOM} = -0.0008(28.7)^2 - 0.155(28.7) + 120\$perKvar$$

$$C_{STATCOM} = -0.66 - 4.449 + 120\$perKvar$$

$$C_{STATCOM} = 115\$perKvar$$

Similarly, An overall cost for reactive power 28.704MVAr, STATCOM ranges from $115 to $120 per kVAr. As result above sahows, STATCOM is a source of reactive power compensation that is more expensive than SVC because of the used power electronics components like IGBT. But when replacing STATCOM by SVC we can reduce the size of rating by i.e 60MVAr-28.704MVAr = 31.296MVAr.

The cost of net reactive power will be:

$$C_{STATCOM} = 0.0004(31.296)^2 - 0.3225(31.296) + 128.75\$perKvar$$

$$C_{STATCOM} = 0.39 - 10 + 128.75\$perKvar$$

$$C_{STATCOM} = 120\$perKvar$$

$$C_{STATCOM} = -0.0008(31.296)^2 - 0.155(31.296) + 120\$perKvar$$

$$C_{STATCOM} = -0.78 - 4.85 + 128.75\$perKvar$$

$$C_{STATCOM} = 123\$perKvar$$

An overall cost for net reactive power 31.296 MVAr, STATCOM ranges from $120 to $123 per kVAr. So ADAMA II wind farm substation can save net reactive power cost of $120 to $123 per kVAr by replacing STATCOM.

CHAPTER FOUR

RESULTS AND DISCUSSION

4.1 Developed Complete Simulink Model and analysis

The developed complete model of the study is shown in Figure 4-1. The model consists: the main supply source of the grid which is represented by three phase AC source, DFIG wind turbine, STATCOM and nonlinear load. The three-phase grid generates balanced voltages (V_A, V_B,,and V_C,) having constant frequency and magnitude. The DFIG wind turbine model, which consists: aerodynamics wind turbine, rotor side converter, DC bus capacitor, grid side converter and filter, is integrated to the grid at PCC. A STATCOM is coupled in shunt and it consists: voltage source IGBT based six-pulse inverter and a DC voltage source capacitor linked at its DC bus. The bang-bang controller uses a hysteresis current controlled technique to generate gate pulsing signal that commands ON/OFF state of semiconductor IGBT switches of voltage source inverter. Using this technique, the controller retains the control system variable between boundaries of hysteresis area and gives switching signal pulse for STATCOM operation.

Figure 4-2 shows the existing system Simulink model which consists: the main supply source of the grid which is represented by three phase AC source, DFIG wind turbine, SVC and nonlinear load. The three-phase grid generates balanced voltages (V_A, V_B,,and V_C,) having constant frequency and magnitude. The DFIG wind turbine model, which consists: aerodynamics wind turbine, rotor side converter, DC bus capacitor, grid side converter and filter, is integrated to the grid at PCC. A SVC is coupled in shunt and it consists: Fixed capacitor bank and thyristor-controlled reactor. The firing angle is used to generate trigger pulsing signal that commands ON/OFF state of thyristor valves.

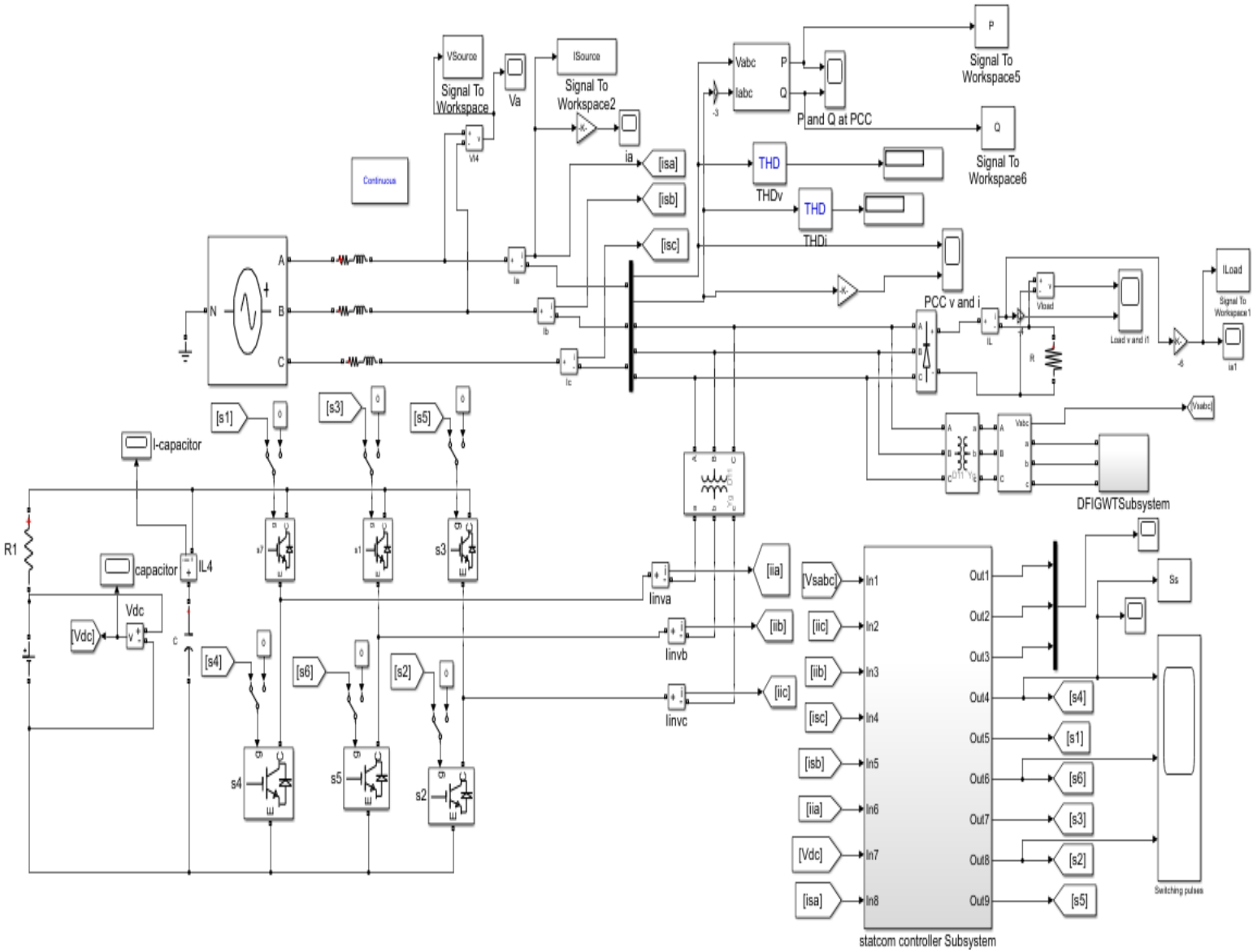

Figure 4-1: Developed Simulink model of the complete developed system.

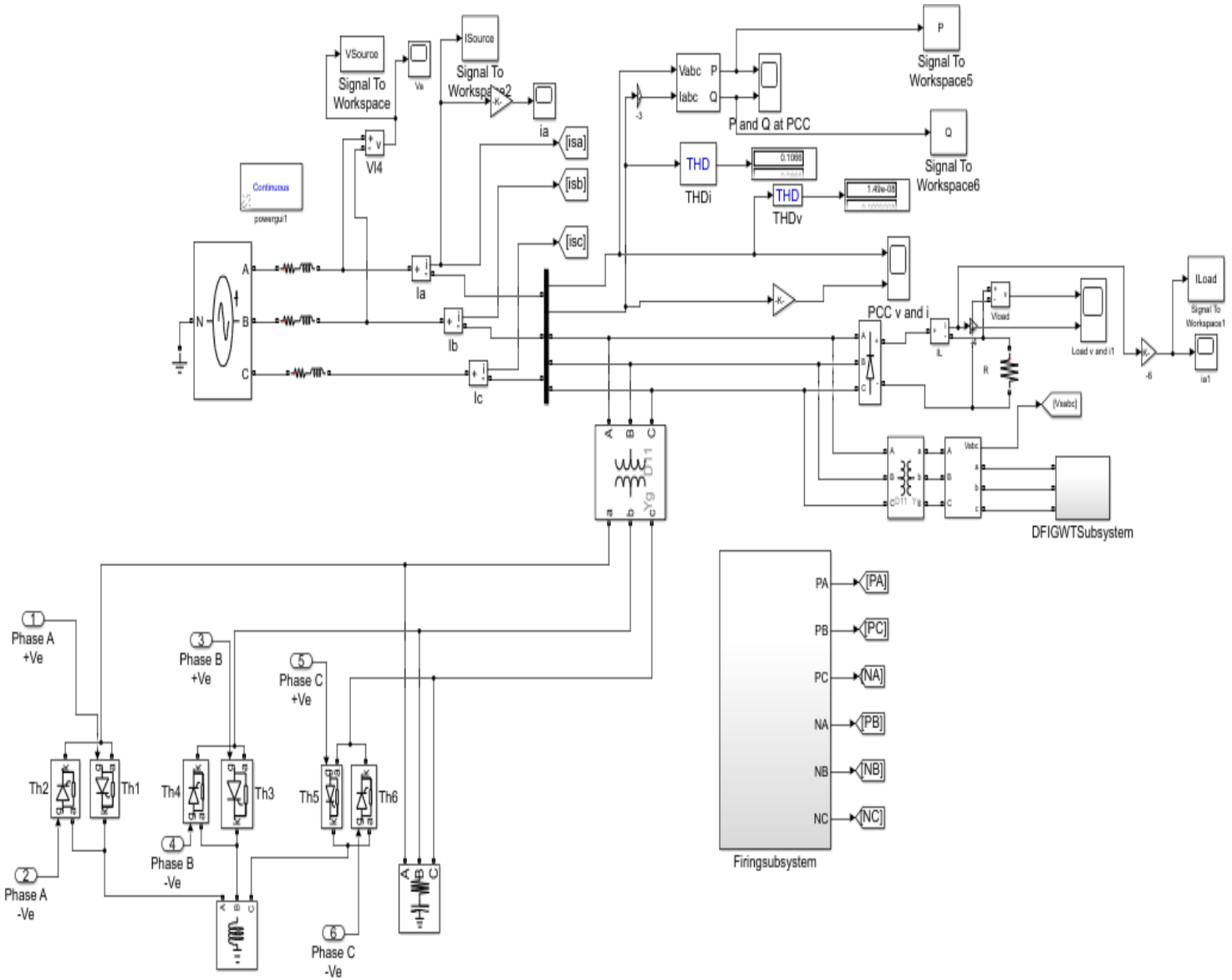

Figure 4-2: Simulink model of the existing system with SVC.

4.1.1 Simulink Model of DFIG Wind Turbine

Figure 4-3 shows, DFIG which consists wind turbine, rotor side controller and grid side controller with back-to-back bi-directional power converter and DC link bus. DFIG is controlled by using vector control technique. DFIG can operate at different operating frequency i.e. at sub synchronous speed, synchronous speed and super synchronous speed.

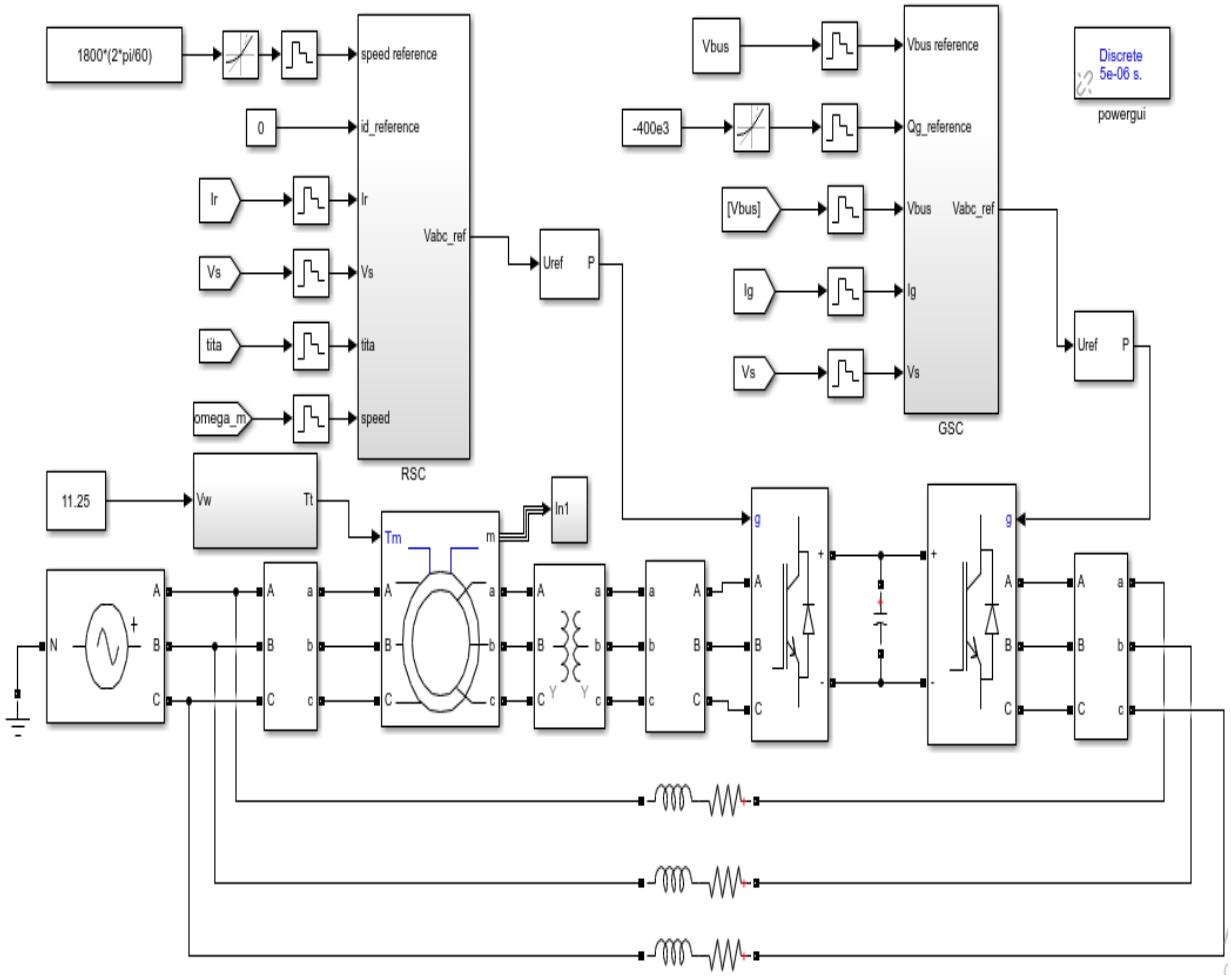

Figure 4-3: Developed Simulink model of DFIG wind turbine.

I. Simulink Model of Wind Turbine Aerodynamic

In Figure 4-4, two inputs such as wind speed and the rotational velocity of wind turbine are needed as inputs to generate the mechanical output torque of the wind turbine. The model consists of tip speed ratio (λ), blade radius (R), wind speed (V_W), gear box ratio(N) and the torque coefficient (C_t). Pitch control technique is used to protect the wind turbine from damage and overload of turbine blades during maximum wind speed by maintaining the rated wind power. Pitch control

technique is applied to get the optimized tip speed ratio using MPPT to which the maximum toque is achieved. Torque coefficient represents the wind turbine does not extract all the available kinetic energy of the flowing air stream according to betz law. Wind speed of low speed shaft is converted into high speed shaft using the gear box. Wind turbine model represent the mechanical torque of the turbine which is used as an input for DFIG.

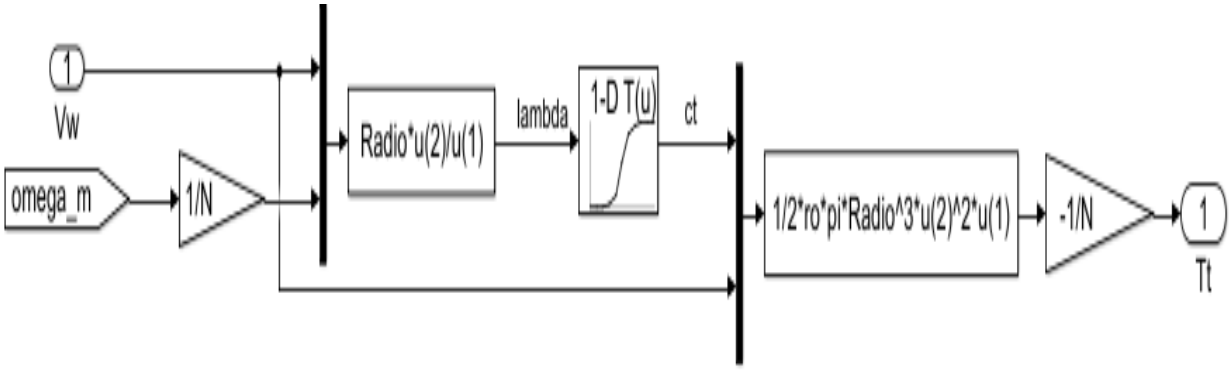

Figure 4-4: Wind turbine model.

II. Simulink Model of Rotor Side Controller

The rotor current control loop is studied to describe the vector control of DFIG wind turbine. In an equivalent way to the classic vector control techniques of other different machines, the vector control specifically, the stator flux vector control is used to decouple both active and reactive power to control them independently. DFIG can be performed in a synchronously rotating dq frame, in which the d-axis is aligned with the stator flux space vector. The space vector transformation is used in order to represent the three-axis coordinate system parameters in to two -axis coordinate system. In the Figure 4-5, RSC uses the measured values of rotor current, stator voltage, stator current, mechanical rotor speed, and the rotational angle of the rotor. The rotor side circuit is modeled by using the grid side as compacted as DC voltage source. The rotor side converter is connected to the grid side converter by the DC link. Two-level six-Pulse Width Modulation generator is used for generating and supplying the pulse into the VSI.

MPPT block in Figure 4-6 is used to get the optimal rotational velocity of wind turbine for variable wind speed to achieve corresponding mechanical torque. The PI controllers are used to control rotor dq-axis current. Synchronous reference frame generates the rotor reference voltage signal.

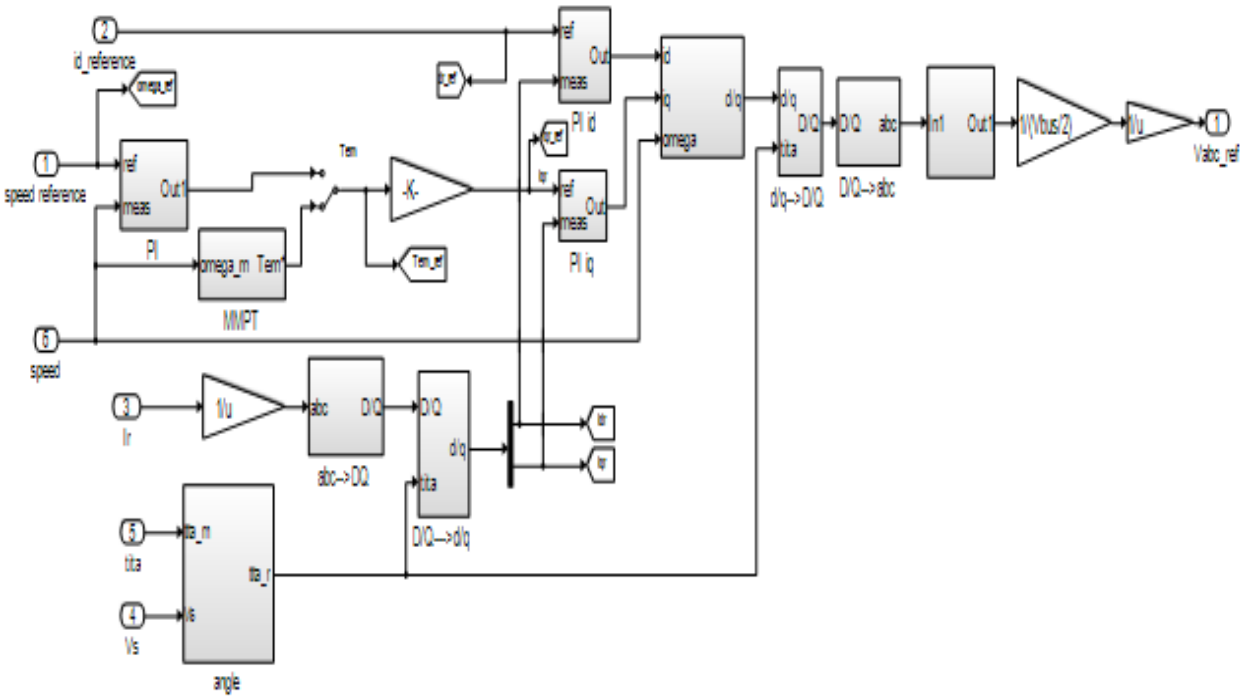

Figure 4-5: Developed Simulink model of RSC.

III. Maximum power point tracing strategy

It is used to control the wind turbine of the DFIG using indirect speed control of MPPT control strategy. The rotational speed is used to produce the optimized torque reference as an output. In the Simulink model shown in Figure 4-6 the parameters are referred to low-speed shaft and converted in to high speed shaft using gear box ratio.

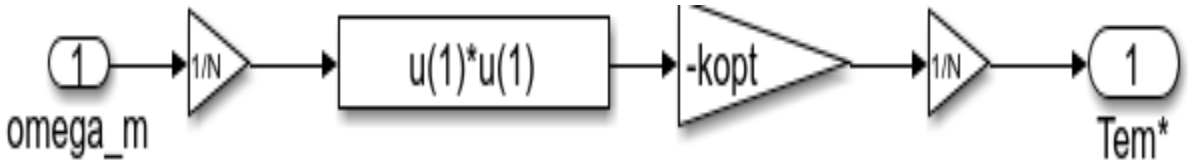

Figure 4-6: Indirect speed control.

IV. Simulink Model of Grid Side Controller

In Figure 4-7, the GRC uses voltage-oriented vector control technique. The space vector transformation is used to estimate the reference signal of the controller. The measured value includes: grid current, DC-link bus voltages and stator voltage are used to estimate the controller reference signal. PI controllers are used to control grid dq-axis currents, and DC-link bus voltage. The synchronous reference frame generates the grid reference voltage signal.

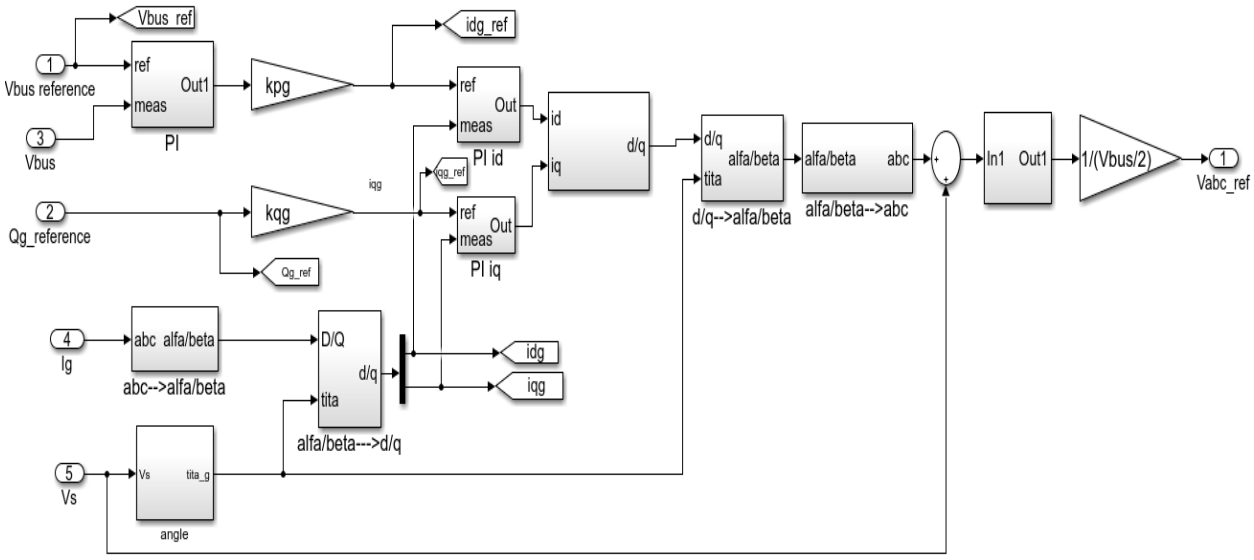

Figure 4-7: Developed Simulink model of GSC.

4.1.2 Simulink Model of STATCOM

STATCOM consists of DC bus capacitor bank, LC lowpass filter, IGBT based VSI coupled to grid through coupling transformer. DC bus capacitor generates the DC input voltage whereas the VSI fabricates the AC voltages using the hysteresis band current control modulation technique. Due to the switching operation of IGBT, the output voltages of VSI is distorted and LC filter eliminates the harmonic distortion to the range of acceptable limit set by IEEE STD 519.

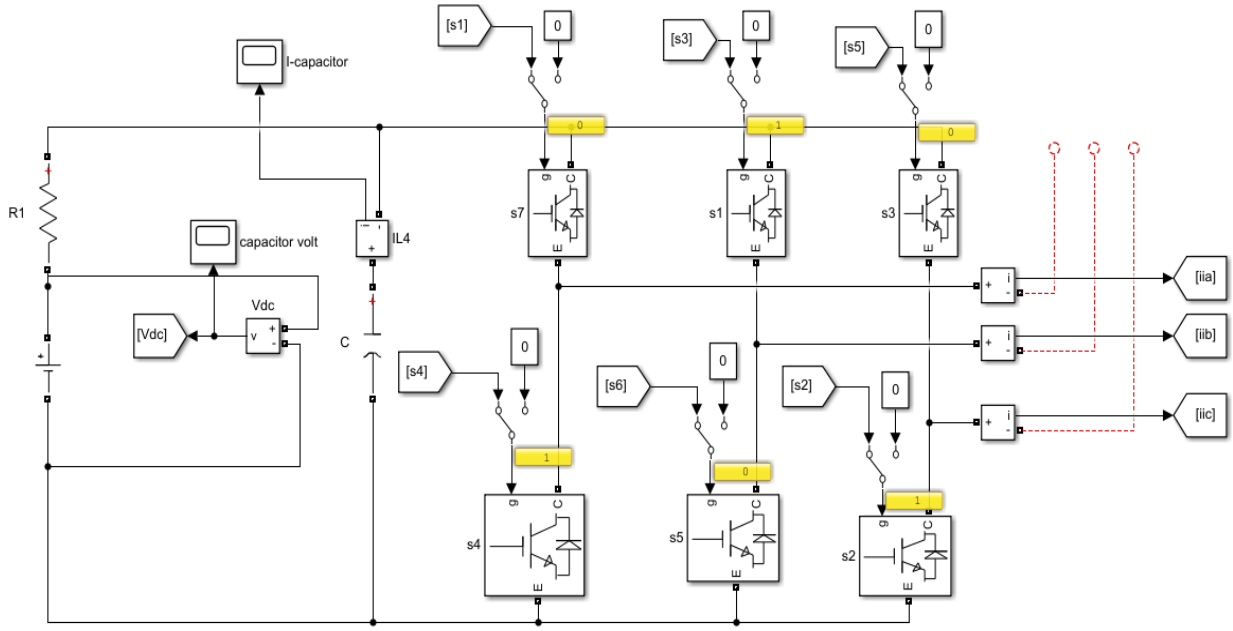

Figure 4-8: Developed Simulink model of STATCOM.

I. Simulink Model of Developed STATCOM Controller

In Figure 4-9, STATCOM is controlled by using the synchronous reference frame technique which decouples the voltages and current of PCC to control them independently and generates the reference current signal. In Figure 4-9, PLL is used to synchronize on the positive sequence component of the three-phase voltage of PCC. The output of the PLL is θ=ωt and it is used to compute the direct-axis and quadrature axis components of the AC (3Φ) currents (Id and Iq). The DC measurement system in Figure 4-9 provides the measurement of the DC voltage Vdc. HCC is used to produce the gate switching pulse signal of VSI.

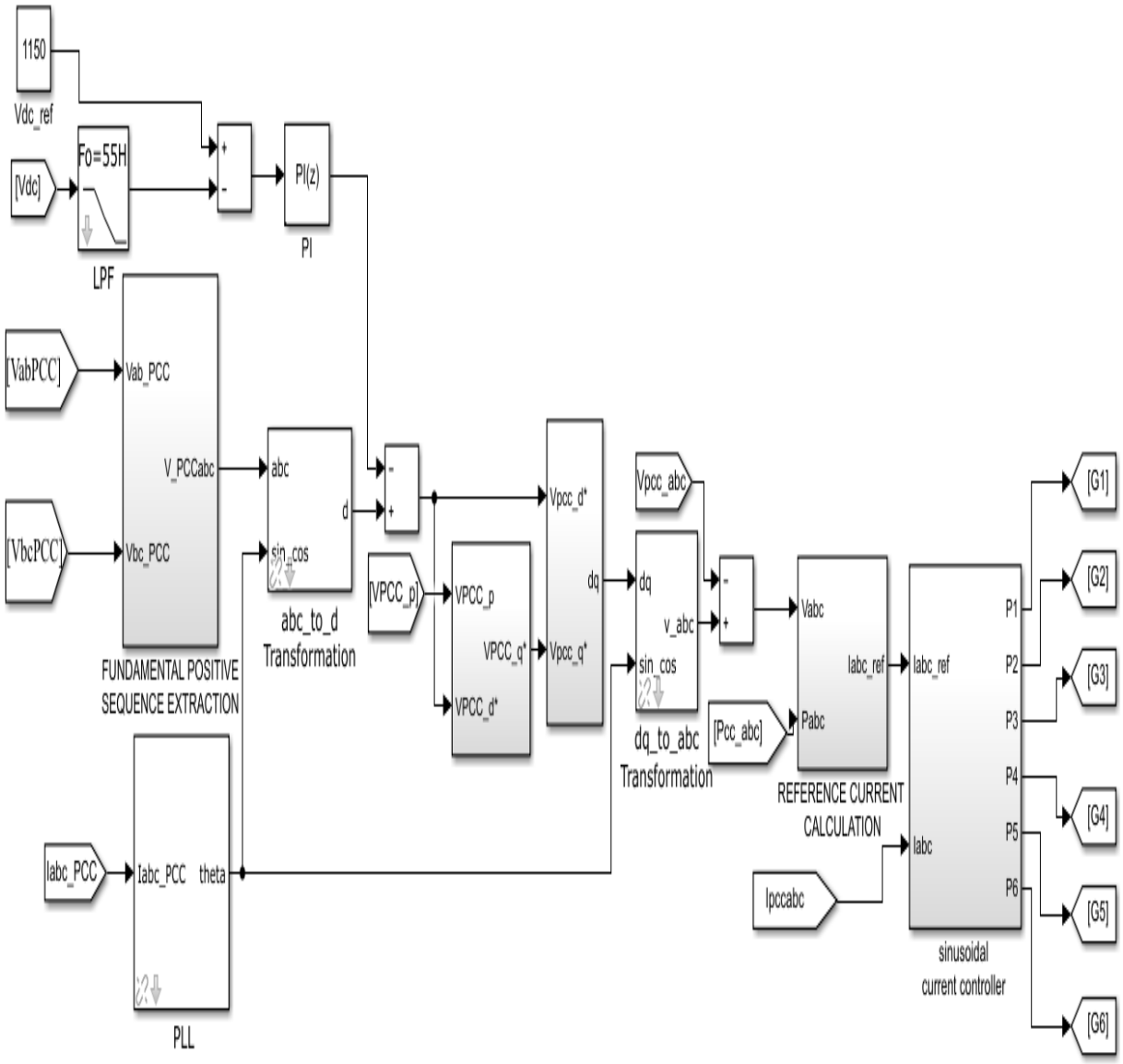

Figure 4-9: Developed Simulink model of STATCOM controller.

II. Simulink Model of HCC of STATCOM

In fig 4-10, it shows the structure of hysteresis current controller where P_1, P_2, P_3, P_4, P_5, P. These switching signals are generating by comparison of actual current as ia, ib, ic. in the respective phase with the reference signal as ia, ref, ib,ref and ic, ref in the respective phase.

In the Figure 4-10, HCC forces the actual current to track the reference current within the hysteresis band. if the actual current signal become beyond the upper hysteresis band during the upper switch of leg A ON, HCC sends a signal to switch OFF the upper switch whereas lower switch become ON. Therefore, the actual current tracks the reference current signal with in the hysteresis band and generates switching pulse signal of VS. Hysteresis band in this study is calculated as 0.05A.

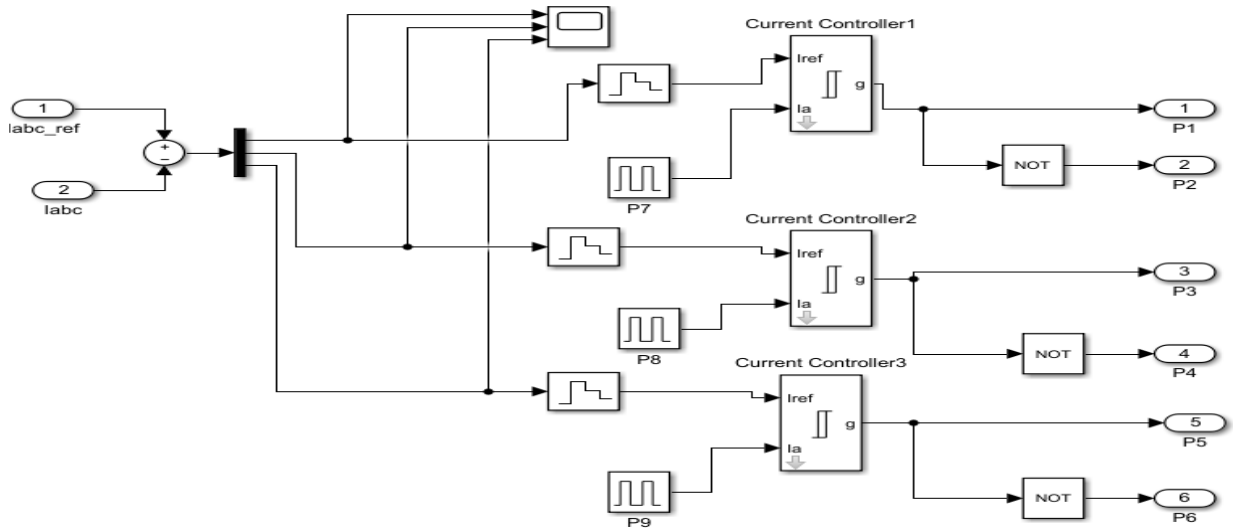

Figure 4-10: Developed Simulink model of HCC.

4.2 Simulation Result of DFIG Wind Turbine

I. Extraction of Maximum Power from Wind Turbine

The power which is available in the wind is not totally transferred into the mechanical input power. According to Albert Betz law, turbine cannot extract all available power in the wind. Turbine only extracts a maximum of 59.3% of power theoretically. However, it only extracts approximately 35%-45% practically.

A variable-speed wind turbine follows the $C_{P,max}$ to capture the maximum power up to the rated speed by varying the rotor speed to keep the system at the optimum TSR, λ_{opt}. Figure 4-11, shows relationship between the wind speed and the power captured by the wind turbine. As shown in the

Figure 4-11 (b), the blades start to move around 4 m/s which is cut-in speed in most cases, and optimal aerodynamic efficiency is achieved up to the rated wind speed, about 11.25 m/s. Between the rated wind speed and cut-out speed, 25 m/s, the power delivered is limited in order to avoid overloading on the wind turbine system. Over the cut-out wind speed, the turbine has to be stopped in order to avoid damages. During the optimal efficiency wind speed range, the wind generator may be adjusted to follow the maximum power point by performing MPPT control for wind turbines.

Figure 4-11 (a) shows the simulation output result of pitch-controlled wind turbine power coefficient versus tip speed ratio curve. Among all curves, the desired one is the point where pitch angle (β) is found to be zero degree whereas $C_{P,max}$ is 0.44 with the corresponding λ_{opt} is 7.2 so that the turbine can extract the maximum power.

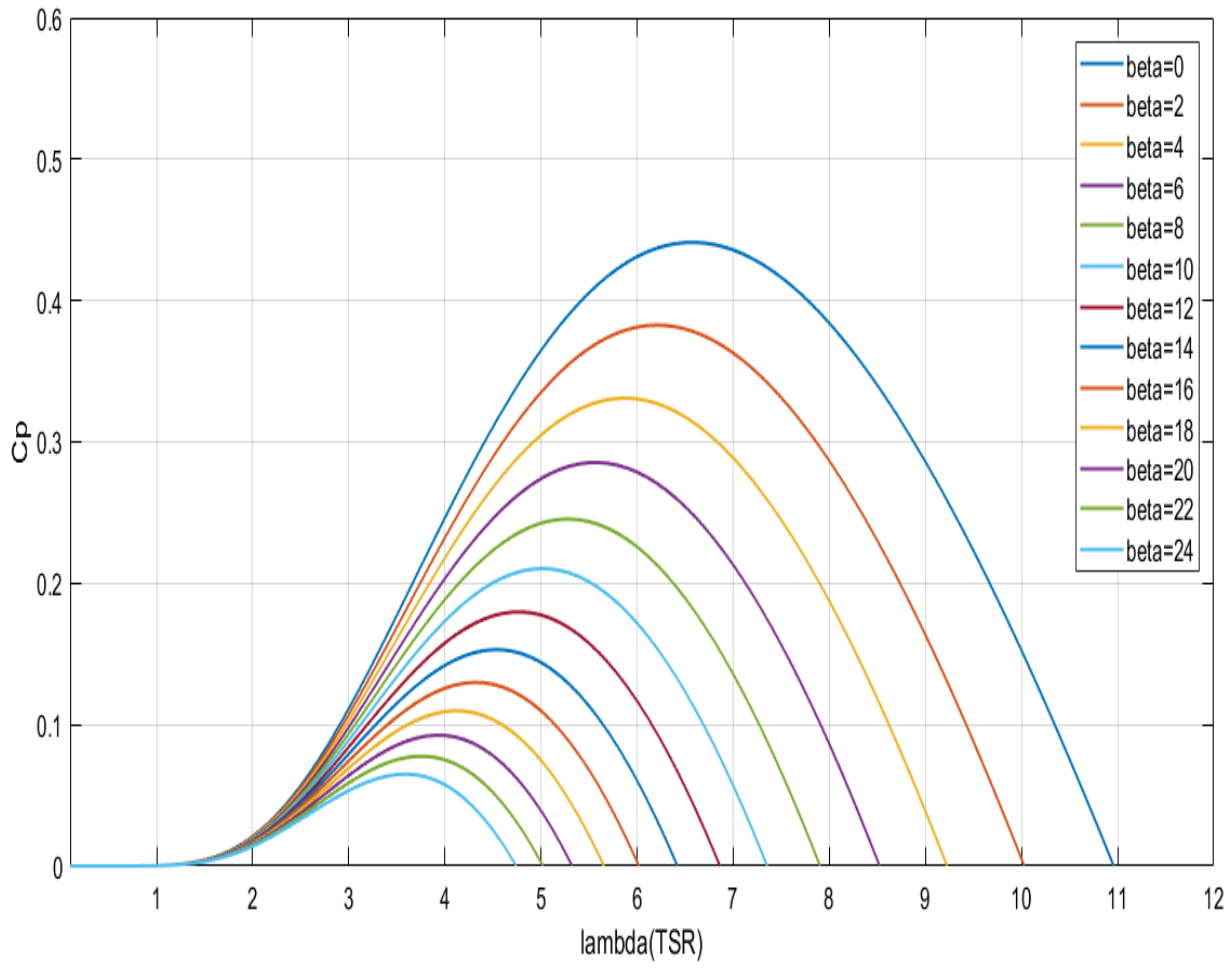

Figure 4-11: Cp Vs λ output at different pitch angle β.

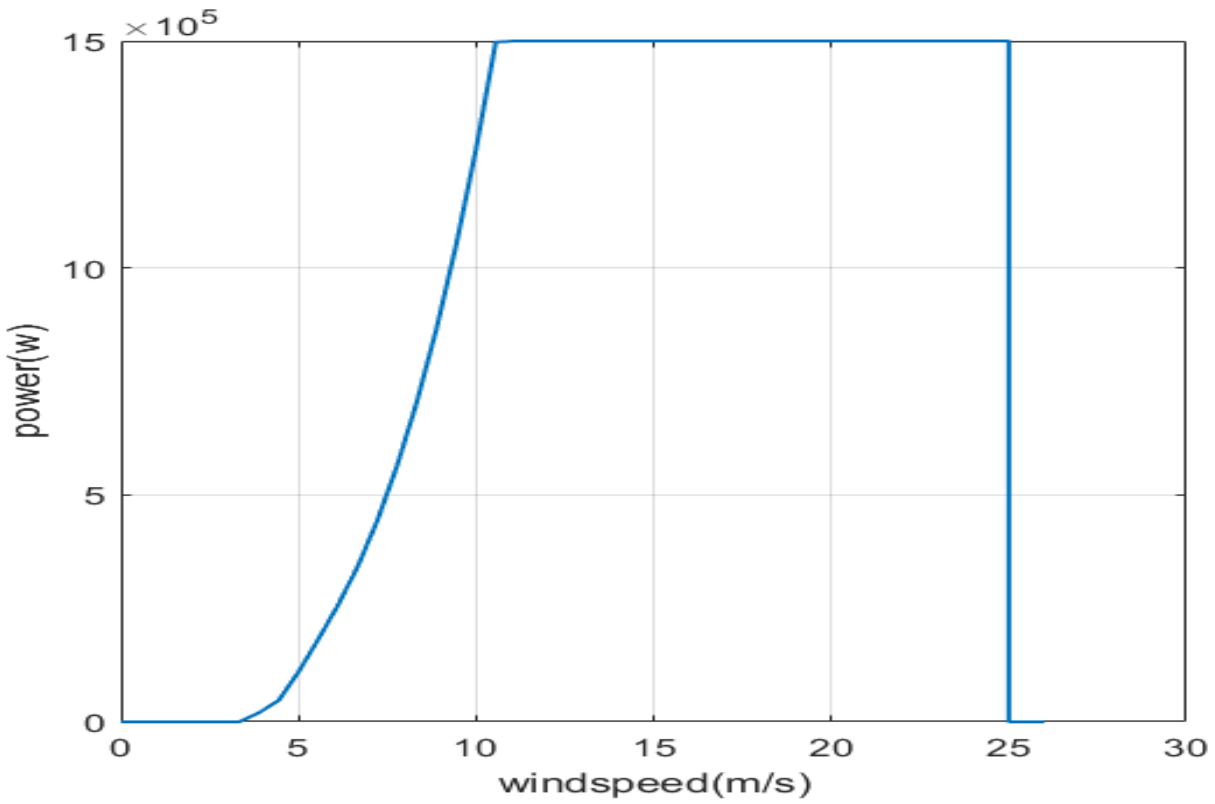

Figure 4-12: Wind power vs wind speed curve.

II. Power Curve

Figure 4-13 shows DFIG can operate at one of the four working mode: Parking, maximum power point tracking, constant power output and the stalling mode. At parking mode, the wind speed is relatively low, i.e. the rotor speed is below the cut-in speed (3.5m/s), which cannot able to generate power. Below the cut-in wind speed 3.5m/s, the power in the wind is too low for useful energy production and so the wind turbine remains shut down. The maximum power point tracking mode is applied to ensure a maximum power conversion efficiency of the wind energy conversion system, when the input wind speed is between 3.5 m/s and 11.25 m/s. At higher wind speeds but below the rated wind speed, the wind turbine power output increases due to a cubic relationship with wind speed. When the speed is greater than 11.25 m/s and below cut-off speed, the power generated reaches the rated output power of the machine. In this case, the wind energy conversion system works in constant power output mode. Under severe weather conditions such as high wind season, the wind speed can be faster than the cut-off speed; the wind energy conversion system enters the stalling mode. In this case, there is no electrical power output, and the generator stops working.

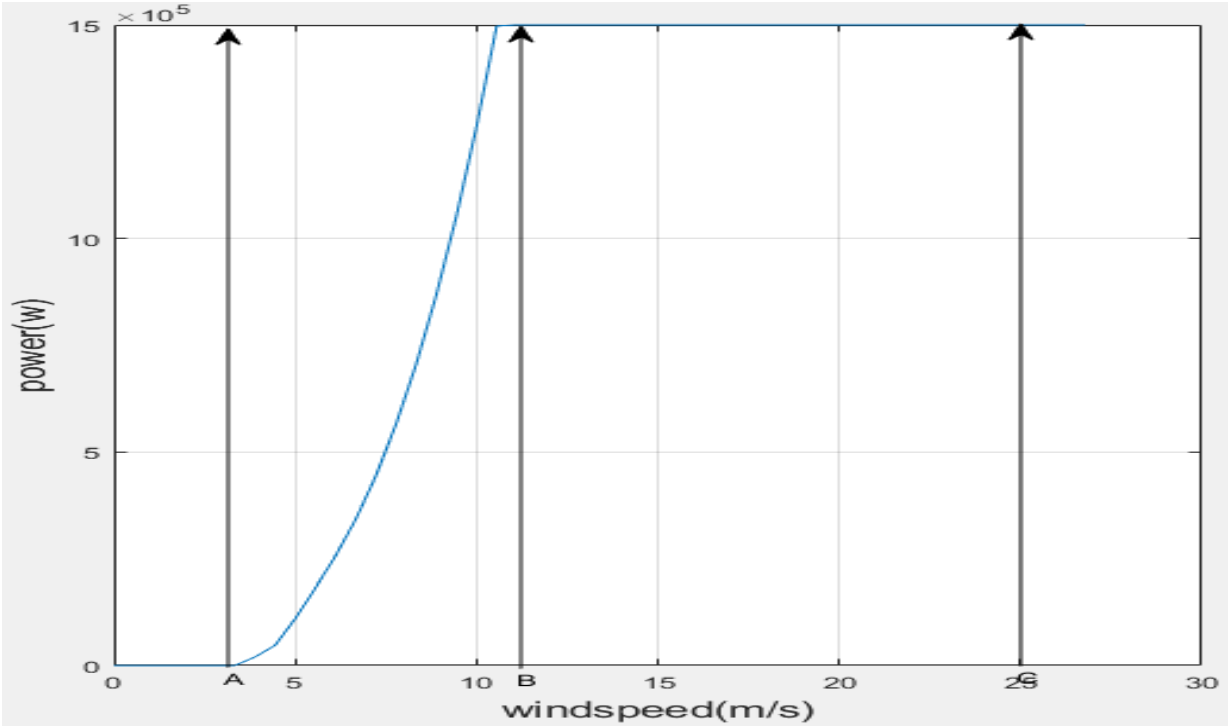

Figure 4-13: Power curve output at different wind speed range.

Figure 4-14 shows wind power can be expressed in terms of turbine torque i.e. aerodynamic torque is obtained from the power received and the speed of rotation of the turbine.

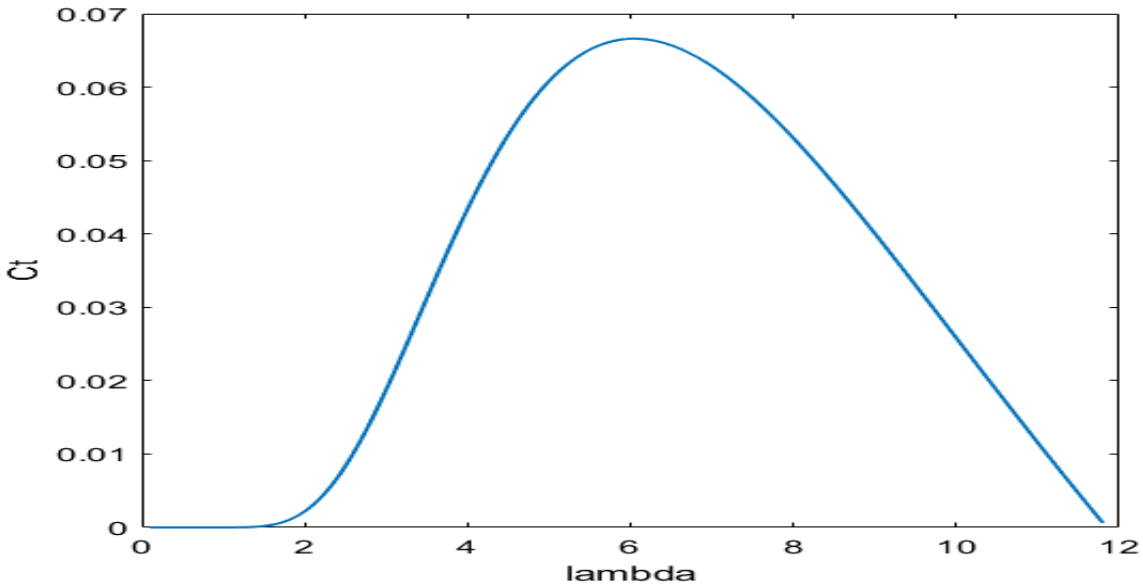

Figure 4-14: C_t Vs λ output curve.

Figure 4-15 shows power curve during pitch angle is zero which indicates the maximum power is captured at this point on curve.

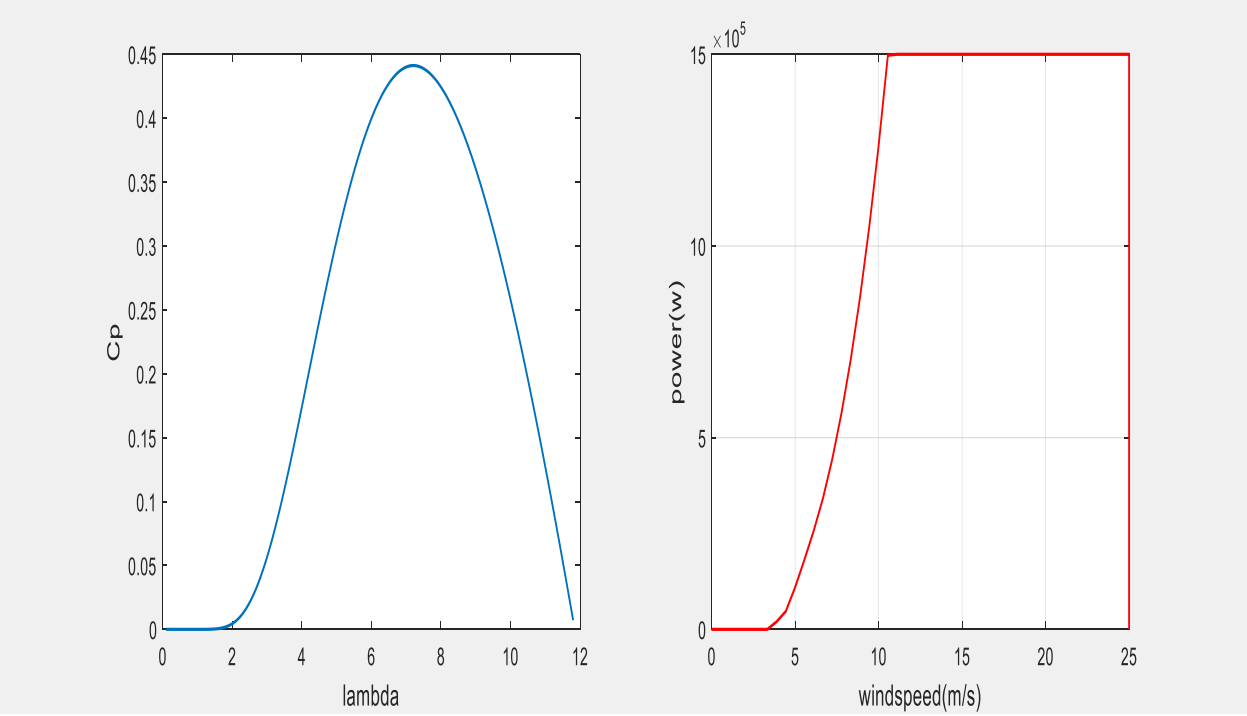

Figure 4-15: Power curve of DFIG.

Figures 4-16 and 4-17 shows the Sany Electric Ltd, manufacture given curve of SE77/15 DFIG wind turbine.

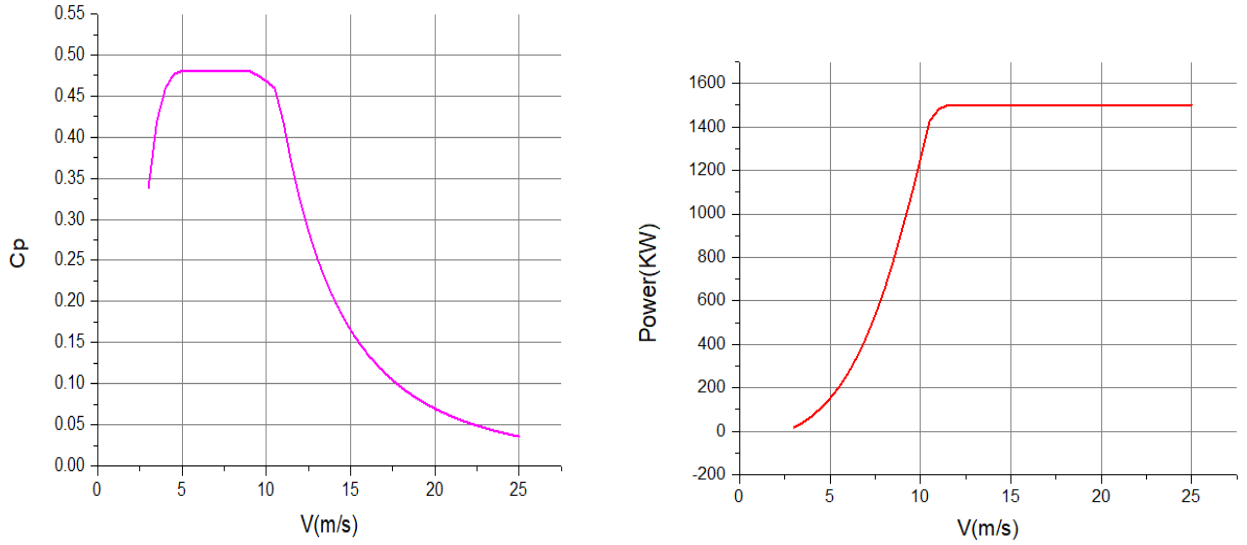

Figure 4-16: Manufacturer: (a) Cp Vs wind speed curve (b) power Vs wind speed curve.

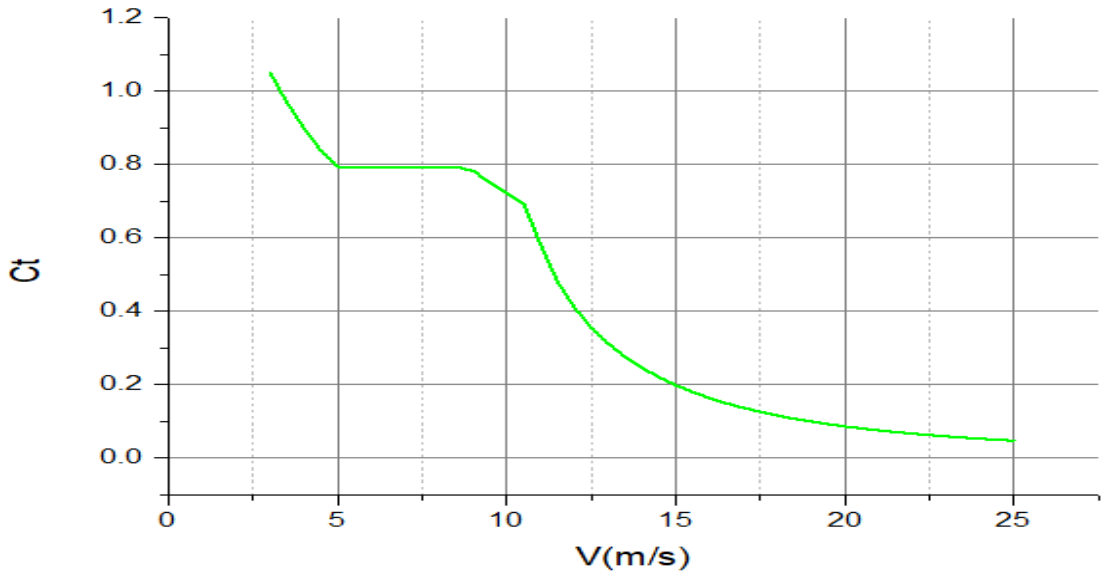

Figure 4-17: Manufacturer Ct Vs wind speed curve.

4.2.1 Dynamic Analysis of Adama II DFIG Wind Turbine

I. Rotor Side Controller Analysis

The equation that relates ω_s (frequency of stator voltages and currents), ω_r (frequency of rotor voltages and currents) and ω_m (rotor electrical speed) is as follows:

$$\omega_s = \omega_r + \omega_m$$

The relation between the mechanical speed of the shaft Ω_m and the electrical speed depends on the pole pairs of the machine:

$$\omega_m = \rho\Omega_m$$

The units of these two equations are given in rad/s. The slip s of the machine is defined as follows:

$$s = \frac{w_s - w_m}{w_s} = \frac{w_r}{w_s}$$

In this case, the stator windings are directly connected to the grid and thus, ω_s is constant. This frequency is also known as the synchronous frequency.

However, ω_r obviously depends on the shaft's electrical speed ω_m, which leads to three operating modes of the machine dependent on the speed:

$\omega_m < \omega_s \Rightarrow \omega_r > 0 \Rightarrow s > 0 \Rightarrow$Sub synchronous operation

$$s = \frac{157.0796 - 141.3717}{157.0796} = 0.1$$

Figure 4-18 shows the results of the DFIG is operating at sub synchronous speed of 141.37rad/sec of mechanical speed. As shown in the Figure 4-18, the DFIG is oscillating up to approximately 1second due to its startup problem. This start up is not properly made in terms of reality but for sake of simplicity we have avoided this startup methods. The stator voltage and current are sinusoidal and have synchronous angular frequency of 50Hz. The rotor voltage and current are different from synchronous angular frequency. The rotor dq current is at synchronous references frame is constant as PI controller of current loops requires the constant quantity at steady state.

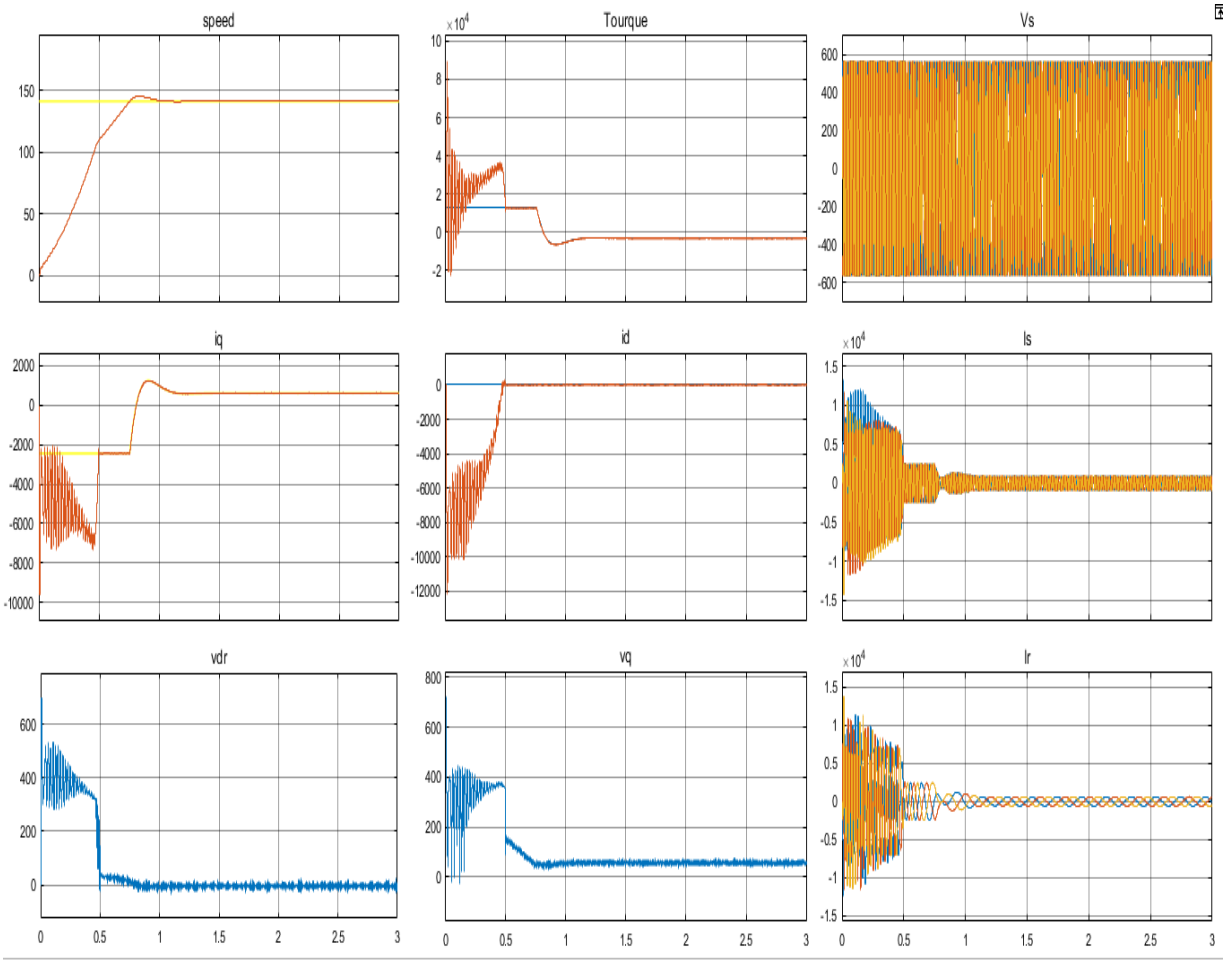

Figure 4-18: DFIG parameters operating characteristics at sub-synchronous speed.

In Figure 4-19 (a) rotor mechanical speed is gradually increases and reaches to the steady state value of 141.37 rad/sec and come to the reference value. In this case the DFIG is operating below the synchronous speed called sub synchronous speed.

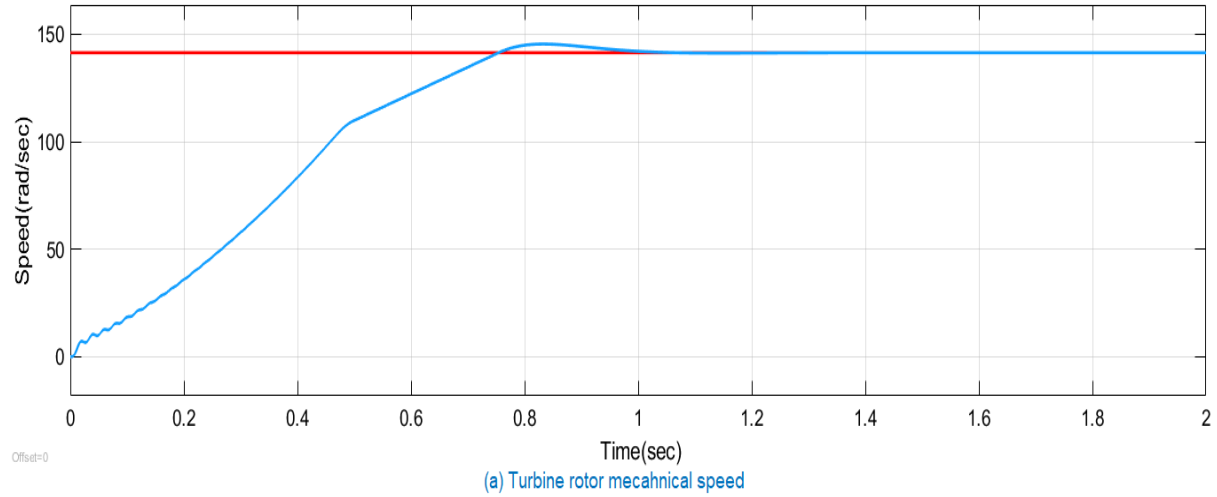

(a) Turbine rotor mecahnical speed

In Figure 4-19 (b) rotor q-axis current varies correspondingly with turbine electromagnetic torque. In stator flux vector control technique of RSC, adjustment of the rotor q-axis current controls the generator torque or stator active power of the DFIG.

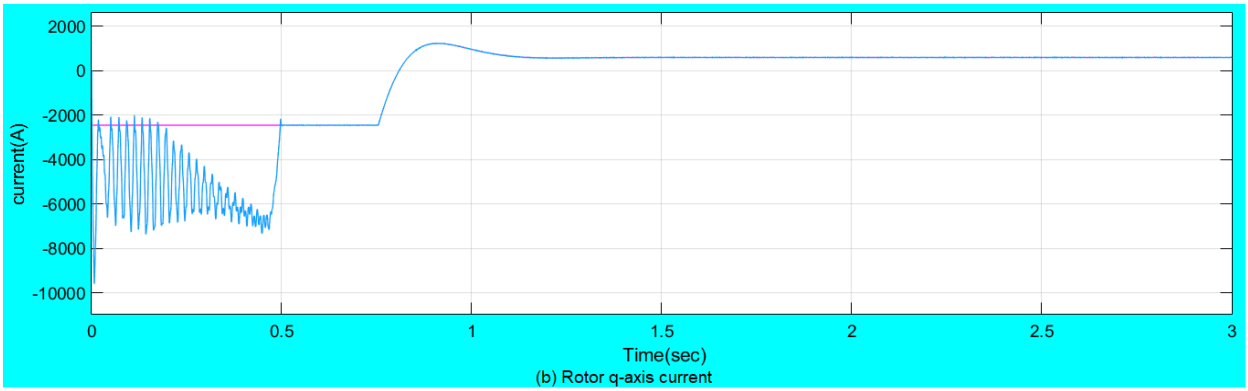

(b) Rotor q-axis current

In Figure 4-19 (c) rotor d-axis reference current is zero; which shows that DFIG is magnetizing through the stator. In stator flux vector control technique of RSC, adjustment of the rotor d-axis current controls the reactive power of the DFIG.

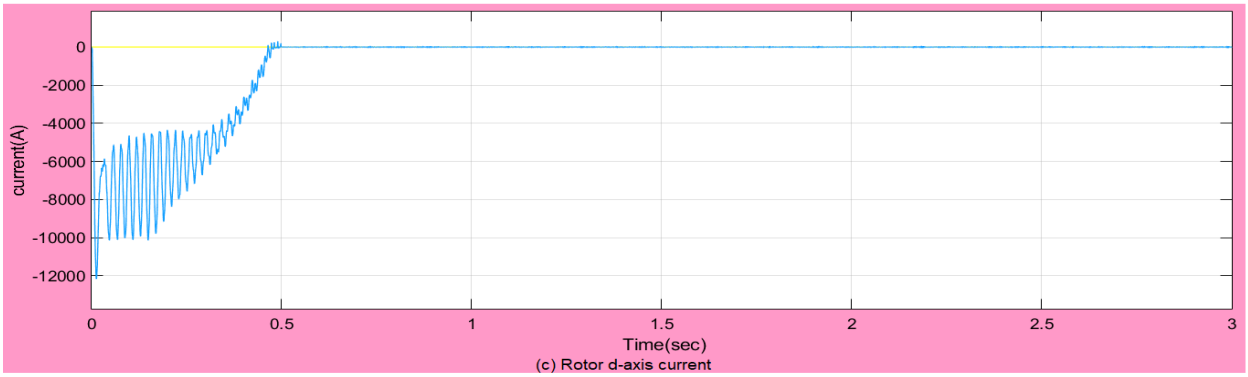

(c) Rotor d-axis current

Therefore, in Figure 4-19 (b) and (c) the rotor reference current is presented with real and imaginary constant values which are used for PI regulator. The id_r is proportional to the stator reactive power and iq_r is proportional to stator torque or active power hence it is used to control the active and reactive power independently.

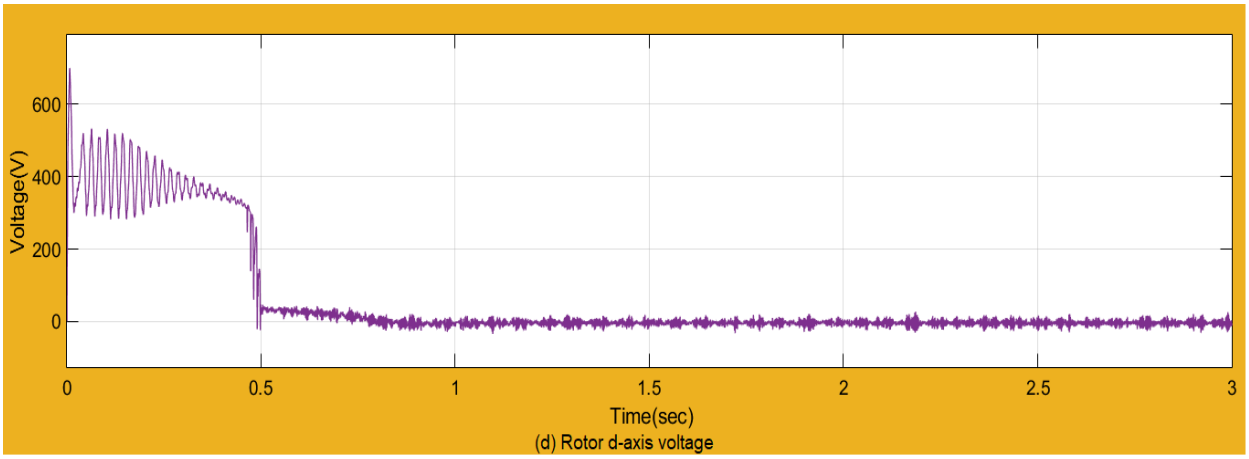

(d) Rotor d-axis voltage

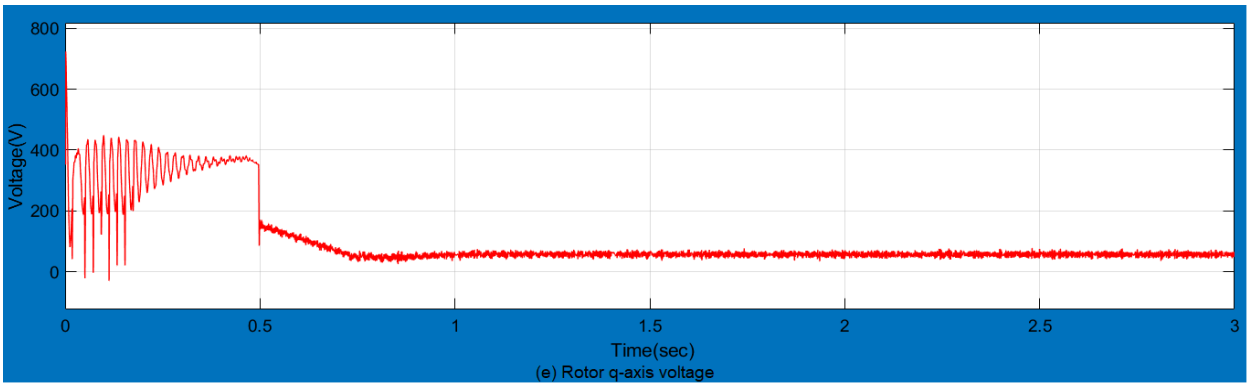

(e) Rotor q-axis voltage

In Figure 4-19 (f) negative sign of the torque indicates that DFIG operating as a generator. The measured value of the torque achieves its reference at steady state.

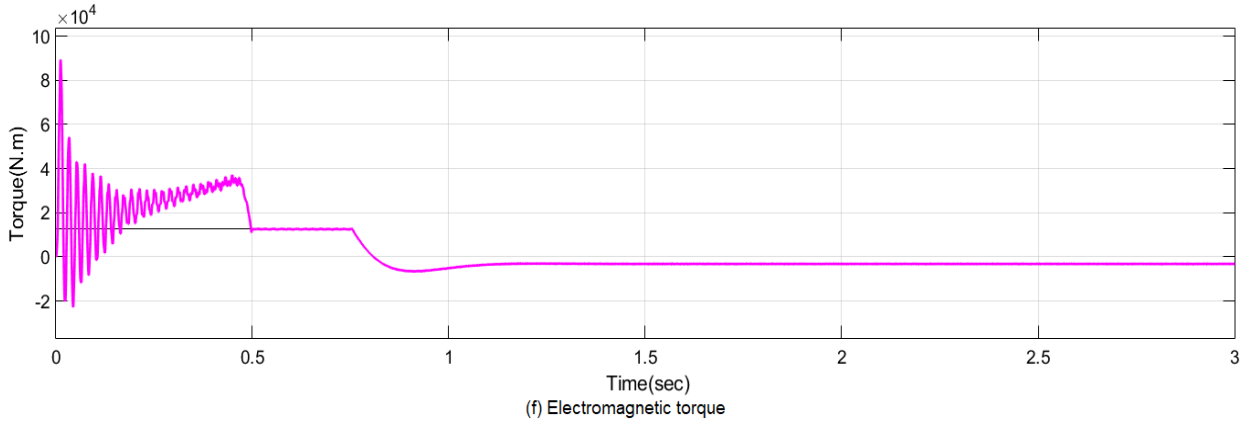

(f) Electromagnetic torque

In Figure 4-19 (f) and (g) stator is supplied by three-phase voltages directly from the grid at constant amplitude and frequency, creating the stator magnetic field. The stator windings are directly connected to the grid and thus, ω_s is constant i.e. 50Hz. The peak value of terminal voltage of DFIG is 563.39V. Thus, the stator voltage and current have the same magnitude and frequency with the grid.

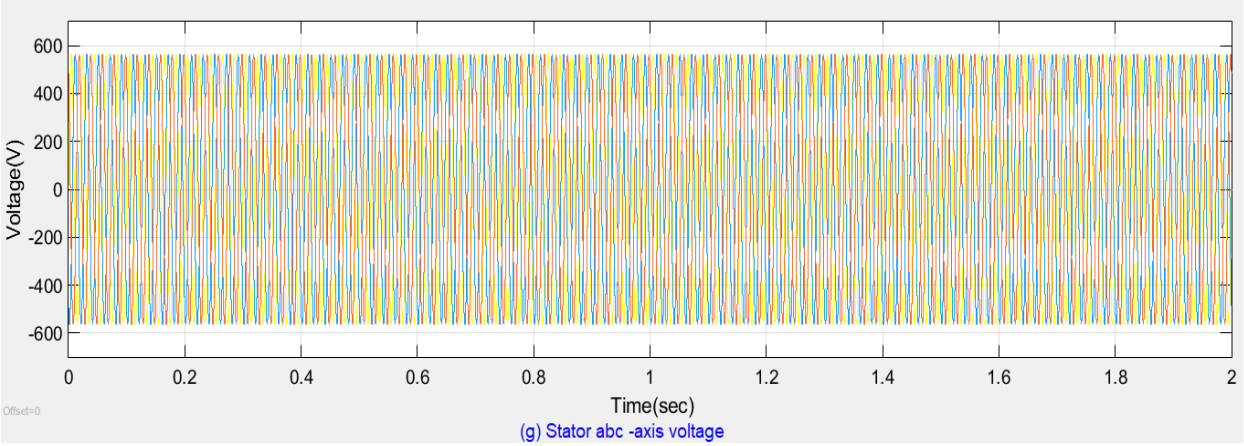

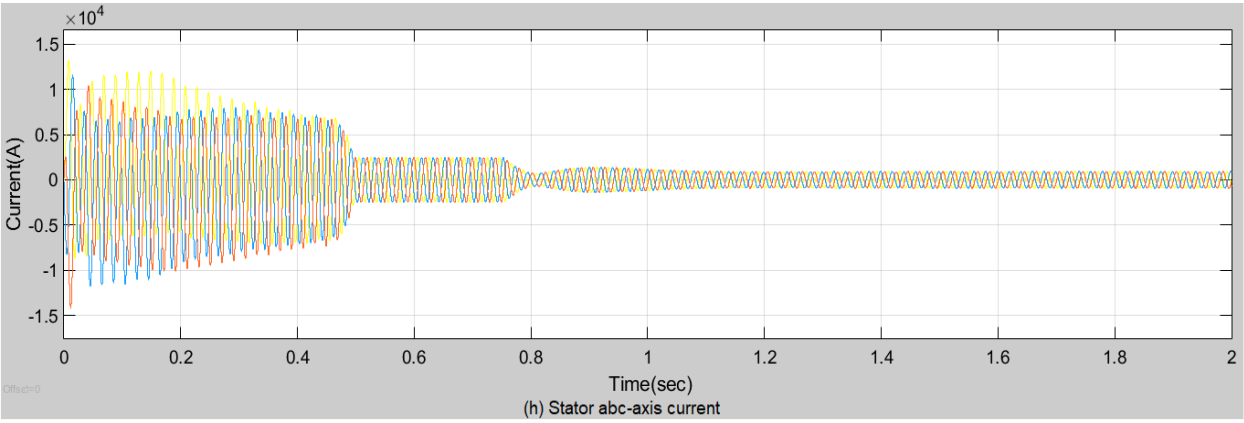

Figure 4-19 (i) shows rotor abc-axis current wave form.

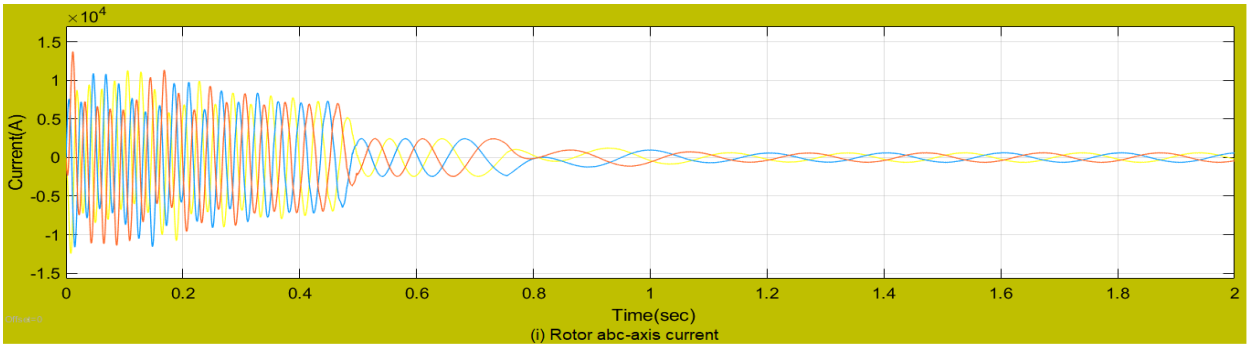

Figure 4-19: RSC parameters operating at sub synchronous speed.

Figured 4-20 and 4-21 shows the zoomed wave form of the stator voltage in abc-axis reference frame.

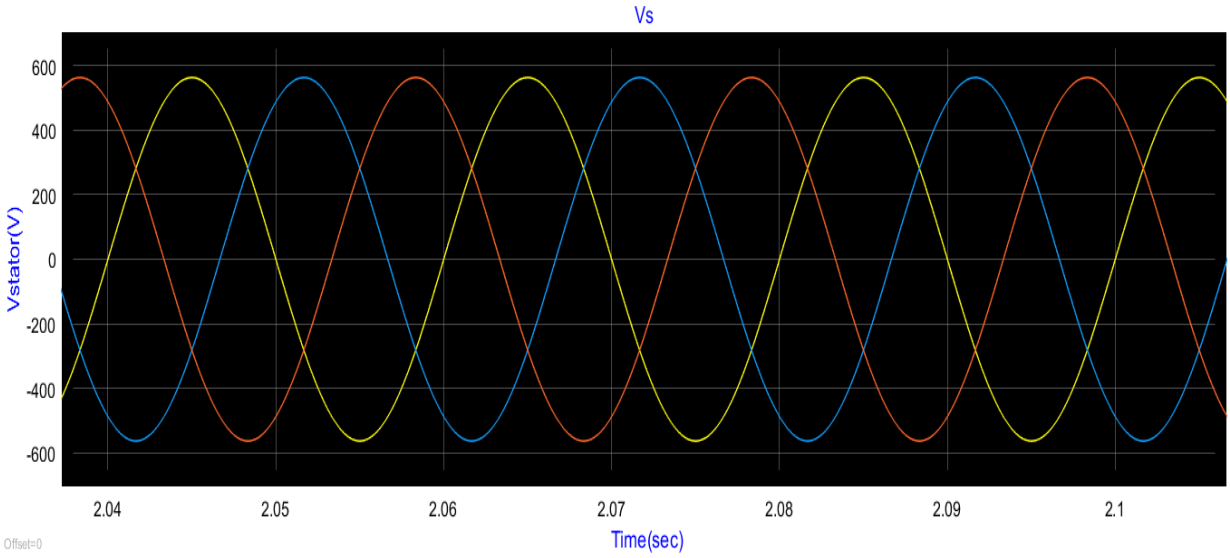

Figure 4-20: Stator voltage of DFIG wind turbine at abc reference frame.

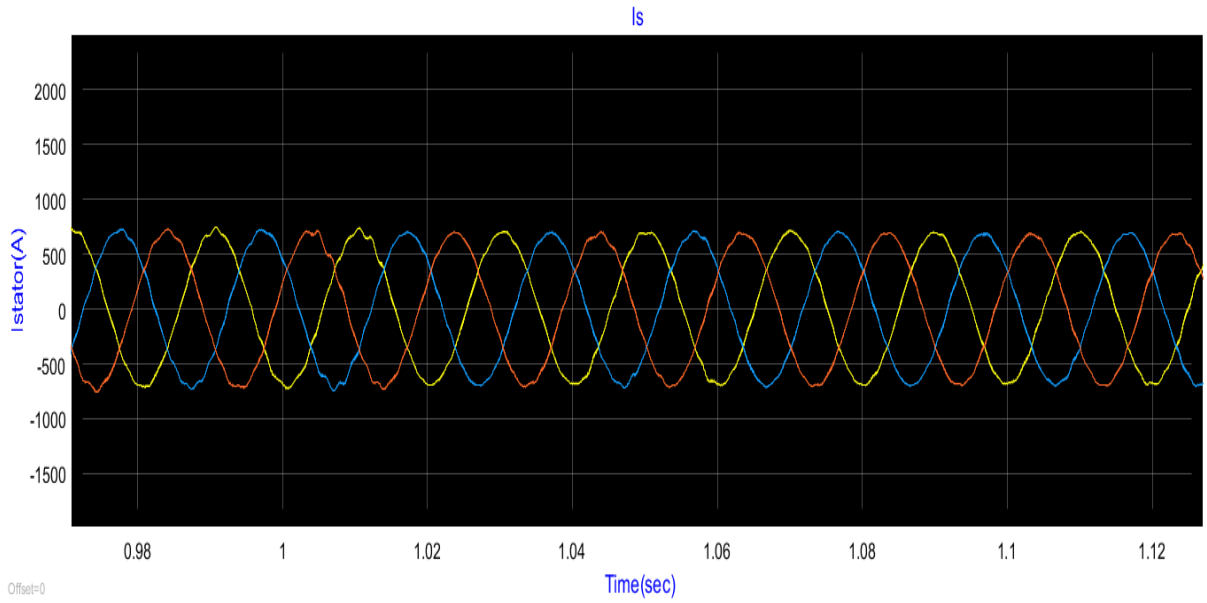

Figure 4-21: Stator current of DFIG wind turbine at abc reference frame.

Figure 4-22 shows that rotor winding of DFIG is also supplied by three-phase voltages but it takes a different amplitude and frequency at steady state.

$$s = \frac{w_r}{w_s}, \qquad w_r = sw_s$$

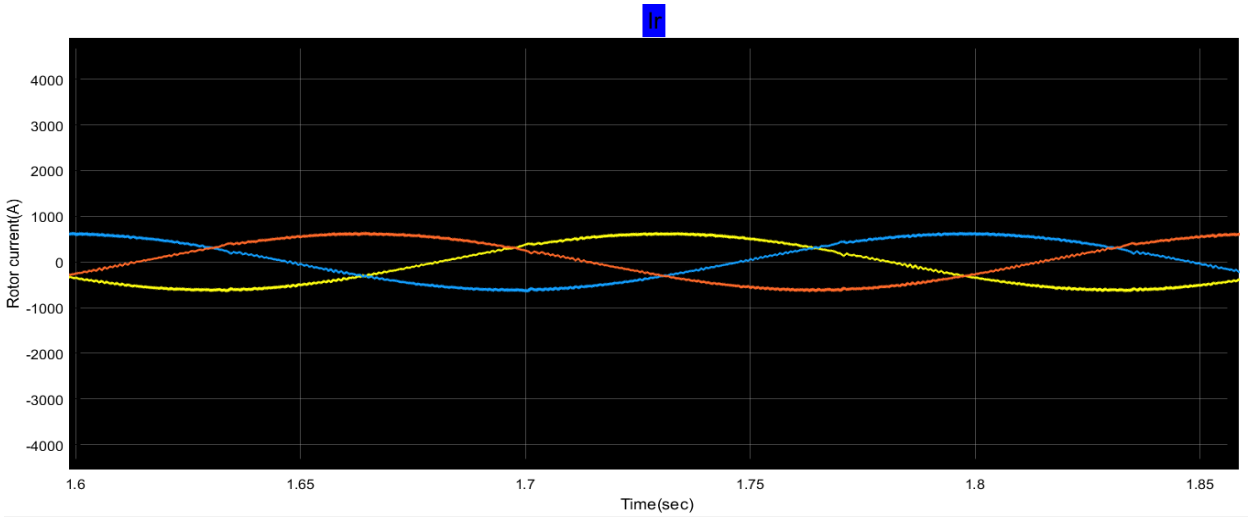

Figure 4-22: Rotor current of DFIG wind turbine at abc reference frame.

$\boldsymbol{\omega_m = \omega_s \Rightarrow \omega_r = 0 \Rightarrow s = 0}$ **⇒Synchronous operation**

Figure 4-23 shows that DFIG is operating at synchronous speed and we see that rotor current are almost DC, they are not sinusoidal.

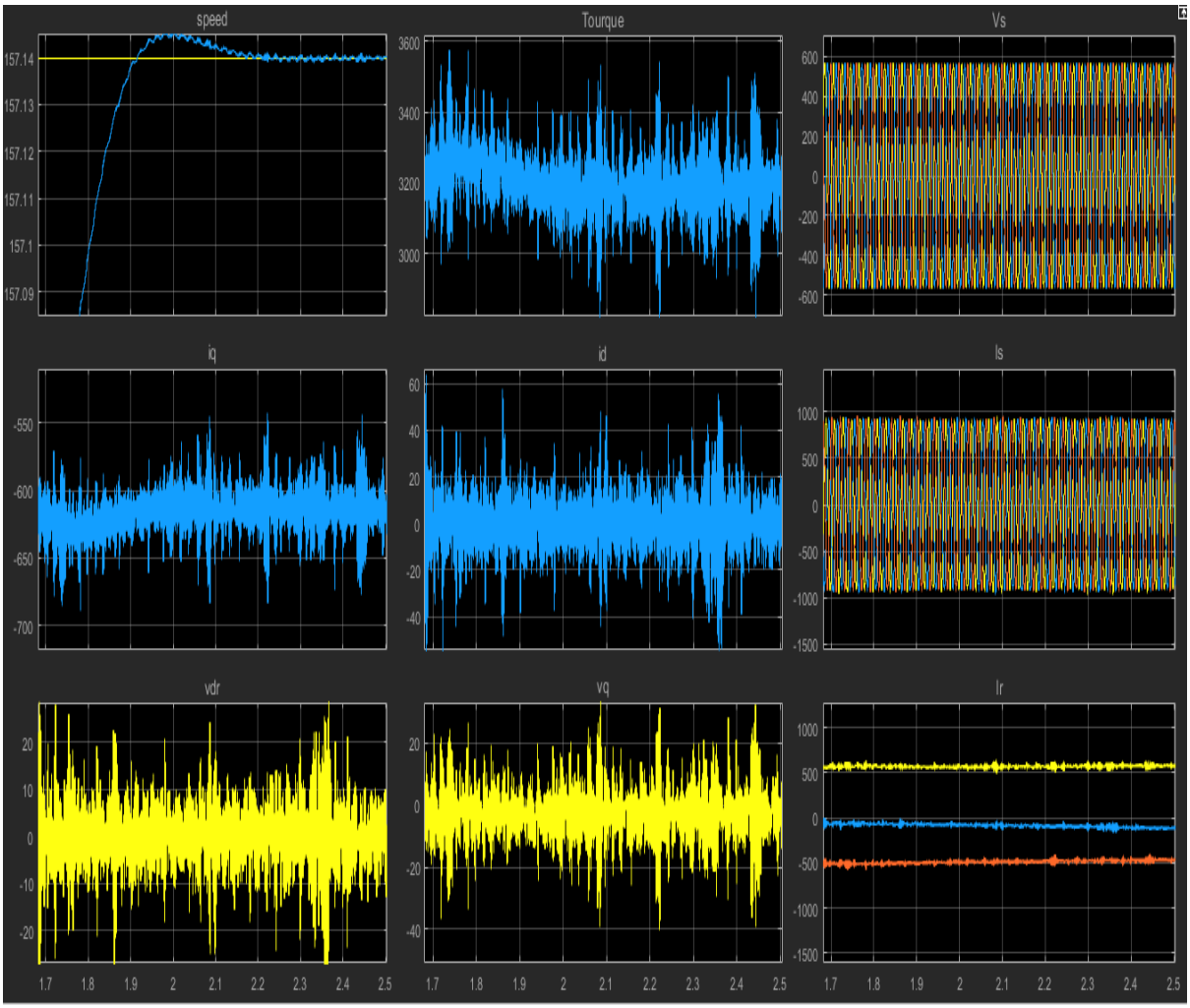

Figure 4-23: DFIG parameters operating characteristics at synchronous speed.

Figure 4-24 shows that the DFIG is operating at synchronous speed. In this mode the rotor current at abc reference frame is constant i.e. it has a DC wave form.

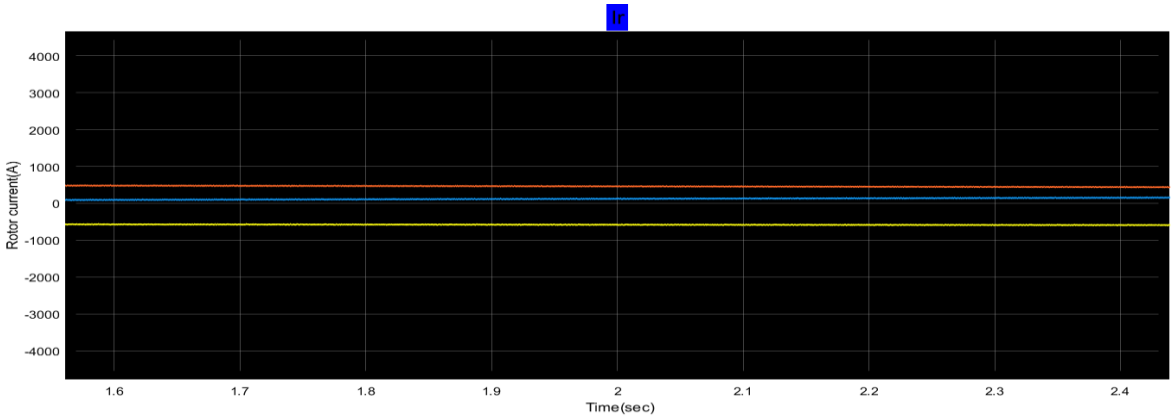

Figure 4-24: Rotor abc-axis current characteristics.

$\omega_m > \omega_s \Rightarrow \omega_r < 0 \Rightarrow s < 0 \Rightarrow$**Hyper synchronous operation**

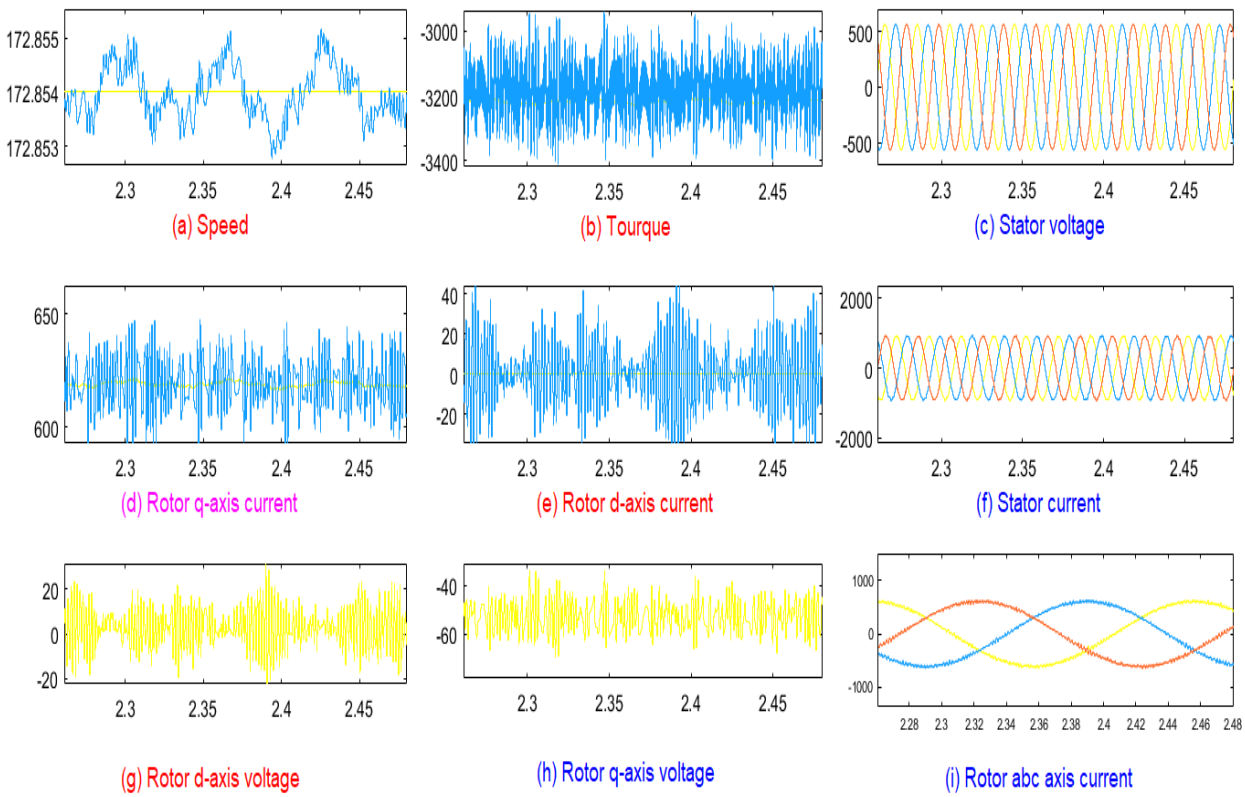

Figure 4-25: DFIG parameters operating characteristics at hypersynchronous speed.

Figure 4-26 shows that the stator currents are operating at different speed i.e. at sub synchronous, synchronous and Hyper synchronous speed operation.

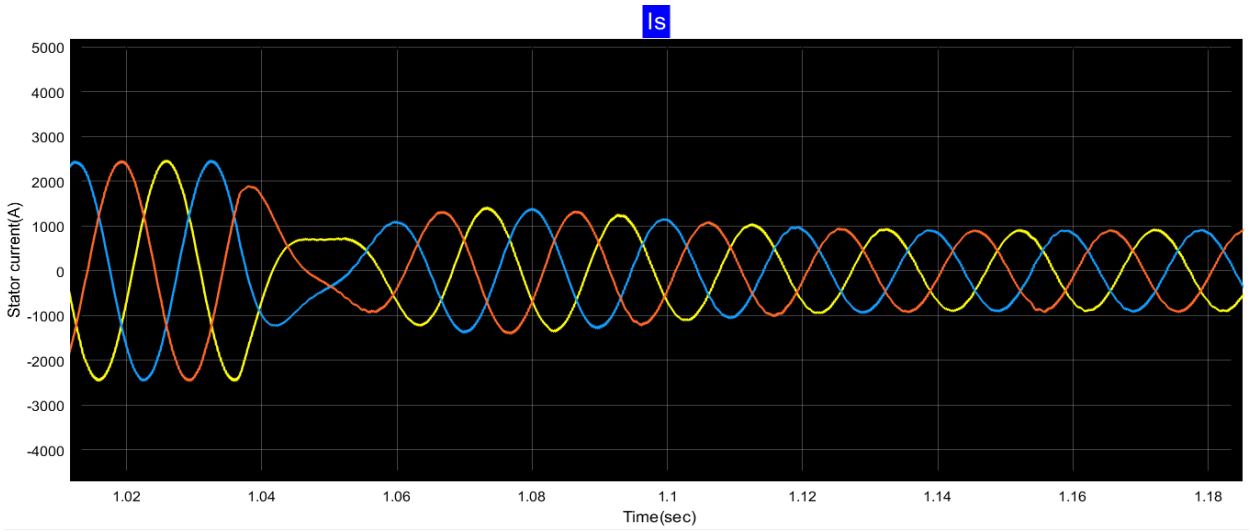

Figure 4-26: Stator abc-axis current characteristics.

The Figure 4-27 shows that the rotor currents are operating at different speed i.e. at sub synchronous, synchronous and Hyper synchronous speed operation. At sub-synchronous speed rotor current is abc positive sequence whereas at Hyper synchronous rotor current is acb negative sequence.

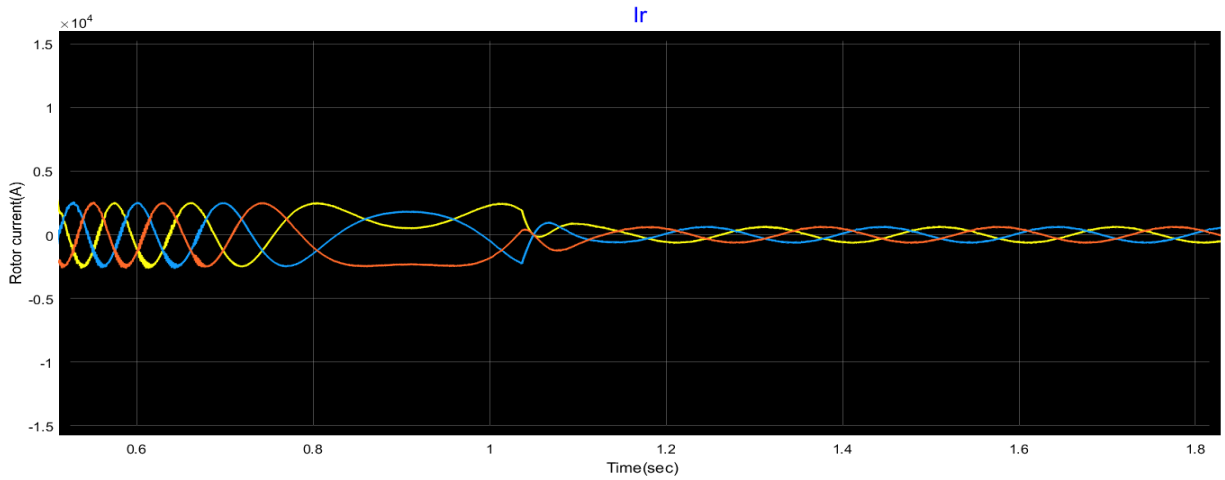

Figure 4-27: Rotor abc-axis current.

Discussion

We have the speed variation that have performed at the reference therefor the actual speed is also varying. We have the torque that has been modified accordingly, therefore the iq_r is has been modified accordingly to the torque, that will be iq_r the voltage reference accordingly to more less this iq_r variations. For id_r, we have maintained all the time zero therefore the voltage reference has been also more less zero, the stator currents and rotor have been like as seen in Figure 4-28. For instance, here we have sub synchronous operations because we have at lower than the synchronous speed therefore, we have abc sequence of stator and rotor currents. The figure 4-28 shows that we were almost at synchronous speed after a few seconds and we have dc currents. Then we have finally reached to hyper synchronous operations again after a few seconds later therefore we have again abc sequence. The Figure 4-28 shows us we have seen abc reference frame and it shows the stator currents and voltages are at 50Hz whereas the rotor voltages and currents are at sw_s of frequency. This are current loop performances and this is how accurate can we achieve speed control, currents loop control and the currency of the torque. we have already implemented the DFIG control and we have made a machine to operate at different operating points.

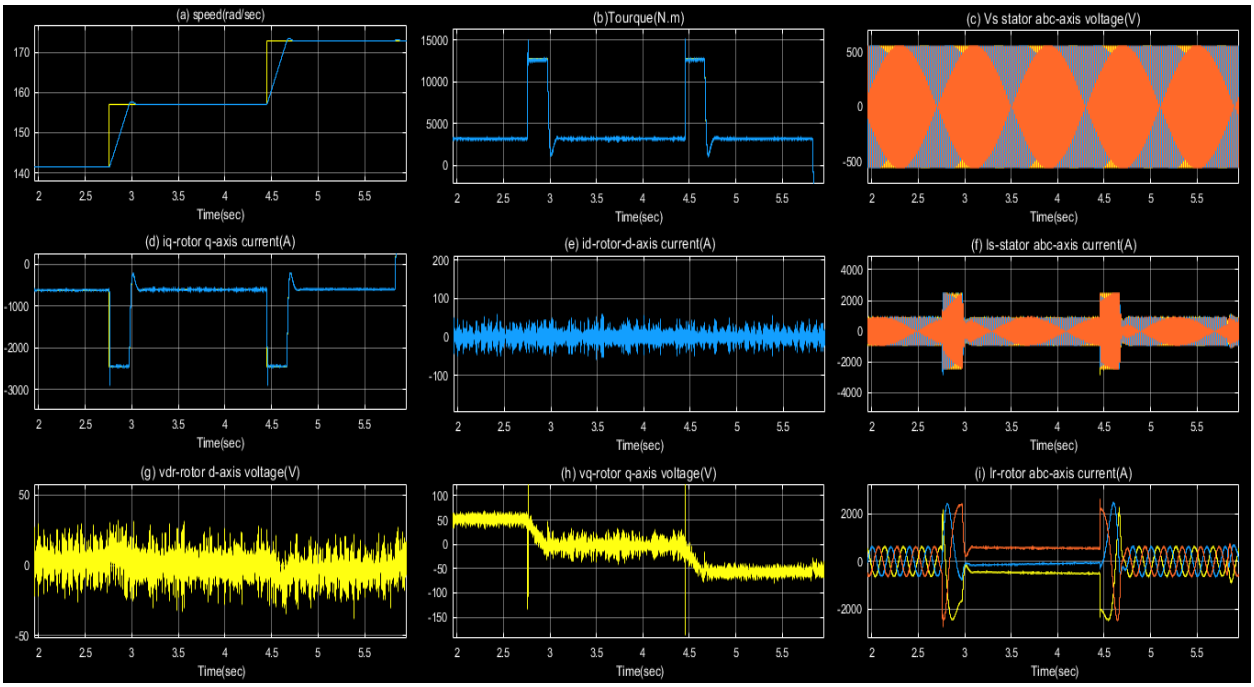

Figure 4-28: DFIG operates at different speed range.

The simulation results of the rotor side convertor control using the vector control strategy of stator flux oriented at synchronous reference frame is implemented. The results show that the direct rotor current is proportional to the stator reactive power, and that the quadrature rotor current is proportional to the torque or active stator power. Therefore, the current loop control and the speed control of rotor side converter is achieved.

At synchronous speed, the magnetic field of the rotor rotates at the same speed as the stator magnetic field. The DFIG then operates as asynchronous machine with DC current in rotor windings such that the rotor power is zero and therefore all active power from the DFIG will flow from the stator of the machine to the grid. When the wind speed enhances gradually, the speed of the rotor increases beyond synchronous speed, which causes a negative slip and super synchronous operation. In this case, power flows to the grid from both the stator windings and the rotor windings. As the wind speed decreases, the rotor speed also decreases and the machine operates in sub- synchronous mode with positive slip. Rotor absorbs active power from the grid such that it consumes power for rotor winding excitation. Hence as a generator, DFIG delivers power at constant voltage and constant frequency through stator, while rotor is supplied through a static power converter at variable voltage and variable frequency. The rotor part of the machine may absorb or deliver electric power.

II. Grid Side Controller Analysis

Figure 4-29 shows the performance of grid side converter parameters. The voltage-oriented vector control technique is used to control the GSC of DFIG. Grid id_g -current axis used to control DC bus voltage whereas iq_g used to control the reactive power. The main role of GRC is to maintain constant DC bus voltage.

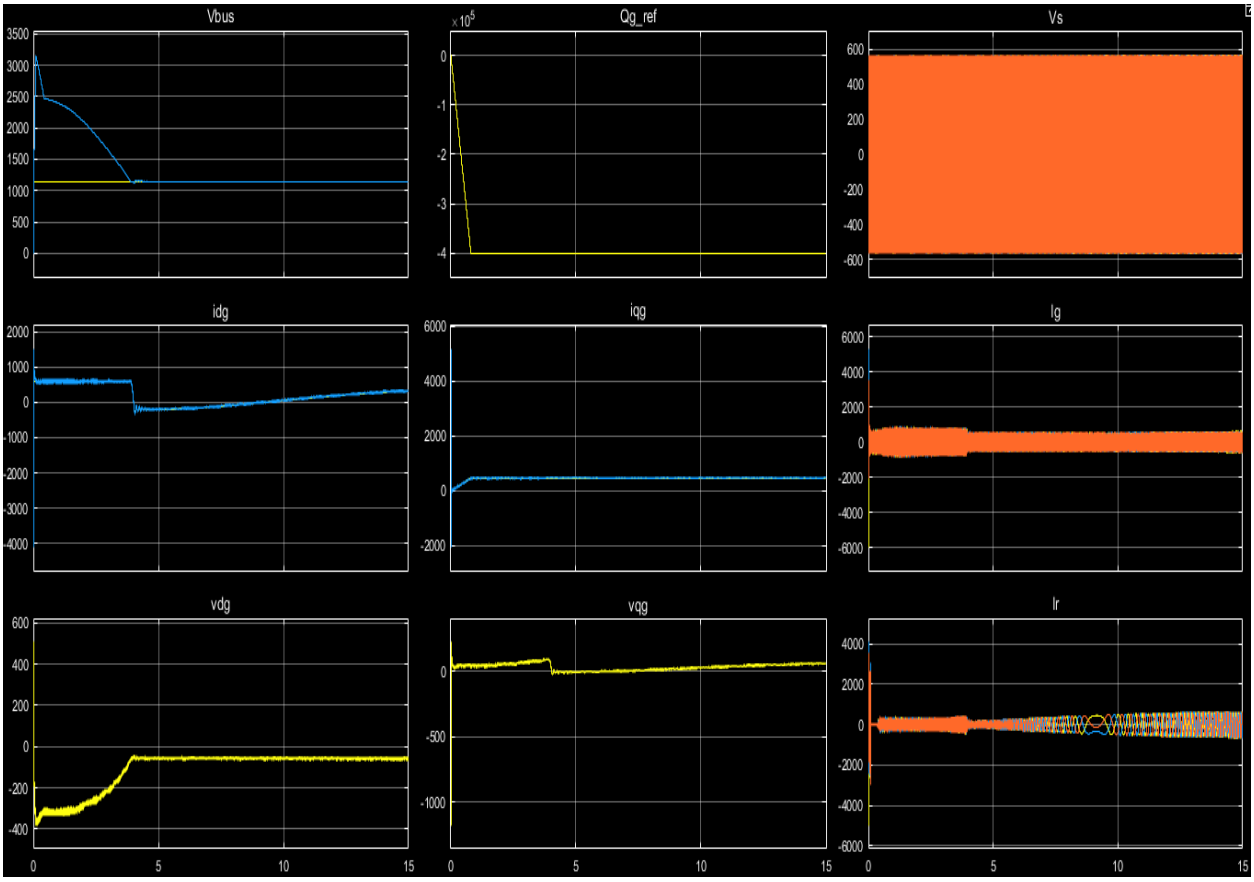

Figure 4-29: Simulink model of GSC.

Figure 4-30 shows the injected current wave form.

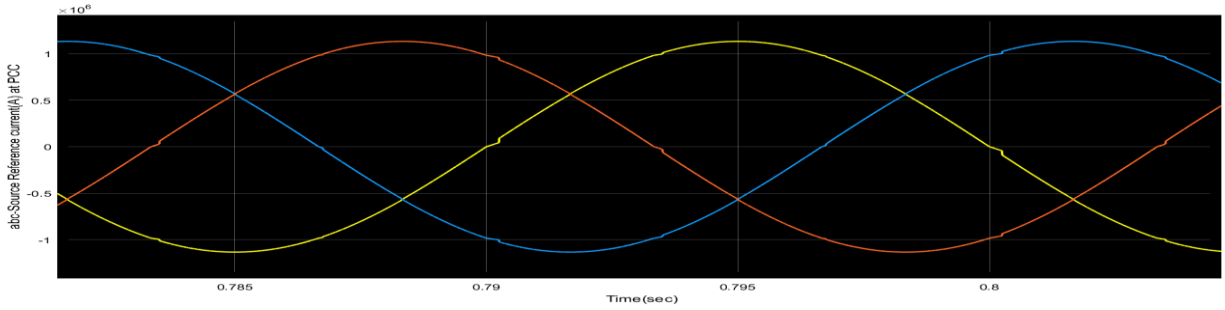

Figure 4-30: STATCOM compensating current.

Figure 4-31 shows the gating pulse signal generated by using hysteresis current control technique. The gate pulses are given to three phase two-level VSC in order STATCOM get in to operation. The signal commands the switching ON/OFF IGBT switch of the six-pulse VSI leg of STATCOM complimentarily. That means, when G_1 ON G_4 will be OFF for leg A (phase A) and similarly the same for other legs(phases). The conduction mode(period) of each switches of the VSC leg is 180^0(0.01sec). So, these switching gate pulses G_1, G_2, G_3, G_4, G_5 and G_6 are given to the voltage source inverter that will produce reactive current to compensate the harmonic and voltage dip produced due both back-to-back VSC of DFIG/nonlinear and linear/nonlinear loads respectively.

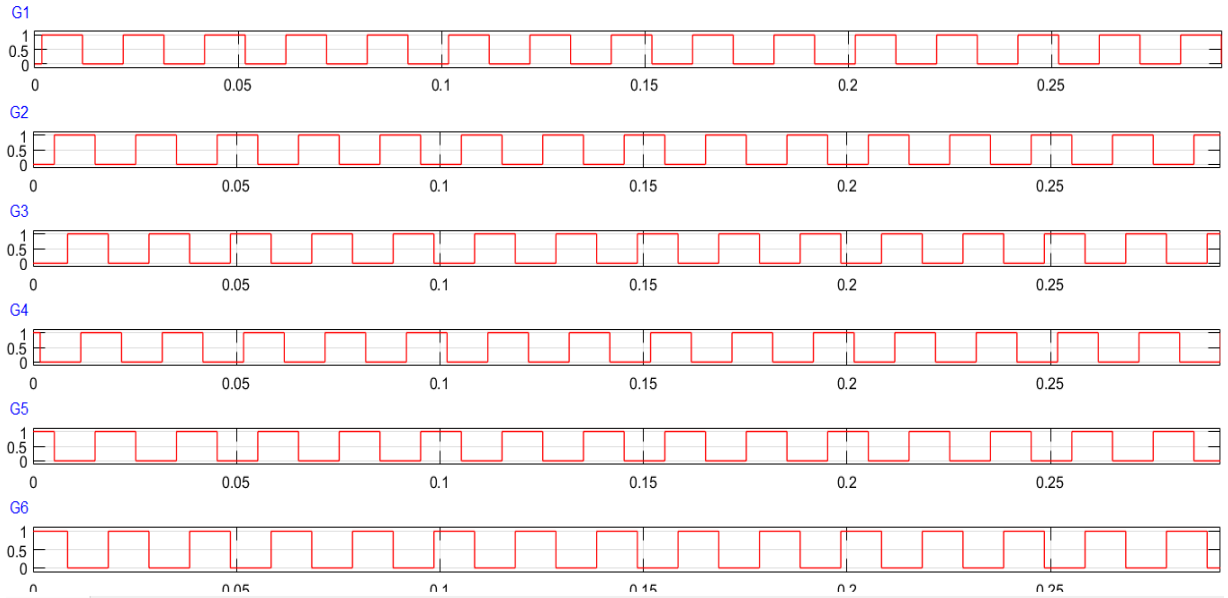

Figure 4-31: Switching gate pulses of STATCOM.

The Figure 4-32 shows the pulse that are given to the thyristor switches so that SVC is get into operation.

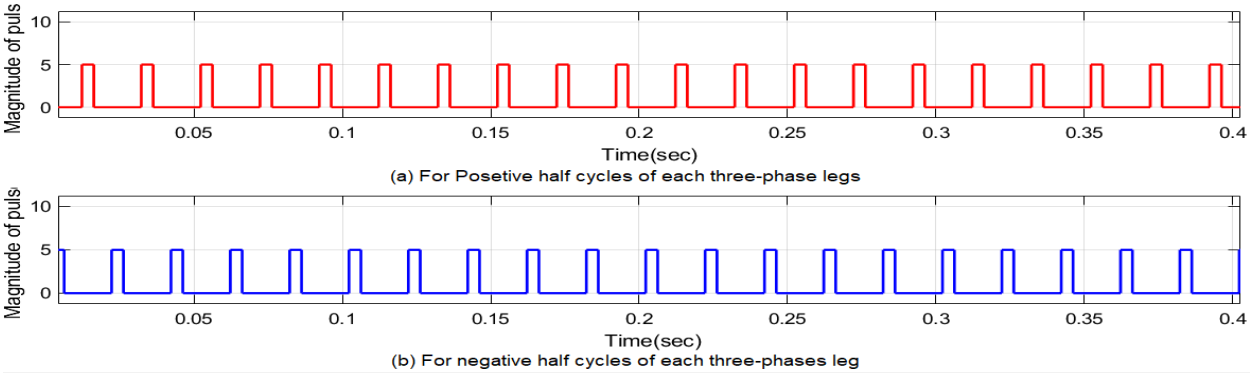

Figure 4-32: Firing pulses for TCR.

Figure 4-33 shows the performance of PI controller to control DC bus voltage of STATCOM.

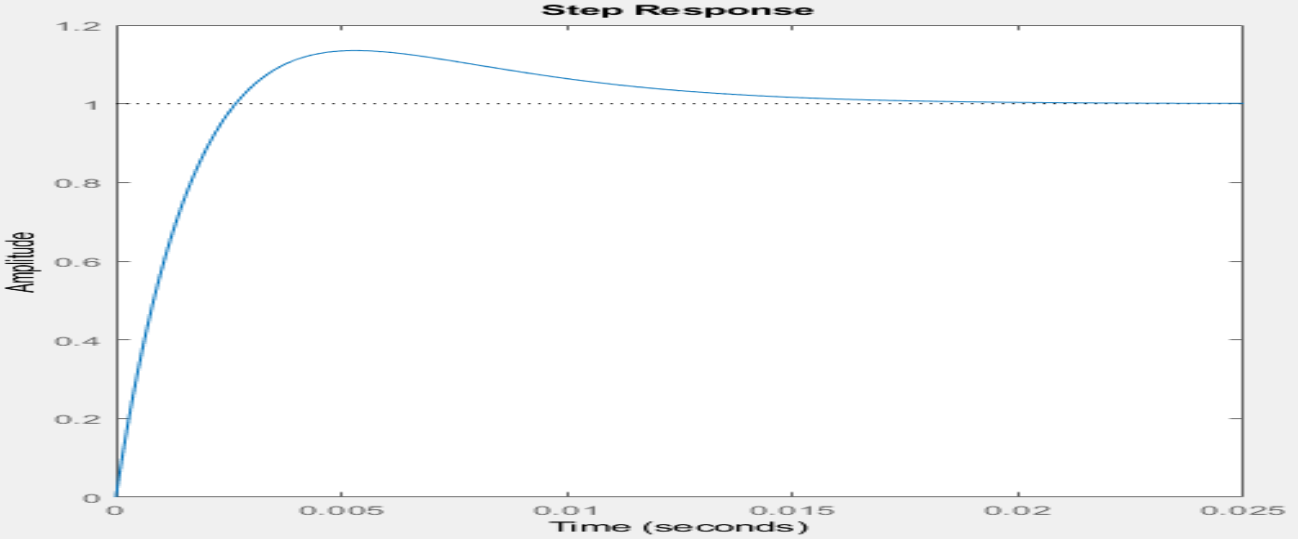

Figure 4-33: Performance of PI controller.

4.2.2 Voltage Dip analysis of Grid Connected System before mitigation.

Figure 4-34 shows the peak value of voltage in pu at PCC in the normal operating condition. As seen in the Figure 4-34, the voltage has pure sinusoidal wave and 1pu magnitude before the connection of linear or nonlinear loads at PCC.

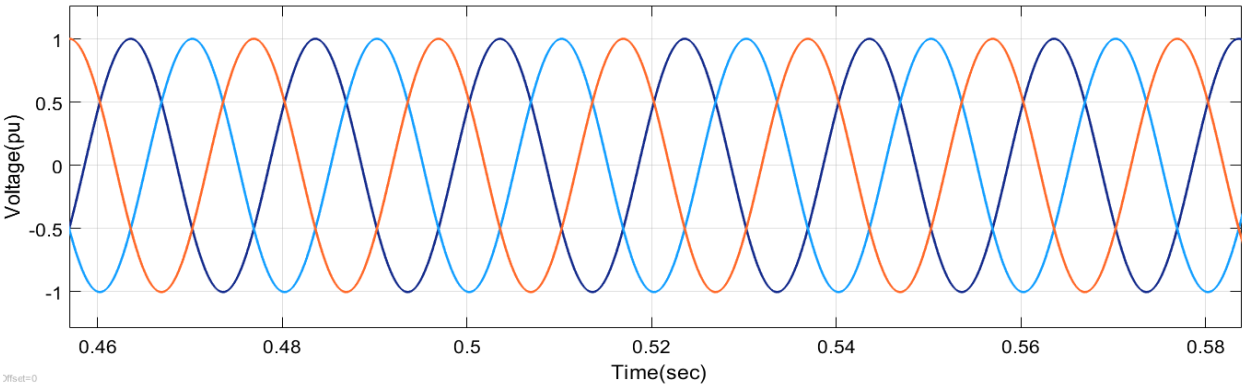

Figure 4-34: Voltage wave form at PCC before connection of loads.

Case I: Grid with a nonlinear load

Figure 4-35 shows the peak value of voltage at PCC when the non-linear load is connected at PCC of grid connected wind power system at t = 1.12sec. As shown Figure 4-35, initially there is no voltage distortion and voltage drop until the time reaches t=1.12sec. after the start of simulation. But the nonlinear load is connected when the circuit breaker one is closed at the instant of

t=1.12sec. and the wave form of the voltage become distorted and its peak value is also decreased to 0.736pu from 1pu.

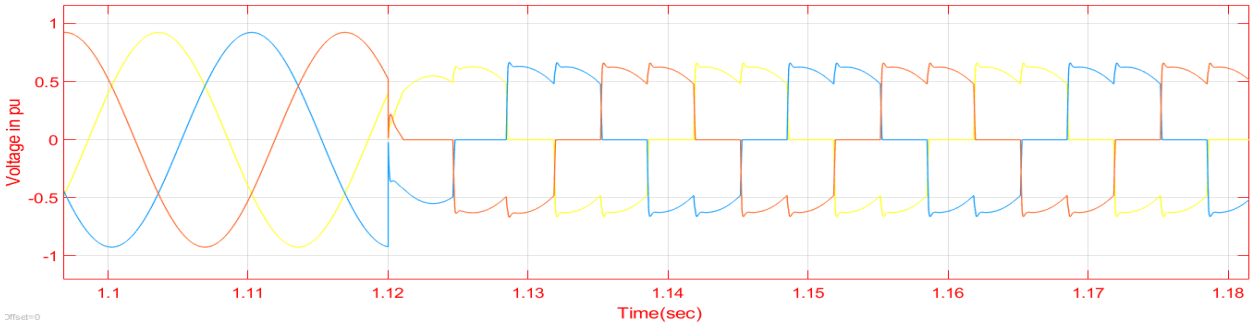

Figure 4-35: Voltage value at PCC when non-linear load is connected.

Figure 4-36 shows the RMS value of voltage at PCC when the nonlinear load is connected to grid. As seen in the Figure, the RMS value of voltage is 1pu before the connection of nonlinear load. But when the nonlinear load is connected at t=1.12sec, the RMS value of voltage start decrease to the value of 0.736pu from 1pu.

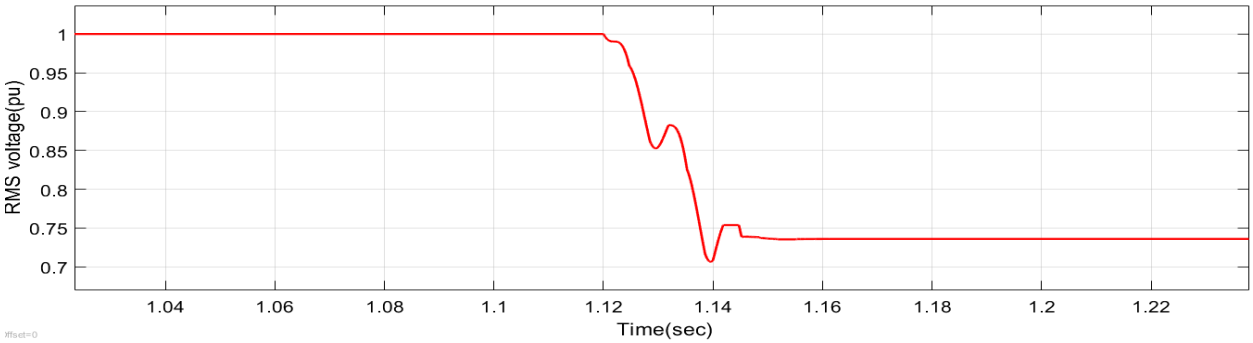

Figure 4-36: Voltage sag when nonlinear load is connected.

Figure 4-37 shows the voltage sag value of 0.736pu after the connection of the nonlinear load at t=1.12sec. at PCC of grid connected wind power before mitigation.

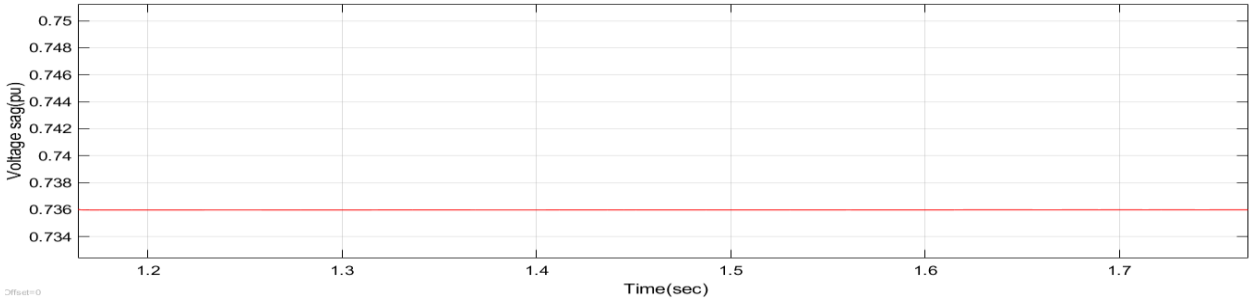

Figure 4-37: Voltage sag after connection of linear load.

Case II: Grid with a linear load

Figure 4-38 shows the peak value voltage at PCC when the linear load is connected at PCC of grid connected wind power system at t = 1.12sec. As shown in Figure 4-38, initially there is no voltage distortion and voltage drop until the time reaches t=1.12sec. The linear load is connected when the circuit breaker is closed once again at the instant of t=1.12sec, the wave form of the voltage is the same with the wave as before the connection of linear load but, the peak value become decreased to 0.6885pu from 1pu.

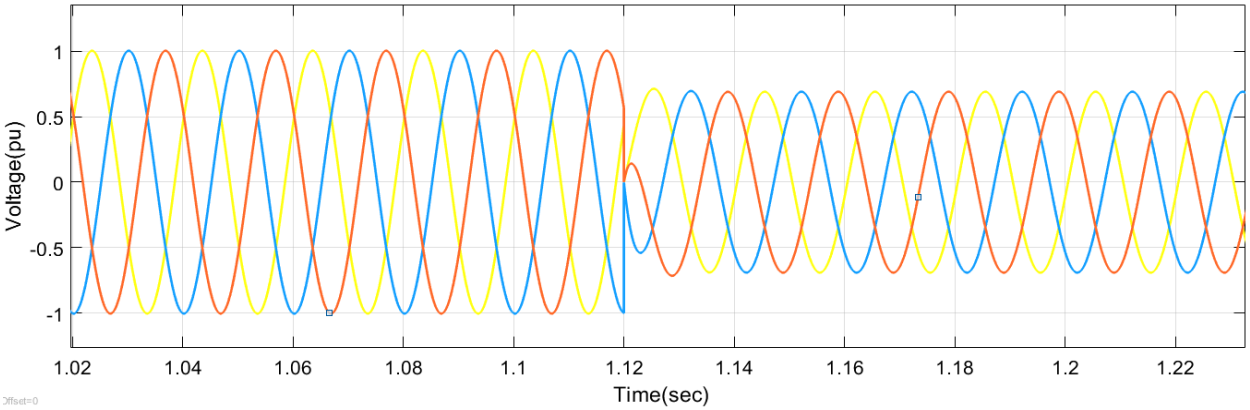

Figure 4-38: Voltage value at PCC when linear load is connected.

Figure 4-39 shows the RMS value of voltage at PCC when the linear load is connected to grid connected wind power. As seen in the Figure 4-39, the RMS value of voltage is 1pu before the connection of linear load. But when the linear load is connected at t=1.12sec, the RMS value of voltage start to decrease the value of 0.6885pu from 1pu.

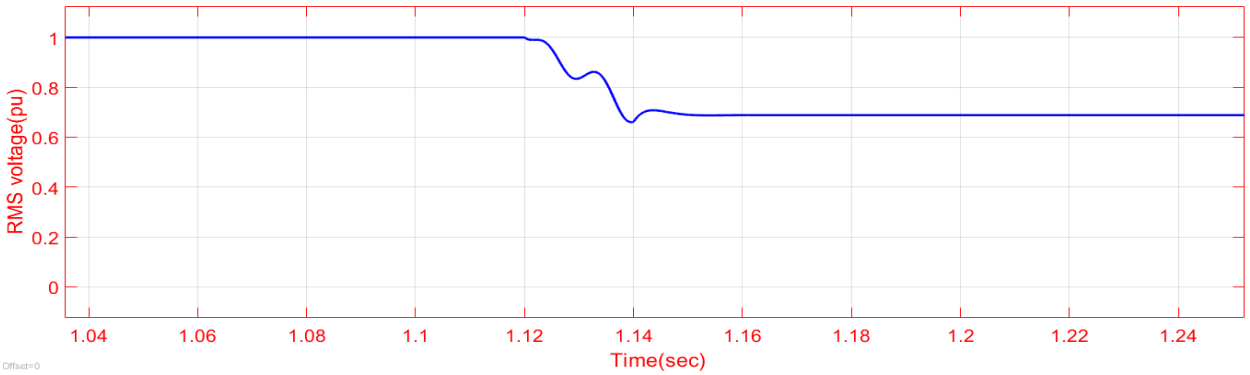

Figure 4-39 : Voltage sag when linear load is connected

Figure 4-40 shows the voltage sag value of 0.6885pu after the connection of the linear load at t=1.12sec. at PCC of grid connected wind power before mitigation.

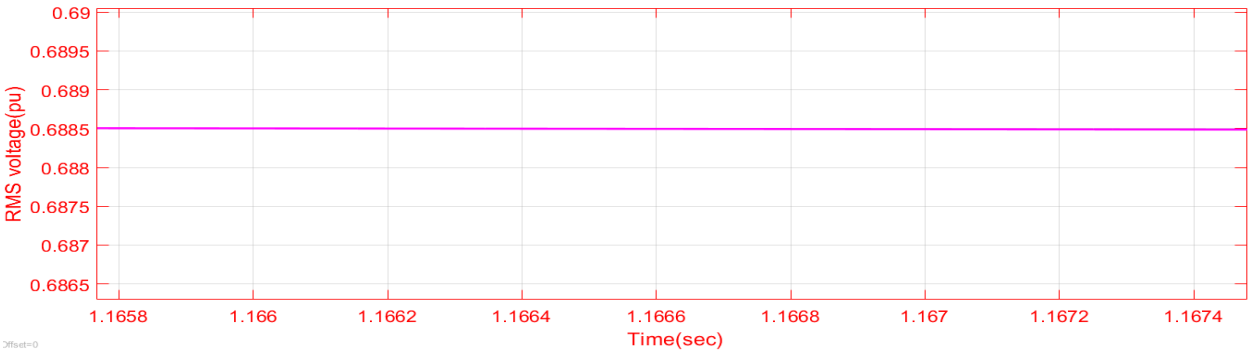

Figure 4-40: Voltage sag after connection of linear load.

4.2.3 Voltage Dip analysis of Grid Connected System with SVC

Case I: Grid with a Nonlinear Load

Figure 4-41 shows the peak value of voltage at PCC when the non-linear load is connected at PCC of grid connected wind power system at t = 1.12sec before mitigation. As shown in Figure 4-41, initially there is no voltage distortion and voltage drop until the time reaches t=1.12sec. But the nonlinear load is connected when the circuit breaker one is closed at the instant of t=1.12sec. And the wave form of the voltage become distorted and its peak value is also decreased to 0.736pu from 1pu before mitigation. In this case, the SVC is connected when circuit breaker two is closed once again at t=1.14sec. and the wave form and its magnitude once again become slightly pure and 0.9184pu of respectively.

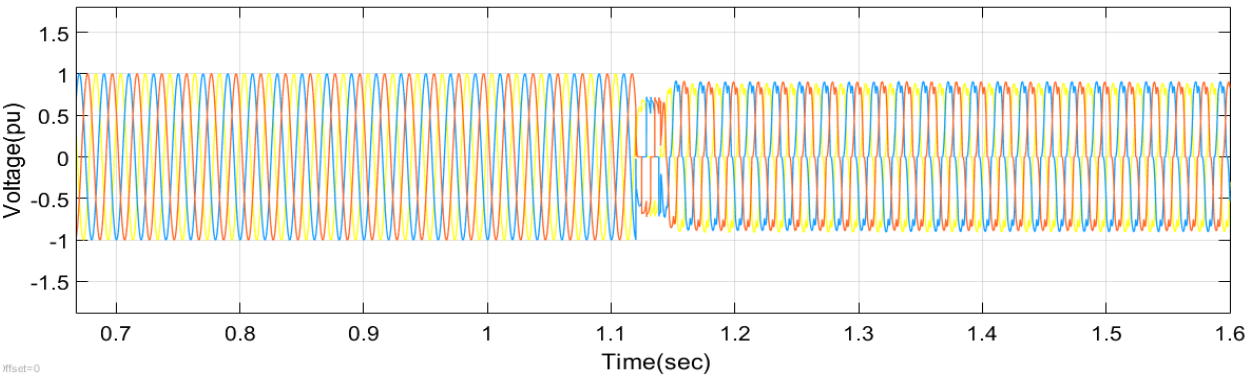

Figure 4-41: Voltage value at PCC after mitigation with SVC.

As shown in Figure 4-42, the RMS value of voltage at PCC is 1pu until connection of the non-linear load at t=1.12sec. But after the connection of non-linear load the RMS voltage is dropped to 0.736pu from 1 pu before mitigation. Now, SVC is connected at PCC when the circuit breaker two is closed at t=1.14sec.and the RMS value of voltages is recovered to 0.9184pu from 0.736pu.

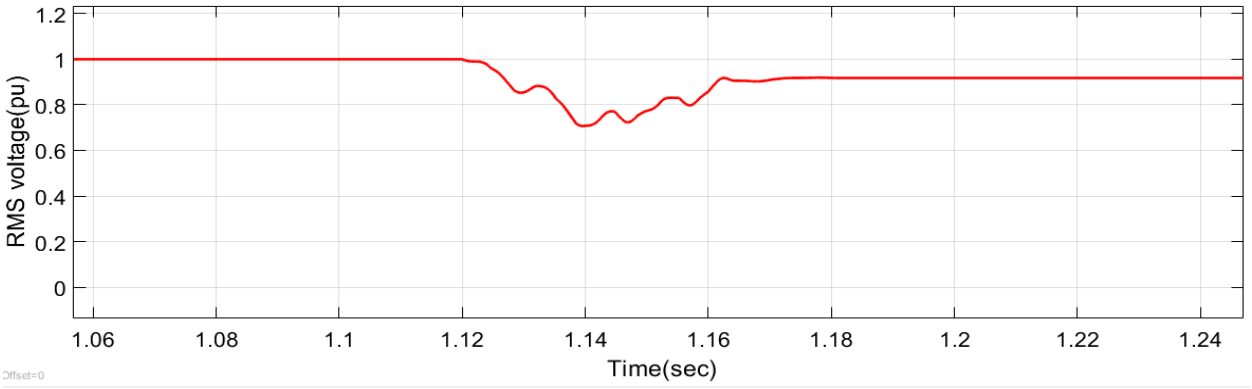

Figure 4-42: Voltage sag after mitigation with SVC

Case II: Grid with a linear load

Figure 4-43 shows the peak value of voltage at PCC when the linear load is connected at PCC of grid connected wind power system at t = 1.12sec before mitigation. As shown in Figure 4-43, initially there is no voltage distortion and voltage drop until the time reaches t=1.12sec. But the linear load is connected when the circuit breaker one is closed once again at the instant of t=1.12sec. and the wave form of the voltage become distorted and its peak value is also decreased to 0.6885pu from 1pu before mitigation. In this case, the SVC is also connected when circuit breaker two is closed once again at t=1.14sec. So, the wave form and its magnitude once again become approximately pure sinusoidal and 0.8865pu of respectively.

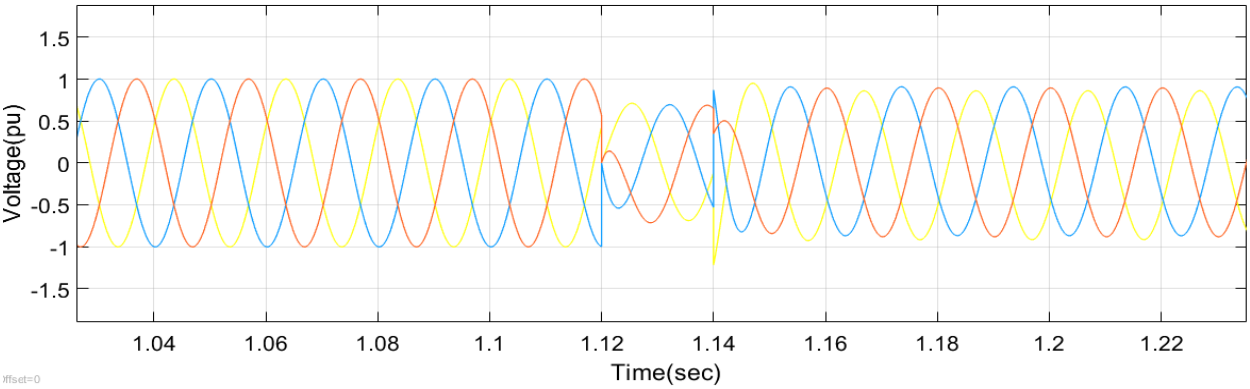

Figure 4-43: Voltage value at PCC after mitigation with SVC.

As shown in Figure 4-44, the RMS value of voltage at PCC is 1pu until connection of the linear load at t=1.12sec. But after the connection of linear load the RMS voltage is dropped to 0.6885pu from 1 pu before mitigation. Now, SVC is connected at PCC when the circuit breaker two is closed once again at t=1.14sec.and the RMS value of voltages is recovered to 0.8865pu from 0.6885pu.

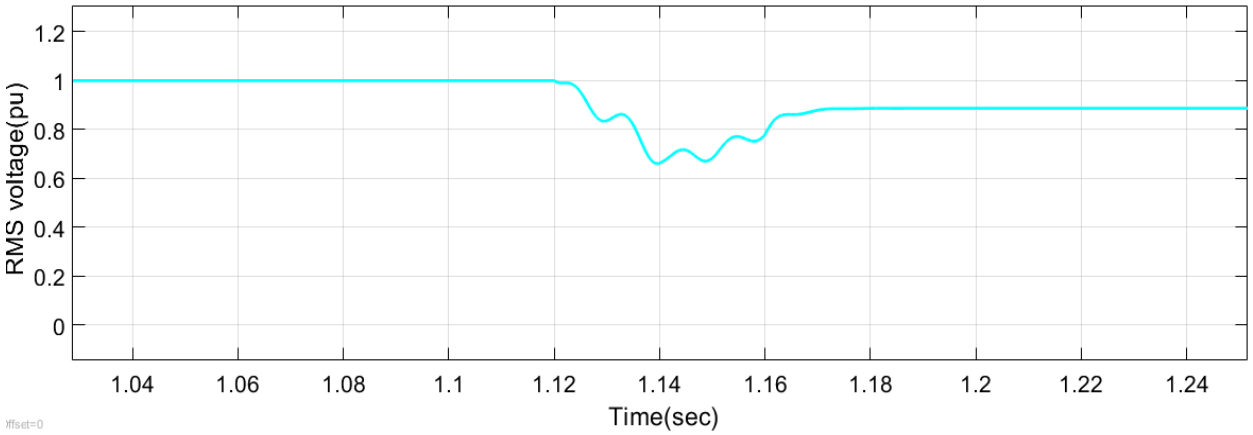

Figure 4-44:Voltage sag after mitigation with SVC.

4.2.4 Voltage Dip analysis of Grid Connected System with STATCOM

Case I: Grid with a nonlinear load

Figure 4-45 shows the peak value of voltage at PCC when the non-linear load is connected at PCC of grid connected wind power system at t = 1. 12sec.before mitigation. As shown in Figure 4-45, initially there is no voltage distortion and drop until the time reaches t=1.12sec. Now, the nonlinear load is connected when the circuit breaker one is closed at the instant of t=1.12sec and the wave form of the voltage become distorted and its peak value is also decreased to 0.736pu from 1pu before mitigation. In this case, STATCOM is connected when circuit breaker two is closed at t=1.14sec. As illustrated in Figure 4-45, the wave form and its magnitude once again become approximately pure and 1.048pu respectively.

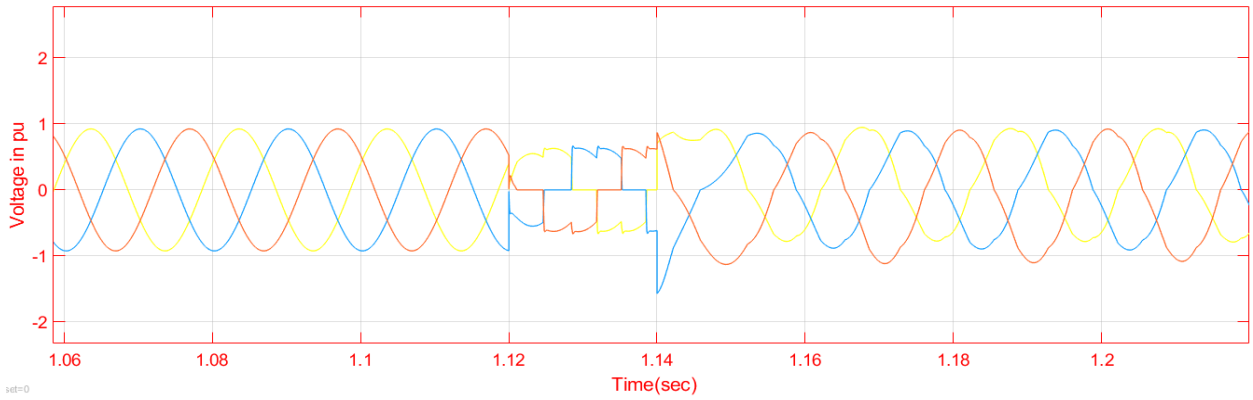

Figure 4-45: Voltage value at PCC after mitigation with STATCOM.

As shown in Figure 4-46, the RMS value of voltage at PCC is 1pu until the connection of the nonlinear load at t=1.12sec. But after the connection of nonlinear load, the RMS voltage is dropped

to 0.736 pu from 1 pu before mitigation. STATCOM is connected at PCC when the circuit breaker two is closed at t=1.14sec. So, the RMS value of voltages is recovered to 1.048pu from 0.736 pu.

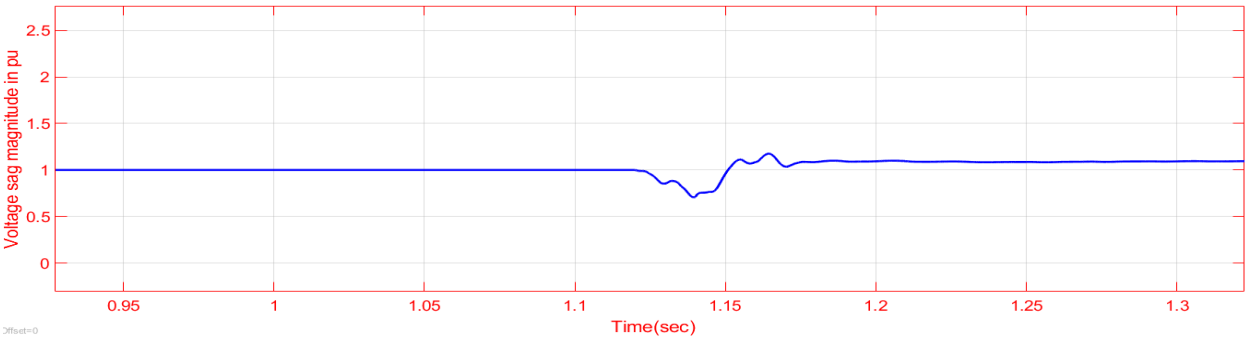

Figure 4-46: Voltage sag after mitigation with STATCOM.

Case: II Grid with a Linear Load

Figure 4-47 shows the peak value of voltage at PCC when the linear load is connected at PCC of grid connected wind power system at t = 1.12sec. As shown in Figure 4-47, initially there is no voltage distortion and voltage drop until the time reaches t=1.12sec. The linear load is connected when the circuit breaker one is closed once again at the instant of t=1.12sec, the wave form of the voltage is the same with the wave form as before the connection of linear load but the peak value is also decreased to 0.6885 pu from 1 pu before mitigation. But When the STATCOM is connected at t=1.14sec., the magnitude of voltage at PCC once again recovered from drop of 0.6885pu to the value of 0.9957pu.

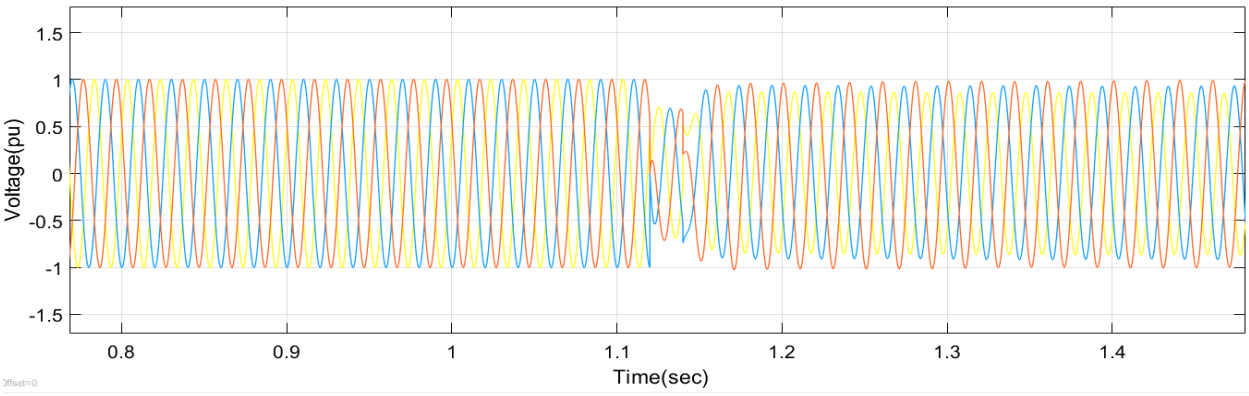

Figure 4-47: Voltage value at PCC after mitigation with STATCOM.

As shown in Figure 4-48, the RMS value of voltage at PCC is 1pu until the connection of the linear load at t=1.12sec. But after the connection of linear load the RMS voltage is dropped to 0.6885pu from 1 pu before mitigation. STATCOM is connected at PCC when the circuit breaker two is

closed once again at t=1.14sec. Now, the RMS value of voltages is recovered to 0.9957pu from 0.6885pu.

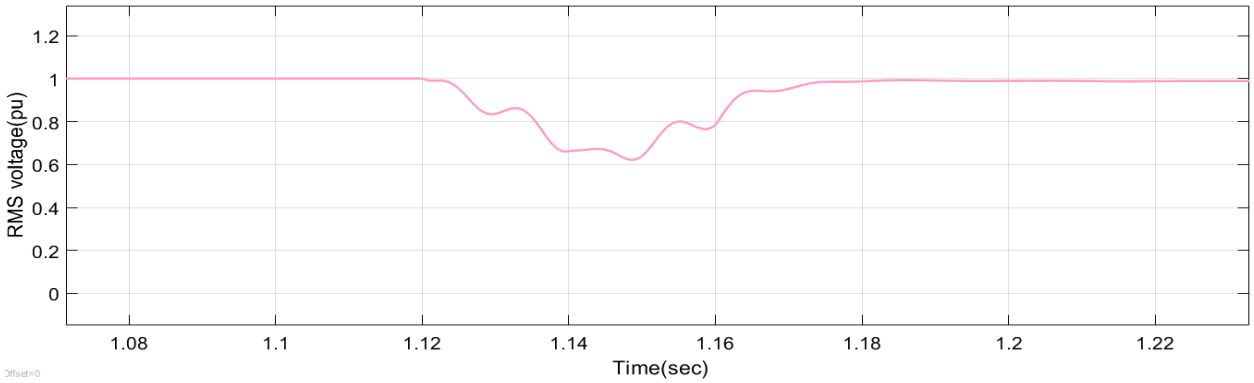

Figure 4-48: Voltage sag after mitigation with STATCOM.

summary

Figure 4-34 shows the voltage value at PCC which is pure sinusoidal and magnitude of 1pu before the connection of linear/nonlinear loads. But as seen in Figures 4-35 - 4-40, there is voltage variation and wave form distortion when linear/non-linear loads are connected to grid before mitigation. The developed grid connected system with two cases i.e. with non-linear and linear loads have been simulated using both SVC and STATCOM. First case is, grid connected with nonlinear load at PCC using SVC and STATCOM. As shown in Figure 4-42, the RMS value of voltage at PCC is 1pu until connection of the linear load at t=1.12sec. But after the connection of non-linear load the RMS voltage is dropped to 0.736pu from 1 pu before mitigation. Now, SVC is connected at PCC when the circuit breaker two is closed at t=1.14sec. and the RMS value of voltages is recovered to 0.9184pu from 0.736pu. Again, as shown in Figure 4-46, STATCOM is connected at PCC when the circuit breaker two is closed once again at t=1.14sec. and the RMS value of voltages is recovered to 1.048pu from 0.736 pu.

Second case is, grid connected with linear load at PCC using SVC and STATCOM. As shown in Figure 4-44, the RMS value of voltage at PCC is 1pu until connection of the linear load at t=1.12sec. But after the connection of linear load the RMS voltage is dropped to 0.6885pu from 1 pu. Now, SVC is connected at PCC when the circuit breaker two is closed once again at t=1.14sec.and the RMS value of voltages is recovered to 0.8865pu from 0.6885pu. Again, As shown in Figure 4-48, STATCOM is connected at PCC when the circuit breaker two is closed once again at t=1.14sec. Now, the RMS value of voltages is recovered to 0.9957pu from 0.

6885pu.Therefore, the result of voltage sag improved by using STATCOM is in permissible limit i.e. +/- 3% as per standard of IEEE 519-1992.

4.2.5 FFT Analysis of Grid Connected System

Case: 1 Existing system without harmonic mitigation

Figure 4-49 (a) and (b) shows the waveform of three phase voltage and current at PCC. The distortion of both the voltage and current wave forms are due to both VSC of DFIG and nonlinear loads that are connected at PCC of grid connected wind power without harmonic mitigation. As seen in the Figure 4-49 harmonics is injected in to network at PCC resulting in both waveform distortion.

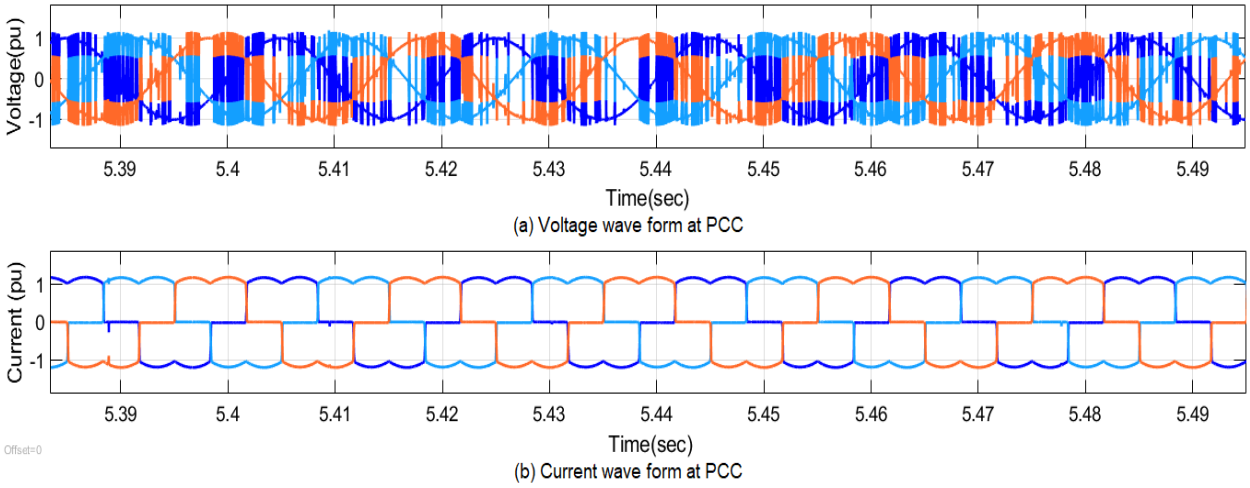

Figure 4-49: Voltage and current wave form at PCC without STATCOM.

Figure 4-50 (a) and (b) shows the distorted current magnitude signal and FFT output respectively at PCC without harmonic mitigation.

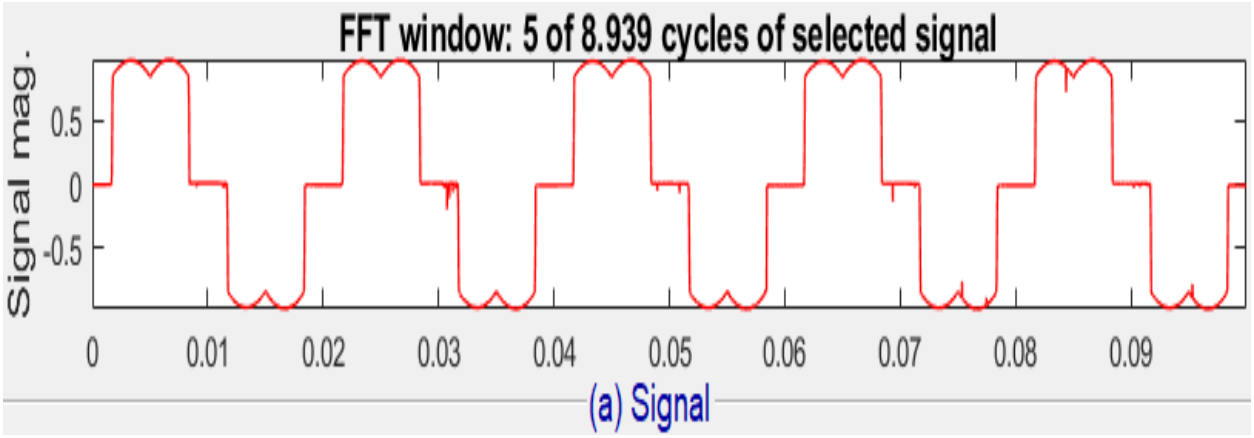

As Figure 4-50 (b) illustrates, FFT analysis result shows the THD of current at PCC is 30.21% which is not in permissible limit i.e. 5% due to the connection of both back-to-back VSC of DFIG and nonlinear load which are connected at PCC of grid connected wind power.

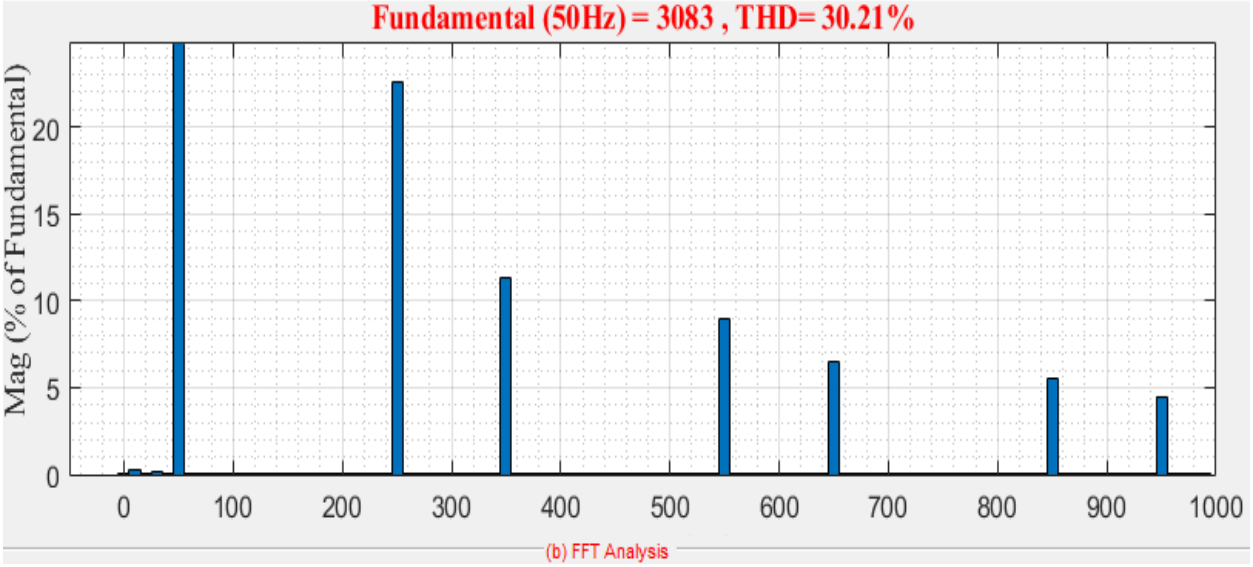

Figure 4-50: FFT output of total harmonic current distortion.

Figure 4-51 (a) and (b) shows the distorted voltage magnitude signal and FFT analysis result respectively at PCC without harmonic mitigation.

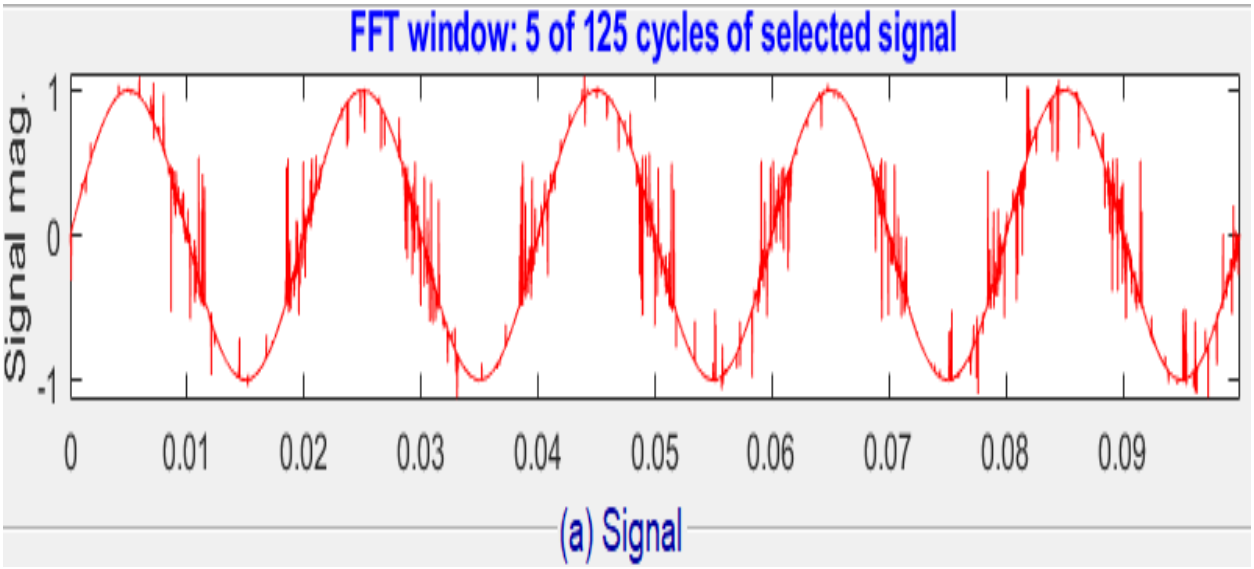

As Figure 4-51 (b) illustrates, FFT analysis result shows the THD of current at PCC is 5.18% due to the connection of both back-to-back VSC of DFIG and nonlinear load which are connected at PCC of grid connected wind power without harmonic mitigation.

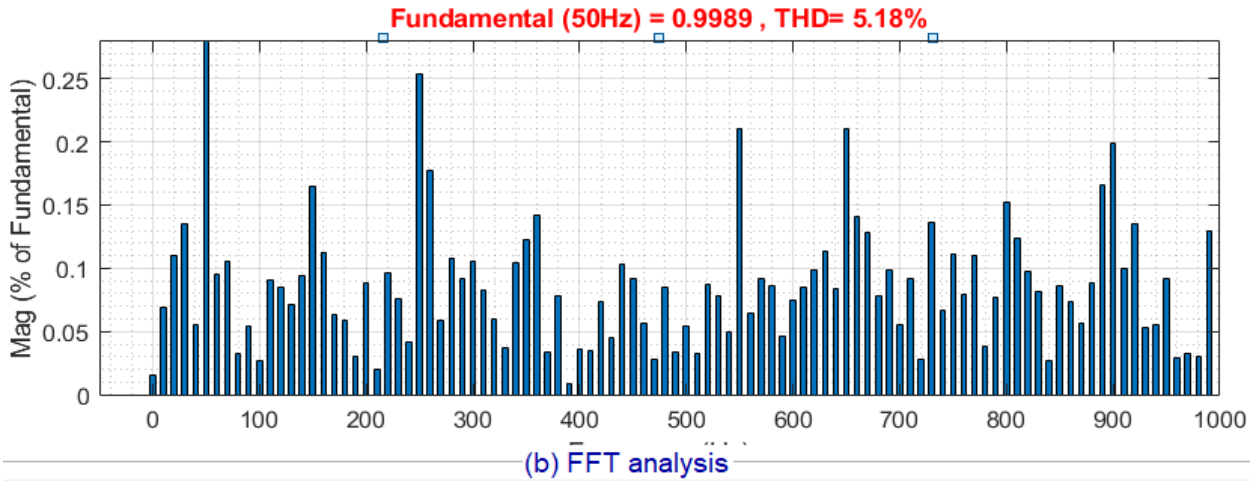

Figure 4-51: FFT output of total harmonic voltage distortion.

Case: 1I Existing system with SVC

Figure 4-52 (a) and (b) shows the waveform of three phase voltage and current at PCC. The distortion of both voltage and current wave forms are due to both back-to-back VSC of DFIG and nonlinear loads that are connected at PCC of grid connected wind power. As seen in the Figure 4-52 harmonics is injected in to network at PCC resulting in both waveform distortion especially current wave form.

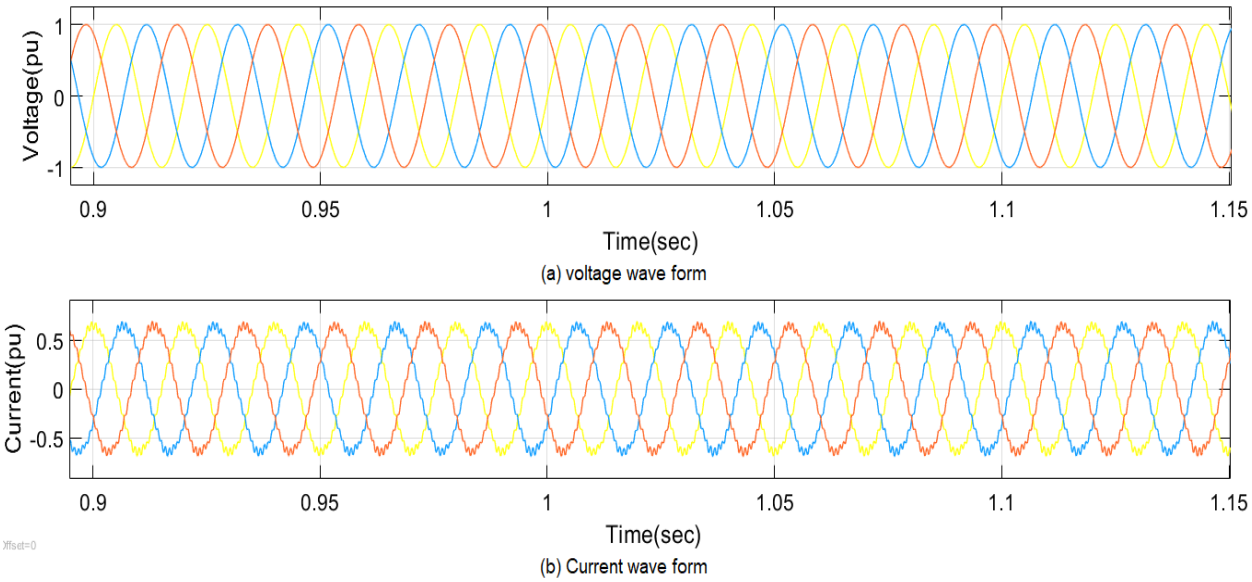

Figure 4-52: Voltage and current wave form with filter.

Figure 4-53 (a) shows the distorted current magnitude signal at PCC and Figure 4-53 (b) gives the FFT analysis result of current at PCC of existing system with SVC.

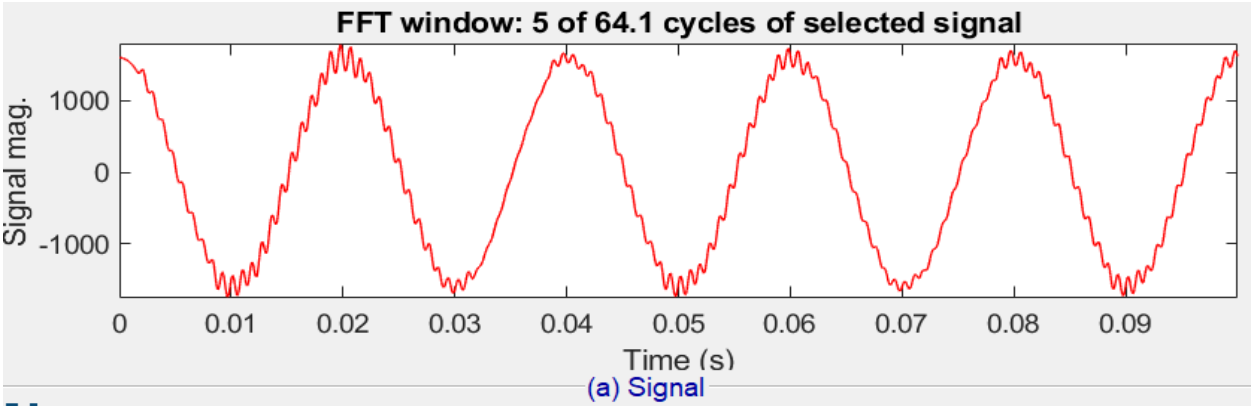

As Figure 4-53 (b) illustrates, FFT analysis result shows the THD of current at PCC is 6.69% due to the connection of both back-to-back VSC and nonlinear load connected at PCC.

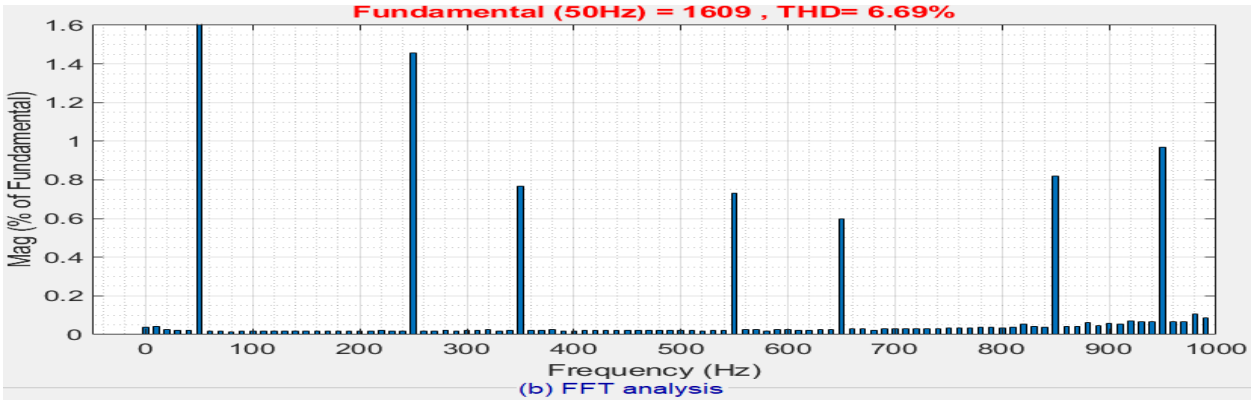

Figure 4-53: FFT output of total harmonic current distortion.

Figure 4-53 (a) shows the voltage magnitude signal at PCC and Figure 4-53 (b) gives the FFT analysis result of voltage at PCC of existing system with SVC.

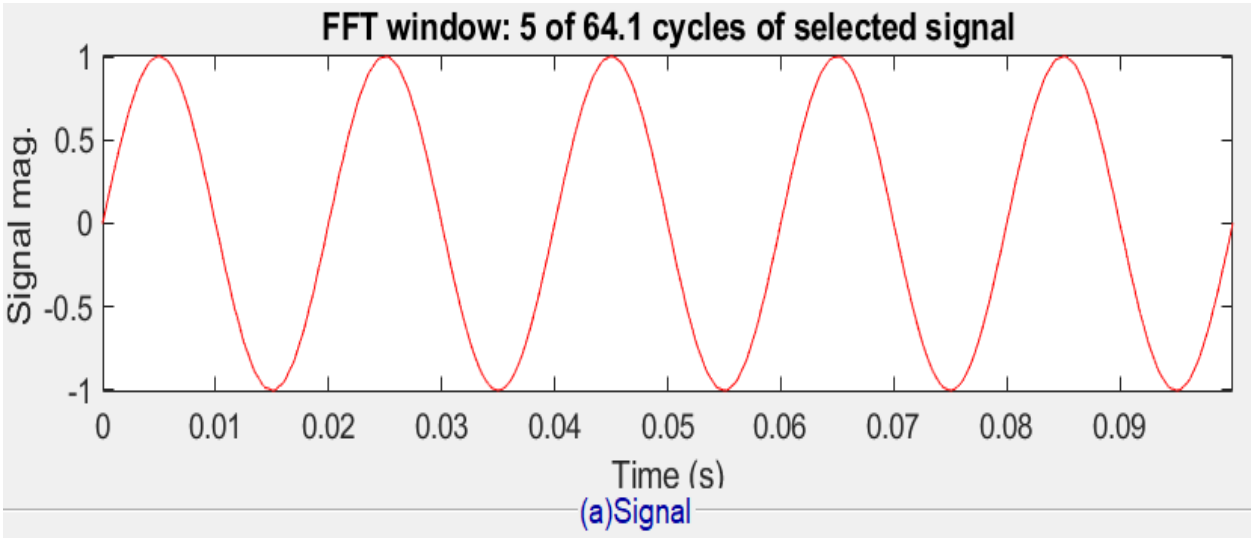

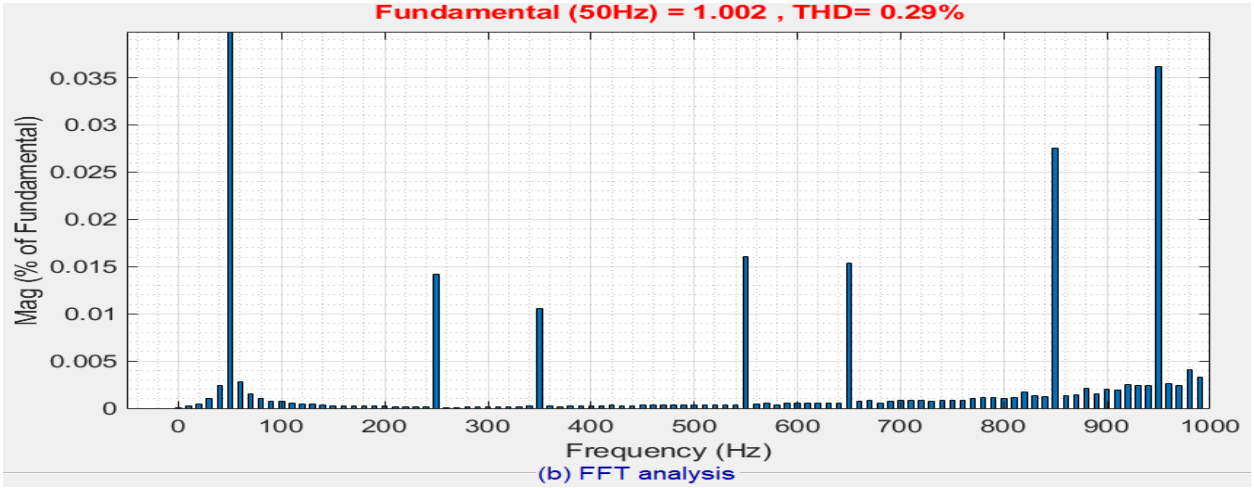

Figure 4-54: FFT output of total harmonic voltage distortion.

Case: 1I Grid connected system with STATCOM

Figure 4-55 (a) and (b) shows the waveform of three phase voltage and current at PCC. The total harmonics distortion of both voltages and currents are reduced and the wave shape become approximately pure when STATCOM is connected at PCC. The wave form shows that both voltage and current are in phase resulting in a unity power factor.

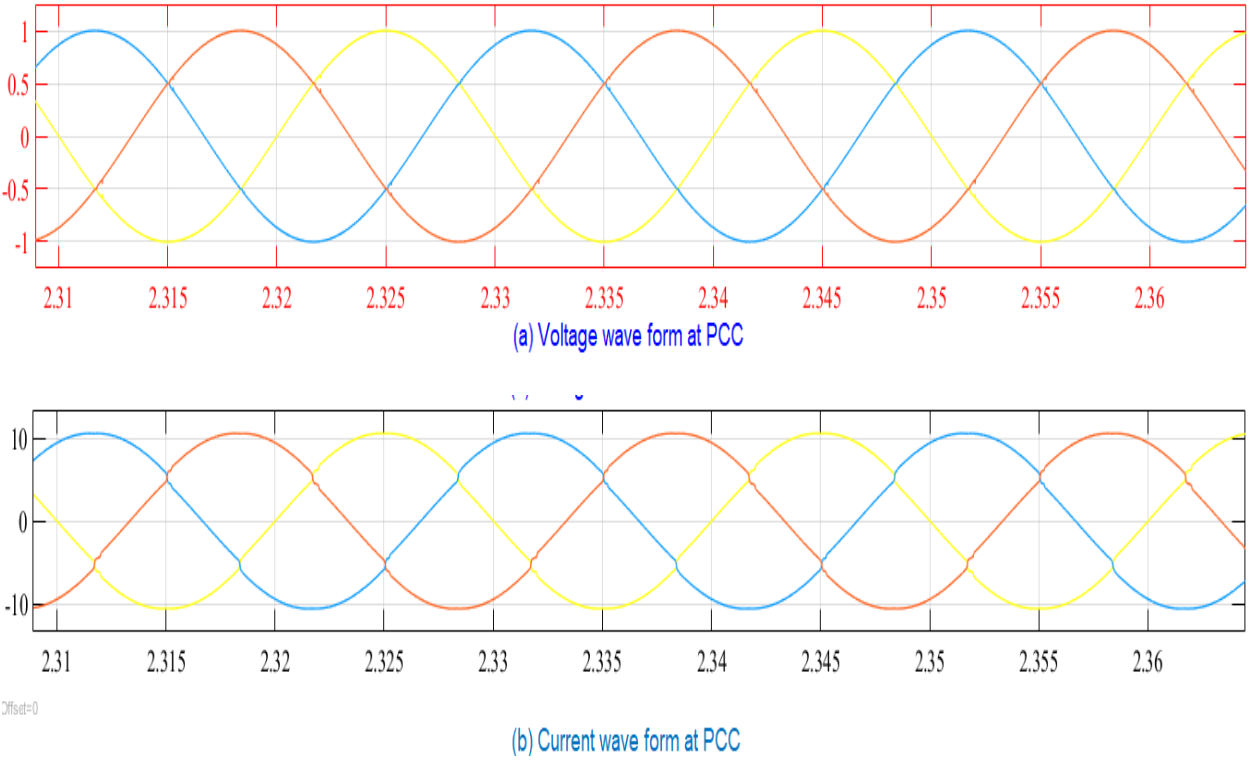

Figure 4-55: Voltage and current wave form at PCC.

Figure 4-56 (a) shows the voltage magnitude signal at PCC and Figure 4-56 (b) gives the FFT analysis result of voltage at PCC with STATCOM.

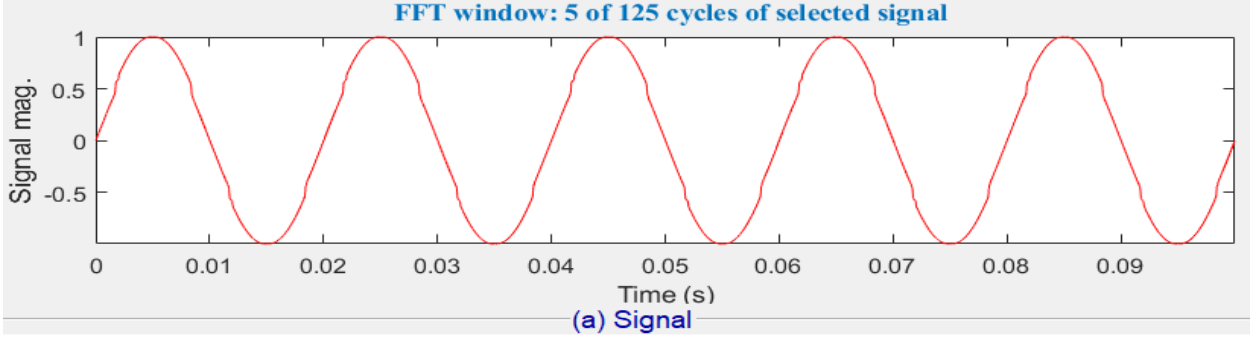

As Figure 4-56 (b) illustrates, FFT analysis result shows the THD of current at PCC is 3.39% due to the connection of both back-to-back VSC and nonlinear load connected at PCC with STATCOM.

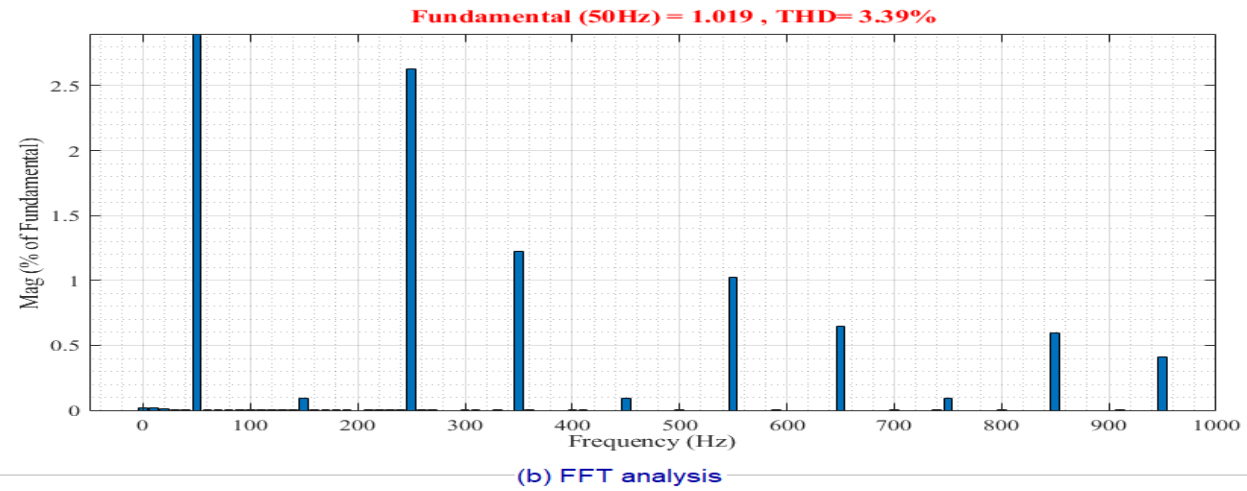

Figure 4-56: FFT output of total harmonic current distortion.

Figure 4-57 (a) shows the voltage magnitude signal at PCC and Figure 4-57 (b) gives the FFT analysis result of voltage at PCC of existing system with STATCOM.

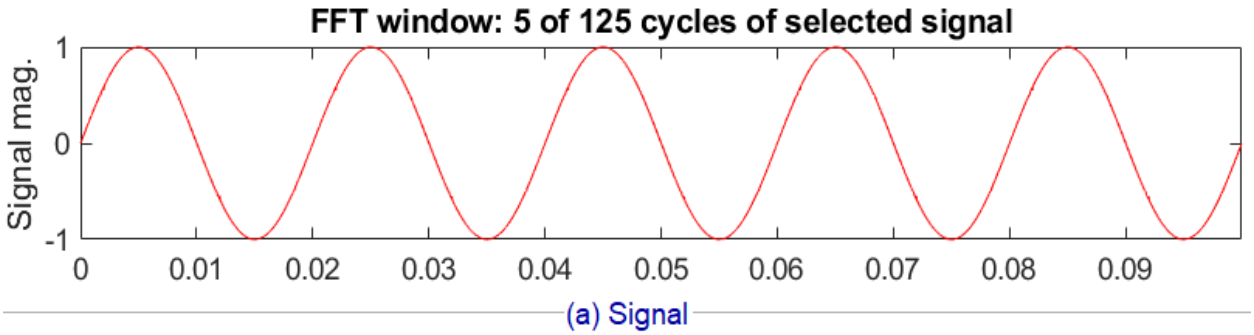

As Figure 4-57 (b) illustrates, FFT analysis result shows the THD of voltage at PCC is 0.25% due to the connection of both back-to-back VSC and nonlinear load connected at PCC with STATCOM.

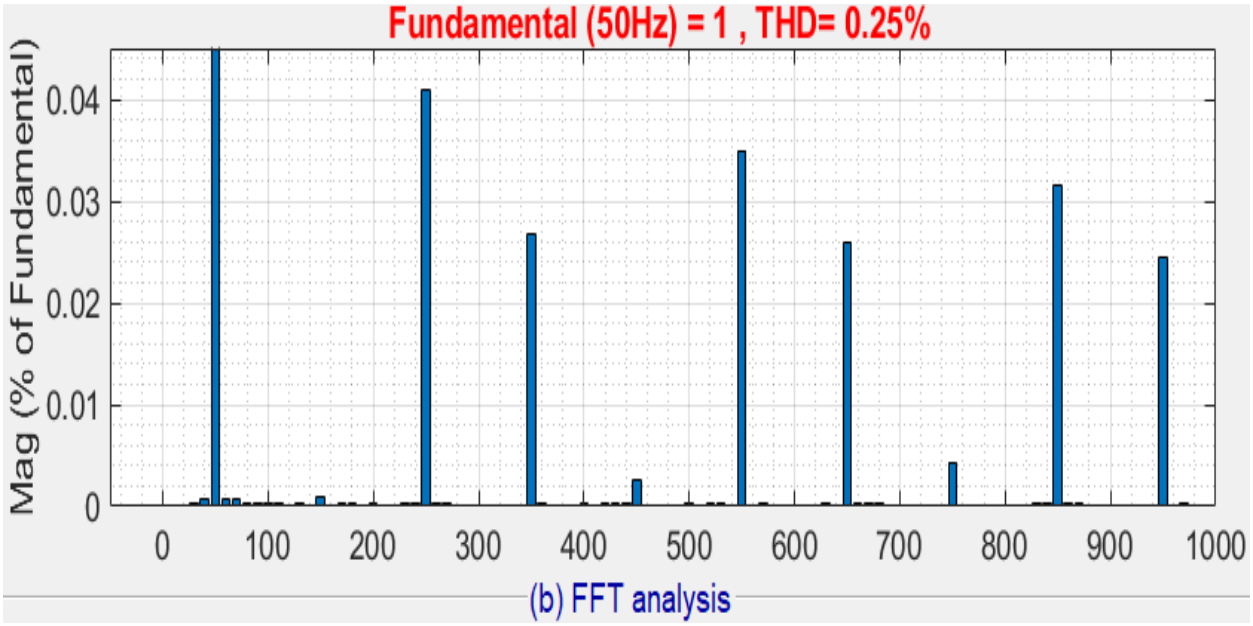

Figure 4-57: FFT output of total harmonic voltage distortion.

Discussion

The developed grid connected system with three cases have been simulated. First case is grid connected existing system without harmonic mitigation. As shown in Figure 4-49 (a) and (b), both the voltage and current waveforms are distorted respectively. The distortions are caused by connection of both back-to-back VSC of DFIG and nonlinear load at PCC. The FFT analysis results i.e. (30.21% and 5.18%) of both current and voltages are depicted in Figures 4-50 (b) and 4-51 (b) respectively. These, FFT analysis of THD of both voltage and current results, are not in permissible i.e. (5.18% >3% and 30.21% >5%) as per IEEE 519-1992. In second case, Adama II wind farm is using SVC at PCC. But as Figure 4-53 (b) shows, the FFT analysis of THD of current is beyond the permissible standard i.e. (6.69% > 5%). In case three, in order to improve the harmonic distortion, we have used STATCOM. As shown in Figures 4-56(b) and4-57(b), FFT analysis result of THD of current and voltage are 3.39% and 0.25% respectively. Also, the shape of the voltage and current wave, in Figure 4-55 (a) and (b) respectively, are approximately pure and sinusoidal. Therefore, the % THD of voltages and current have been improved from 5.18 % and 30.21 % to 0.25 % and 3.39 % respectively after mitigation by using STATCOM.

Table 4-1: Total Harmonics Distortion values.

Total harmonic distortion	Without harmonic mitigation	With SVC	With STATCOM
THD_i	30.21 %	6.69%	3.39 %
THDv	5.18 %	0.29%	0.25 %

Table 4-2: Voltage Sag/Dip Values.

Voltage Variation	Normal operating value	Without voltage dip mitigation		With SVC		With STATCOM	
Voltage sag/Dip	1 pu	Linear load	Nonlinear load	Linear load	Nonlinear load	Linear load	Nonlinear load
		0.6885pu	0.736pu	0.8865	0.9184pu	0.9957pu	1.048pu

CHAPTER FIVE

CONCLUSION, RECOMMENDATION AND FUTURE WORK

5.1 CONCLUSION

A STATCOM has been investigated for power quality problems of voltage variation and harmonic improvement at PCC of grid connected DFIG wind turbine power system. The simulation results show that HCC scheme of STATCOM, developed in MATLAB, for mitigation of voltage variation and harmonics is performed effectively. The performance of STATCOM is analyzed by selecting proper design parameters of its component. STATCOM reduced the total harmonic distortion of current and voltage values of 30.21 % and 5.18 % to 3.39 % and 0.25 % at PCC respectively. The FFT analysis confirms that the THD of the voltage and current is reduced to an acceptable value of 3 % and 5 % of IEEE 519-1992 standard respectively. Voltage dip is analyzed by in comparison by using SVC and STATCOM with linear or nonlinear loads. SVC recovered the RMS voltage sag values to 0.8865pu and 0.9184pu from 0.6885pu and 0.736 pu due to linear and nonlinear loads respectively. And also, STATCOM improved the RMS voltage Sag from 0.6885pu and 0.736 pu to 0.9957pu and 1.084pu due to linear and non-linear loads respectively. Therefore, based on the above findings, it is clear that the shunt connected STATCOM in grid connected DFIG wind power system improves the voltage Dip/Sag and harmonic at PCC effectively more efficient and effectively than SVC.

5.2 RECOMMENDATION

- Based on the findings of this research, it is recommended that STATCOM controllers may be used for harmonics mitigation and voltage regulation in the Adama-II 33/230kV busbar of main substation.

5.3 FUTURE WORK

- This configuration can be tested in hardware to verify the simulation results.
- In this work the voltage across DC link is regulated by using PI controller, some more artificial intelligent control approaches need to be developed for much better regulation.
- This work can be implemented to the grid connected with renewable energy resources.
- This work is carried out by using two-level voltage source inverter STATCOM but it is possible to do with a multi-level STATCOM.

REFERENCES

[1] G. M. P. K. P. V. Reddy, "Implementation of a Standalone Solar Photovoltaic Hybrid System Using Fuzzy Logic Controller," *International Journal of Advanced Engineering Research and Science,* vol. 6495, no. 5, pp. 157-163, 2017.

[2] P. Ramanathan, "A Statcom-Control Scheme for Grid Connected Wind Energy System for Power Quality Improvement," *Middle-East Journal of Scientific Research ,* vol. 20, no. 1, pp. 57-61, 2014.

[3] A. O. P. T. K. S. N. M. S. M. Prakash, "Reactive Power Compensation and Mitigation of Current Harmonics in Grid Connected Wind Turbine Generating System (GCWTGS) using STATCOM," *International Journal of Engineering Research & Technology,* vol. 3, no. 2, pp. 912-918, 2014.

[4] S. M. M. Sasthri, "Power quality improvement in grid connected wind energy conversion systems by using custom power device," *International Research Journal of Engineering and Technology,* vol. 04, no. 06, pp. 3254-3259, 2017.

[5] M. K. A. N. a. L. L. L. Hacil, "Harmonic current cancellation and control of a grid-connected synchronous generator entrained by a wind turbine," *Revue des Energies Renouvelables,* vol. 12, no. 3, pp. 405-418, 2009.

[6] J. E. S. W. D. Rocha, "The energy processing by power electronics and its impact on power quality," *International Journal of Renewable Energy Development,* vol. 1, no. 3, pp. 99-105, 2012.

[7] M. G. Mishra, "Voltage Oscillation Mitigation Of Wind Farm Using An Statcom," *International Journal for Research in Applied Science and Engineering Technology,* vol. V, no. XI, pp. 1605-1609, 2017.

[8] M. R. Patel, wind and solar power systems Desighn Analysis and Operation second edition, New York, U.S.A.: CRC press, 2006.

[9] G. W. J. L. J. Y. D. S. L. Ren, "Analysis of wind power intermittency based on historical wind power data," *Energy,* vol. 150, pp. 482-492, 2018.

[10] C. Rica, "GLOBAL WIND STATISTICS 14.2.2018," Global wind energy council, 1040 Brussels, Belgium, 2017.

[11] G. A. A. Bekele, "Investigation of wind farm interaction with Ethiopian electric power corporation's grid," *Energy Procedia*, vol. 14, no. 0, pp. 1766-1773, 2012.

[12] D. Derebew, "Ethiopia's Renewable Energy Power Potential and Development Opportunities," Abu Dhabi, UAE , 2013.

[13] "Feasibility study report for Ethiopian ADAMA II wind power project," HYDROCHINA CORPORATION, 2012.

[14] P. V. S. K. K. G. K. A. B. Deve, "POWER QUALITY IMPROVEMENT FOR A WIND FARM CONNECTED GRID incorporating UPFC controller," *International Journal of Emerging Technology in Computer Science & Electronics*, vol. 20, no. 2, pp. 241-246, 2016.

[15] P. H. K. M. V. C. V. Ku, "Improving Power Quality of Grid Connected Renewable Energy Systems by Using Variable Structure Control Facts Devices," *International Journal of Engineering Science and Computing,*, vol. 6, no. 8, 2016.

[16] M. T. A. A. M. M. Baig, "Mitigation of Harmonics in a grid connected DFIG Wind Power System," *International Journal of Emerging Engineering Research and Technology* , vol. 3, no. 8, pp. 145-153, 2015.

[17] A. B. Mahapatra, "Dfig Converter Controllers Used in Wind Farms To Improve Power Transfer Capability Over Long Distances," *International Journal of Innovative Research in Advanced Engineering*, vol. 07, no. 3, pp. 2349-2763, 2016.

[18] N. (. A. I. F. S. Hasan, "Dynamic Performance Analysis of DFIG based Wind Farm with STATCOM and SVC," *International Journal of Emerging Technology and Advanced Engineerin*, vol. 2, no. 7, pp. 6-14, 2012.

[19] P. P. P. Tare, "Enhancement of power quality of Grid connected wind energy system using STATCOM," *International Research Journal of Engineering and Technology*, vol. 04, no. 04, pp. 2654-2659, 2017.

[20] R. S. Kumbhare and H. Naidu, "Implementation of STATCOM- Control Scheme for Power Quality Improvement using PI and Fuzzy logic controller," *International Journal of Multidisciplinary Research Hub*, vol. 2, no. 8, pp. 28-47, 2015.

[21] V. K. A. A. K. V. H. K. Patel, "Comparative Analysis between IG and DFIG for Wind Energy Conversion Systems using STATCOM," *International Journal of Energy and Power Engineering*, vol. 3, no. 6-2, pp. 21-26, 2014.

[22] CTS power filter compensation scheme," *Journal of Electrical Systems,* no. 9-1, pp. 73-83, 2013A. A. Abdelsalam and M. E. S. A. M. Desouki, "Power quality improvement using FA.

[23] T. Magesh and C. Chellamuthu, "Simulation and study of power quality issues in a fixed speed wind farm substation," *Scientific World Journal,* vol. 2015, p. 10, 2015.

[24] A. Ghosh and G. Ledwich, POWER QUALITY ENHANCEMENT USING CUSTOM POWER DEVICES, New York : Springer Science+Business Media, 2002.

[25] R. C.Dugan, electrical power system quality second edition, McGraw-Hill, 2004.

[26] M. Andewalem, "AN ADAPTIVE HYSTERESIS BAND CURRENT CONTROL SCHEME OF STATCOM FOR POWER QUALITY IMPROVEMENT OF GRID CONNECTED WIND ENERGY SYSTEM," NATIONAL INSTITUTE OF TECHNOLOGY , WARANGAL,India, 2014.

[27] A. Choudhary and P. Gaur, "A Study of Hysteresis Band Current Control Scheme For Shunt Active Power Filter Used For Harmonics Mitigation," *International Journal of Advanced Research in Computer Engineering & Technology,* vol. 4, no. 6, pp. 2842-2847, 2015.

[28] C. Tejavoth, M. Trishulapani, V. Rao and Y. Rambabu, "Power Quality Improvement for Grid Connected Wind Energy System using STATCOM-Control Scheme," *IOSR Journal of Engineering ,* vol. 3, no. 7, pp. 51-57 , 2013.

[29] M. H. Firouz, B. Alefy and M. Montazeri, "Voltage Disturbances Improvement of Gird-Connected Wind Turbines in Distribution System Using STATCOM at Weak-Grid Connection Point," *International Journal of Information and Communication Technology Researc,* vol. 4, no. 6, pp. 230-234, 2014.

[30] P. Rathika and D. Devaraj, "Fuzzy Logic – Based Approach for Adaptive Hysteresis Band and Dc Voltage Control in Shunt Active Filter," *International Journal of Computer and Electrical Engineering,* vol. 2, no. 3, pp. 404-412, 2010.

[31] M. Vijayalakshmi and M. Saratha, "GRID CONNECTED WIND ENERGY SYSTEM BASED ON A STATCOM CONTROL SCHEME FOR POWER QUALITY IMPROVEMENT," *International Research Journal of Engineering Sciences,* vol. 3, no. 2, pp. 34-43, 2017.

[32] D. I. B. Djalel, A. Rezaiguia and Z. Abada, "Improving the Electric Power Quality by UPFC Systems in Electrical Networks," *INTERNATIONAL JOURNAL OF ENERGY,* vol. 6, no. 4, pp. 115-122, 2012.

[33] K. S. Kumar, K. S. Kumar and S. Baji, "A New Control Scheme for Power Quality Improvement with STATCOM," *International Journal of Engineering Research and Applications,* vol. 3, no. 4, pp. 2555-2561, 2013.

[34] M. Abbasi, S. Khazaee and B. Tousi, "APPLICATION OF AN ONLINE CONTROLLER FOR STATCOM TO MITIGATE THE SSR OSCILLATIONS," *Journal of Engineering Science and Technology* , vol. 13, no. 9, pp. 2945-2963, 2018.

[35] K. Dosoglu, A. Ozturk, G. Poyraz and U. Guvenc, "Recovering the voltage dip analysis with STATCOM of DFIG in multi-machine wind farm," *PRZEGLĄD ELEKTROTECHNICZNY (Electrical Review),* no. 10, pp. 166-171, 2012.

[36] M. EL-Shimy, "Steady State Modeling and Analysis of DFIG for Variable-Speed Variable-Pitch Wind Turbines," *Journal of Electrical Engineering* , vol. 2, pp. 1-13, 2010.

[37] M. V. Aware, "Power Quality Issues and its Improvement in Wind Energy Generation Interface to Grid System," *MIT International Journal of Electrical and Instrumentation Engineering,* vol. 1, no. 2, pp. 116-122, 2011.

[38] B. Fox, L. Bryans, D. Flynn, N. Jenkins, D. Milborrow, M. O. Malley, R. Watson and O. Anaya-Lara, Wind Power Integration Connection and System Operational Aspects, 2nd Edition, London, United Kingdom: The Institution of Engineering and Technology, London, United Kingdom, 2014.

[39] A. Hortensia, A. Monica and A. O. Carlos, Reactive Power Management of Power Networks with Wind Generation, Madrid, Spain: Springer, 2013.

[40] S. Bhowmick, Flexible AC Transmission Systems (FACTS) Newton Power-Flow Modeling of Voltage-Sourced Converter Based Controllers, US: CRCpress, 2016.

[41] S. V. S. A. K. Murari Lal Azad, "IMPROVING VOLTAGE PROFILE OF A GRID, CONNECTED TO WIND FARM USING STATIC VAR COMPENSATOR," *International Journal of Advances in Engineering & Technology,* vol. 7, no. 5, pp. 1497-1506, 2014.

[42] D. P. K. &. B. E. KUSHARE, "MITIGATION OF VOLTAGE VARIATIONS IN GRID CONNECTED WIND FARM SYSTEM," *International Journal of Electrical and Electronics Engineering Research* , vol. 3, no. 4, pp. 51-58, 2013.

[43] R. K. Sahu and N. Saxena, "Power Quality Enhancement of Power Transmission System Using Static Var Compensator with PID Controller," *International Journal on Emerging Technologies* , vol. 4, no. 2, pp. 117-120, 2015.

[44] A. P. F. R. M. R. Zahira, "Harmonic Reduction in Wind Power Generating System Using Shunt Active Filter with SPWM Technique," *Circuits and Systems,* vol. 7, pp. 157-165, 2016.

[45] M. K. P. Malathy, "Mitigation of Voltage sag and Harmonics in Grid connected Wind Energy System using STATCOM," *IOSR Journal of Dental and Medical Sciences* , vol. 13, no. 4, pp. 111-119, 2014.

[46] B. K. Dohare and R. P. Singh, "Power Quality Improvement By Usingstatcom To Grid Connected Wind Energy System," *IOSR Journal of Electrical and Electronics Engineering* , vol. 12, no. 3, pp. 01-08, 2013.

[47] G. Rohit and R. Preetha, "STATCOM based mitigation of Voltage Sag in DFIG based Wind connected System," *International Journal of Research* , vol. 2, no. 4, pp. 662-668, 2015.

[48] C. Amit Kumar, M. Abhishek and S. Durga, "A Simulation of a STATCOM-Control for Grid Connected Wind Energy System for Power Quality Improvement," *International Journal of Engineering Research and Applications*, vol. 3, no. 4, pp. 1207-1214, 2013.

[49] O. Noureldeen and H. I., "Design of robust intelligent protection technique for large-scale grid-connected wind farm," Springer, Egypt, 2018.

[50] C. Subramanian, D. Casadei, A. Tani and C. Rossi, "Modeling and Simulation of Grid Connected Wind Energy Conversion System Based on a Doubly Fed Induction Generator (DFIG)," *International Journal of Electrical Energy*, vol. 2, no. 2, pp. 161-166, 2014.

[51] B. Wu, Y. Lan, N. Zargari and S. Kouro, POWER CONVERSION AND CONTROL OF WIND ENERGY SYSTEMS, Canada: John Wiley & Sons, 2011.

[52] H. Abu-Rub, M. Malinowski and K. Al-Haddad, POWER ELECTRONICS FOR RENEWABLE ENERGY SYSTEMS, TRANSPORTATION AND INDUSTRIAL APPLICATIONS, United Kingdom: John Wiley & Sons , 2014.

[53] R. Ann, J. Amalorpavaraj, P. KALIANNAN, S. PADMANABAN, U. SUBRAMANIAM and V. K. RAMACHANDARAMURTHY, "Improved Fault Ride Through Capability in DFIG Based Wind Turbines Using Dynamic Voltage Restorer With Combined Feed-Forward and Feed-Back Control," *IEEE*, vol. 5, 2017.

[54] M. Rashidian, B. Ganji and M. Rahimi, "Mitigation of Power Fluctuation in Variable-Speed Wind Turbine with DFIG," *2017 17th IEEE International Conference on Environment and Electrical Engineering and 2017 1st IEEE Industrial and Commercial Power Systems Europe, EEEIC / I and CPS Europe 2017*, pp. 1-5, 2017.

[55] H.-c. Chen and P.-h. Chen, "Active and Reactive Power Control of a Doubly Fed Induction Generator," *An International Journal of Applied Mathematics and Information Sciences*, vol. 8, no. 1, pp. 117-124, 2014.

[56] M. Harshavardhan and K. Rajesh, "Modelling and Simulation of Grid Side Control of DFIG Using Fuzzy and PI," *International Journal of Computer Science and Mobile Computing* , vol. 5, no. 8, pp. 123-130, 2016.

[57] Baoding Tianwei Group Tebian Electric co, "Proposal for engineering, procurement and construction of Adama II wind power project," Hydrochina and CGCOC joint venture, Bejing, 2012.

[58] E. Muljadi and A. Ellis, "WECC WIND GENERATOR DEVELOPMENT," National Renewable Energy Laboratory , Calfornia, 2010.

[59] Z. J. Meng, F. Xue, K. Chang, J. Zhang, L. Xiang, J. Shi and X. Li, "Applications of an Improved Equivalent Wind Method for the Aggregation of DFIG Wind Turbines," *IEEE*, pp. 151-155, 2011.

[60] F. Shahnia, S. Rajakaruna and A. Ghosh, Static Compensators (STATCOMs) in Power Systems, Singapore Heidelberg New York Dordrecht London : Springer, 2015.

[61] K. L..Ashok, A. Naganathan and R. Vidhyapriya, "Power quality improvement of grid connected wind energy systems using STATCOM-battery energy storage system," *ARPN Journal of Engineering and Applied Sciences*, vol. 10, no. 21, pp. 9872-9879, 2015.

[62] N. EAcha, C. R. Fuerte-Esquivel, H. Ambriz-Pe ´rez and C. A.-C. Angeles-Camacho, FACTS Modelling and Simulation in Power Networks, England: John Wiley & Sons, 2004.

[63] E. Hossain, M. R. Tur, S. Ay and I. Khan, "Analysis and Mitigation of Power Quality Issues in Distributed Generation Systems Using Custom Power Devices," *IEEE Access*, vol. 6, pp. 16816-16833, 2018.

[64] A. Kapidou, "Application for Wind Farm Integration Complying with the Grid Code by Designing an Outer Control Strategy for the Converter.," ABB Corporate Research, STOCKHOLM SWEDEN, 2015.

[65] G. ABAD, Power Electronics and Electric Drives for Traction Applications, Spain: John Wiley & Sons, 2017 .

[66] S. D and L. B. Ganesh, "Mitigation of Harmonics by Hysteresis Control Technique of VSI Based Statcom," *International Journal of Latest Trends in Engineering and Technology* , vol. 2, no. 1, pp. 146-160, 2013.

[67] M. A. Pai and A. M. Stankovic, Power Electronics and Power Systems, New York : Springer, 2013.

[68] P. Yedukondalu, M. B. Subbareddy and M. S. Shaik, "MITIGATION OF POWER QUALITY DISTURBANCES IN WIND TURBINE INTEGRATED POWER GRID BY STATCOM," *International Journal of Engineering Science & Advanced Technology*, vol. 3, no. 4, pp. 140-147, 2013.

[69] C. Roy and A. Sengupta, "Implementation of STATCOM to overcome disturbances in grid connected Wind farm," *IEEE*, pp. 4-7, 2015.

[70] M. Kale and E. Ozdemir, "An adaptive hysteresis band current controller for shunt active power filter," *Electrical Power SystemRresearch*, vol. 73, pp. 113-119, 2005.

[71] S. M. Abedi and V. Hani, "Simplified Calculation of Adaptive Hysteresis Current Control To Be Used In Active Power Filter," *Trends in Applied Science Research*, pp. 1-9, 2012.

[72] F. Ali, M. N. Arbab, G. Ahmed, M. Ashraf and M. Sarim, "An SVC controller for Power Quality Improvement of a Heavily Loaded Grid," *ournal of Engineering Research and Application*, vol. 39, no. 2, pp. 247-256, 2020.

[73] M. M. A. Mahfouz and M. A. H. El-sayed, "Static synchronous compensator sizing for enhancement of fault ride-through capability and voltage stabilisation of fixed speed wind farms," *IET Renewable Power Generation*, vol. 8, no. 1, pp. 1-9, 2014.

[74] N. K. S. Naidu and B. Singh, "Doubly Fed Induction Generator for Wind Energy Conversion Systems with Integrated Active Filter Capabilities," *IEEE*, pp. 1-11, 2015.

[75] M. A. Soomro, S. A. Dayo, A. Ansari and A. M. Soomro, "VOLTAGE SOURCE INVERTER BASED STATIC COMPENSATOR FOR CURRENT HARMONIC MITIGATION AND POWER FACTOR IMPROVEMENT OF THREE-PHASE SIX PULSE CONVERTERS," *The Turkish Online Journal of Design, Art and Communication* , pp. 2660-2667, 2018.

[76] S. VALLURI and A. N. KUMAR, "Design and Simulation of Fuzzy Based D-STATCOM with Reduced DC Link Voltage," *International Journal of Advanced Technology and Innovation Research,* vol. 7, no. 13, pp. 2516-2521 , 2015.

[77] S. Mani Tripathi and P. Ji Barnawal, "Design and Control of a STATCOM for Non-Linear Load Compensation: A Simple Approach," *Electrical, Control and Communication Engineering* , vol. 14, no. 2, pp. 172-184, 2018.

APPENDIX A: Simulink Model of the Developed System

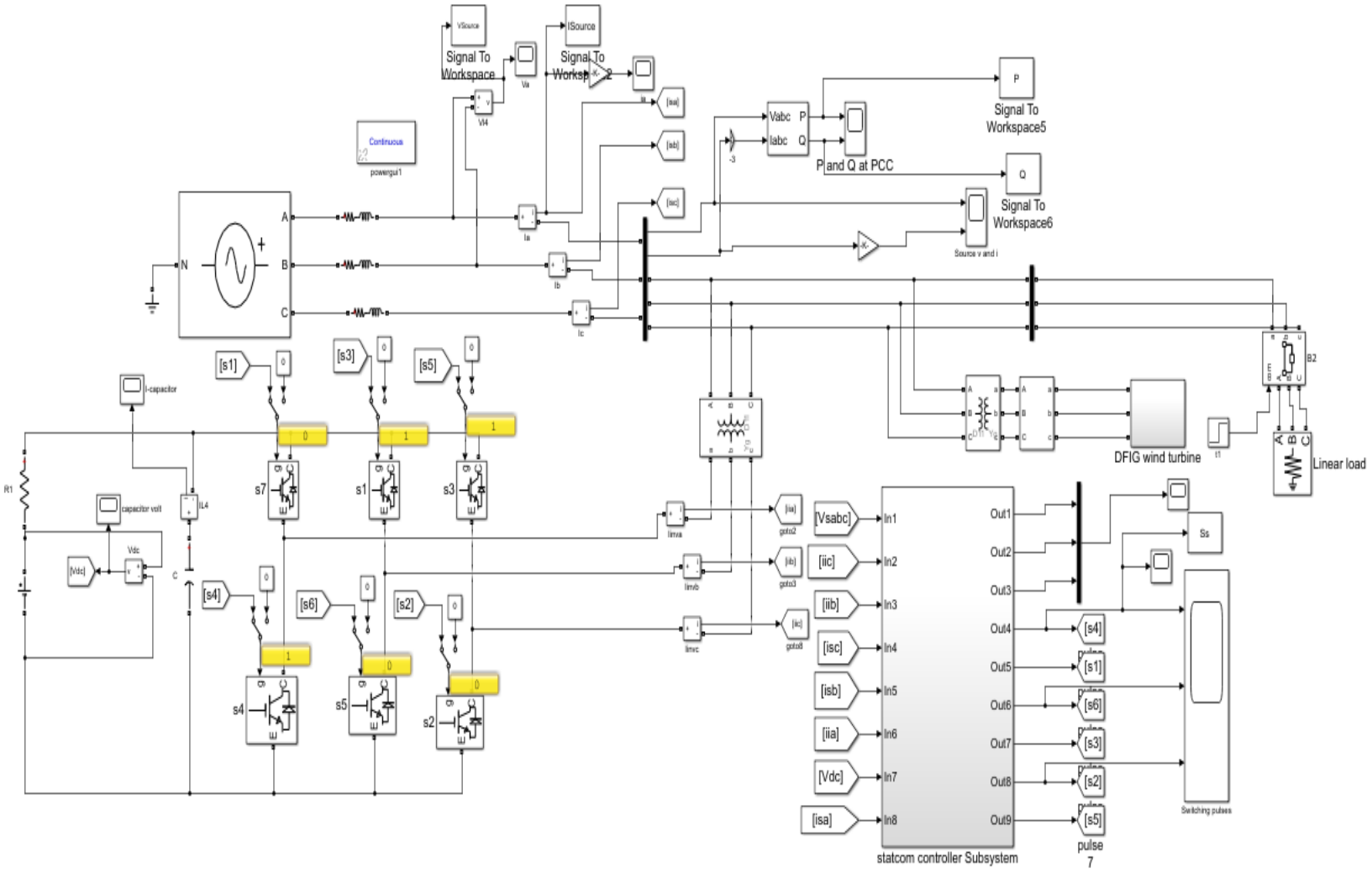

Figure A:1: Simulink model STATCOM with linear load

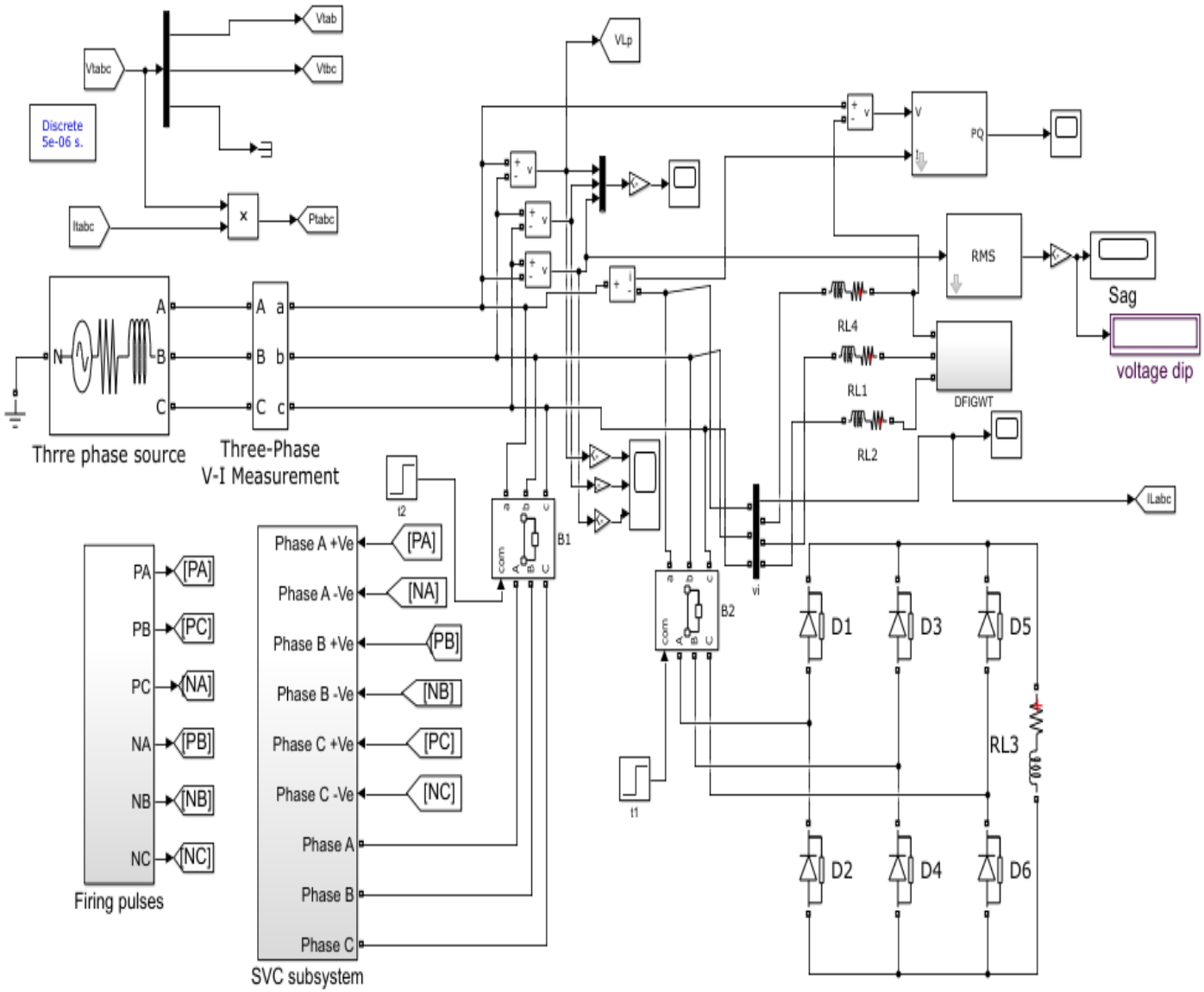

Figure A:2: Simulink model SVC with non-linear load.

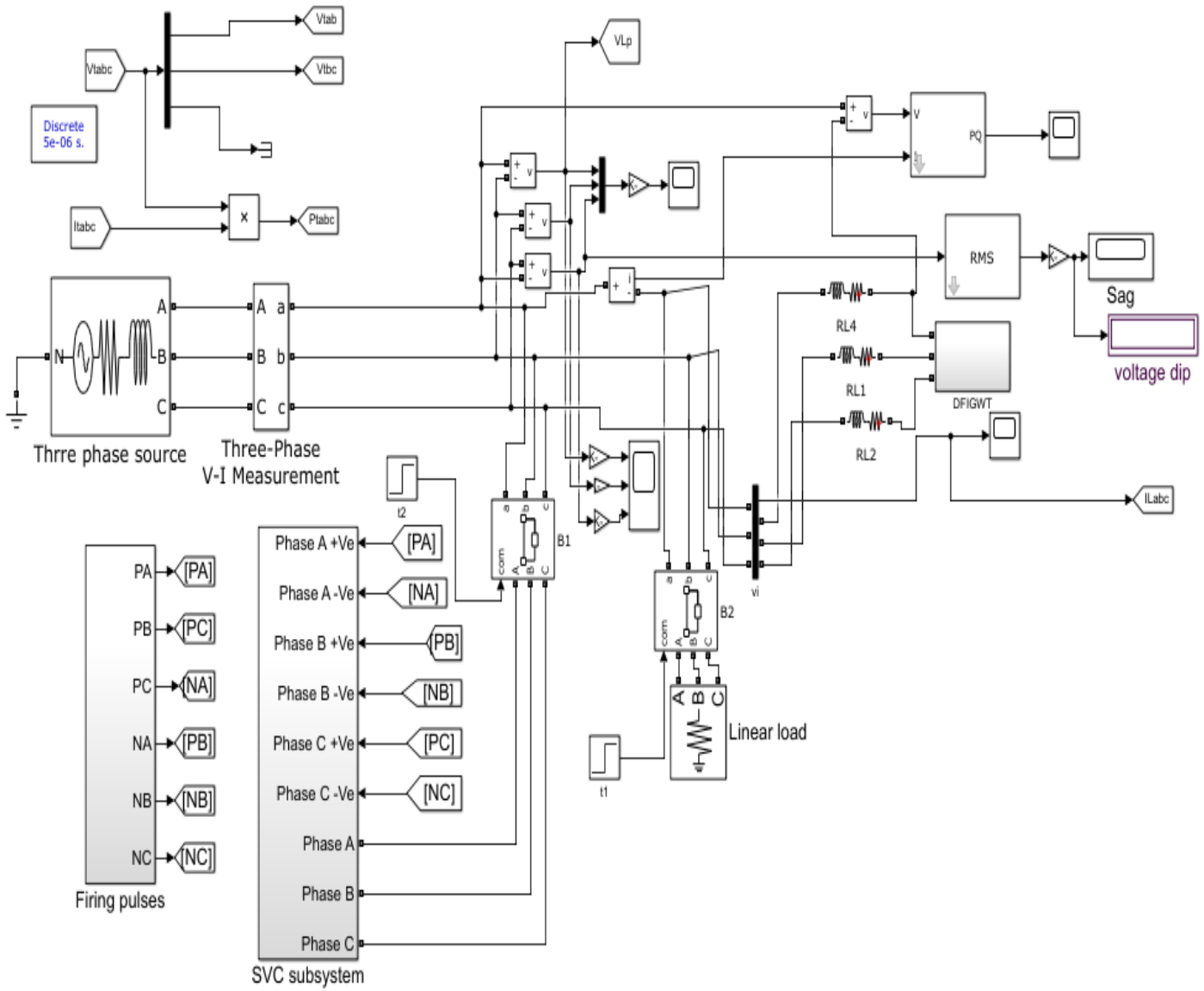

Figure A:3: Simulink model with linear load.

APPENDIX B: System Parameters

Table B:1 DFIG wind parameters

Parameter	Value
Synchronous speed at 50 Hz	150rpm
Rated power	1.5MW
Rated stator voltage	690V
Nominal stator current in rms	1760A
Nominal torque	12.7KNm
Moment of inertia	650kgm^2
Stator connection	star
Pair of poles	2
Rated rotor voltage	2070
Rotor connection	star
Stator rotor turn ratio	1/3
Gera box ratio	1:94.7
Stator resistance	2.6mΩ
Stator leakage inductance	87µH
Magnetizing inductance	2.5mH
Rotor resistance	26mΩ
Rotor leakage inductance	783µH
Rotor resistance referred to stator	2.9mΩ
Rotor leakage inductance	763µH
Stator inductance	2.587mH
Rotor inductance	2.587mH
Rotor rated speed	19rpm
Generator rated speed	1800rpm
Cut-in wind speed	3.5m/s
Rated-wind speed	11.25m/s
Cut-out wind speed	25m/s
Blade number	3
Blade diameter	77m
Swept area	4736m^2
Hub height	70m
Rotating speed	10.6-21.1rpm
Generator power factor	-0.95-+0.95
Unit transformer ratings	1600KVA,33KV
Number of turbines	102

APPENDIX C: Manufacturer Data

Table C:1 Manufacturer power coefficient Vs wind speed of DFIG of Adama wind turbine

v(m/s)	Cp
3	0.3381
3.5	0.4192
4	0.4591
4.5	0.4766
5	0.4809
5.5	0.4809
6	0.4809
6.5	0.4809
7	0.4809
7.5	0.4809
8	0.4809
8.5	0.4809
9	0.4804
9.5	0.4749
10	0.4682
10.5	0.4595
11	0.4188
11.5	0.3665
12	0.3225
12.5	0.2854
13	0.2537
13.5	0.2265
14	0.2031
14.5	0.1829
15	0.1652
15.5	0.1497
16	0.1361
16.5	0.1241
17	0.1135
17.5	0.104
18	0.0956
18.5	0.088
19	0.0812
19.5	0.0752
20	0.0697
20.5	0.0647
21	0.0602

21.5	0.0561
22	0.0523
22.5	0.0489
23	0.0458
23.5	0.0429
24	0.0403
24.5	0.0379
25	0.0357

Table C:2 Power Coefficient Vs Wind speed of DFIG of Adama Wind Turbine

v(m/s)	Ct
3	1.0492
3.5	0.9677
4	0.8983
4.5	0.8372
5	0.7934
5.5	0.7934
6	0.7934
6.5	0.7933
7	0.7934
7.5	0.7934
8	0.7933
8.5	0.7934
9	0.7824
9.5	0.7517
10	0.722
10.5	0.6927
11	0.5806
11.5	0.4804
12	0.4101
12.5	0.355
13	0.3116
13.5	0.2759
14	0.2459
14.5	0.2205
15	0.1989
15.5	0.18
16	0.1638
16.5	0.1496

17	0.1373
17.5	0.1263
18	0.1166
18.5	0.1079
19	0.1001
19.5	0.0931
20	0.0868
20.5	0.0812
21	0.076
21.5	0.0714
22	0.0671
22.5	0.0633
23	0.0597
23.5	0.0564
24	0.0535
24.5	0.0507
25	0.0482

Table C:3 Wind speed Vs power

wind speed(m/s)	Power (KW)
3	17.14
3.5	40.18
4	70.19
4.5	107.37
5	151.67
5.5	204.77
6	268.59
6.5	343.96
7	432.59
7.5	535.17
8	651.45
8.5	785.45
9	934.66
9.5	1087.08
10	1252.82
10.5	1426.19
11	1481.04
≥11.5	1500.69

APPENDIX D: Initialization Program of Wind Turbine

```
% DFIG parametres->rotor parametres referred to stator side
f = 50;                          %stator frequency (Hz)
Ps=1.5e6;                        %stator rated power (W)
n = 1500;                        %rated rotational speed (rpm)
Vs=690;                          %rated stator voltage(V)
Is=1321;                         %rated stator current(A)
Sn=1600e3;                       %rated transformer capacity(VA)
Vsec=33e3;                       %transformer secondary winding  vaoltage.
Tem=9549.3;                      %rated tourque(N.m)
p=2;                             %pole pair
u=1/3;                           %satator/rotor turn ratio
Vr=2070;                         %rated rotor voltage(non-reached(V)
smax=1/3;                        %maximum slip
Vr_stator=(Vr*smax)*u;           %rated rotor voltage referred to stator(V)
Rs=2.6e-3;                       %stator resistance(ohm)
Lsi=0.087e-3;                    %leakage inductance(stator &rotor((H)
Lm=2.5e-3;                      %magnetizing inductance(H)
Rr=2.9e-3;                       %rotor resistance referred to staator(ohm)
Ls=Lm + Lsi;                     %stator inductance(H)
Lr=Lm + Lsi;                     %rotor inductance(H)
Vbus = Vr_stator*sqrt(2);        %DC bus voltage referred to stator(V)
sigma=1-Lm^2/(Ls*Lr);
Fs=Vs*sqrt(2/3)/(2*pi*f);        %stator Flux(apprx.)   (Wb)
J=127;                           %inertia
D= 1e-3;
fsw=4e3;
Ts=1/fsw/f;

%PI controllers
tau_i=(sigma*Lr)/Rr;
tau_n=0.05;
wni=100*(1/tau_i);
wnn=1/tau_n;

kp_id = (2*wni*sigma*Lr)-Rr;
kp_iq = kp_id;
ki_id= (wni^2)*Lr*sigma;
ki_iq=ki_id;
kp_n=(2*wnn*J)/p;
ki_n=((wnn^2)*J)/p;
%three blade wind turbine model
N=94.7;                              % Gearbox ratio
Radio=37;                            % Radio
ro=1.1225;                           % Air density
%Cp and Ct curve
beta=0;
beta1=3;
beta2=6;
beta3=9;
beta4=12;
beta5=15;
beta6=18;
beta7=21;
beta8=24;
```

```
beta9=27;
beta10=30;
beta11=33;
beta12=36;
ind2=1;
for lambda=0.1:0.1:11.8
    lambdai(ind2)=(1./((1./(lambda+0.02.*beta)-(0.003./(beta^3+1)))));
  Cp(ind2)=0.73.*(151./lambdai(ind2)-0.58.*beta-0.002.*beta^2.14-
13.2).*(exp(-18.4./lambdai(ind2)));
  Cp1(ind2)=0.73.*(151./lambdai(ind2)-0.58.*beta1-0.002.*beta1^2.14-
13.2).*(exp(-18.4./lambdai(ind2)));
  Cp2(ind2)=0.73.*(151./lambdai(ind2)-0.58.*beta2-0.002.*beta2^2.14-
13.2).*(exp(-18.4./lambdai(ind2)));
  Cp3(ind2)=0.73.*(151./lambdai(ind2)-0.58.*beta3-0.002.*beta3^2.14-
13.2).*(exp(-18.4./lambdai(ind2)));
  Cp4(ind2)=0.73.*(151./lambdai(ind2)-0.58.*beta4-0.002.*beta4^2.14-
13.2).*(exp(-18.4./lambdai(ind2)));
  Cp5(ind2)=0.73.*(151./lambdai(ind2)-0.58.*beta5-0.002.*beta5^2.14-
13.2).*(exp(-18.4./lambdai(ind2)));
  Cp6(ind2)=0.73.*(151./lambdai(ind2)-0.58.*beta6-0.002.*beta6^2.14-
13.2).*(exp(-18.4./lambdai(ind2)));
  Cp7(ind2)=0.73.*(151./lambdai(ind2)-0.58.*beta7-0.002.*beta7^2.14-
13.2).*(exp(-18.4./lambdai(ind2)));
  Cp8(ind2)=0.73.*(151./lambdai(ind2)-0.58.*beta8-0.002.*beta8^2.14-
13.2).*(exp(-18.4./lambdai(ind2)));
  Cp9(ind2)=0.73.*(151./lambdai(ind2)-0.58.*beta9-0.002.*beta9^2.14-
13.2).*(exp(-18.4./lambdai(ind2)));
  Cp10(ind2)=0.73.*(151./lambdai(ind2)-0.58.*beta10-0.002.*beta10^2.14-
13.2).*(exp(-18.4./lambdai(ind2)));
  Cp11(ind2)=0.73.*(151./lambdai(ind2)-0.58.*beta11-0.002.*beta11^2.14-
13.2).*(exp(-18.4./lambdai(ind2)));
  Cp12(ind2)=0.73.*(151./lambdai(ind2)-0.58.*beta12-0.002.*beta12^2.14-
13.2).*(exp(-18.4./lambdai(ind2)));
  Ct(ind2)= Cp(ind2)/lambda;
  ind2=ind2+1;
end
tab_lambda= [0.1:0.1:11.8];
%kopt for MPPT
Cp_max=0.44;
lambda_opt=6.2;
kopt=((0.5*ro*pi*(Radio^5)*Cp_max)/(lambda_opt^3));

% power curve in the function of wind speed
 P=1.0e+06 *[0,0,0,0,0,0,0,0.0199,0.0472,0.1097,0.1815,0.2568,0.3418,...
    0.4437,0.5642,0.7046,0.8667,1.0518,1.2616,1.4976,1.5000,1.5000,...
   1.5000,1.5000,1.5000,1.5000,1.5000,1.5000,
1.5000,1.5000,1.5000,1.5000,1.5000,1.5000,1.5000,1.5000,1.5000,1.5000,1.5000,1.5000,...

1.5000,1.5000,1.5000,1.5000,1.5000,1.5000,1.5000,1.5000,1.5000,1.5000,1.5000,1.5000,1.5000,1.5000,1.5000];
 V=[0.0000,0.5556,1.1111,1.6667,2.2222,2.7778,3.3333,3.8889,4.4444,...
   5.0000,5.5556,6.1111,6.6667,7.2222,7.7778,8.3333,8.8889,9.4444,...
   10.0000,10.5556,11.1111,11.6667,12.2222,12.7778,13.3333,13.8889,...

14.4444,15.0000,15.0000,15.0000,15.0000,15.5556,16.11111,16.6667,17.2222,17.7
778,18.3333,18.8889,19.4444,20.0000,...
```

```
20.5556,21.1111,21.6667,22.2222,22.7778,23.3333,23.8889,24.4444,25.0000,25.55
56,25.1111,25.6667,26.2222,26.7778]
figure
subplot(1,2,1)
plot(tab_lambda,Cp,'linewidth',0.1)
grid
hold on
plot(tab_lambda,Cp1,'linewidth',0.1)
hold on
plot(tab_lambda,Cp2,'linewidth',0.1)
hold on
plot(tab_lambda,Cp3,'linewidth',0.1)
hold on
plot(tab_lambda,Cp4,'linewidth',0.1)
hold on
plot(tab_lambda,Cp5,'linewidth',0.1)
hold on
plot(tab_lambda,Cp6,'linewidth',0.1)
hold on
plot(tab_lambda,Cp7,'linewidth',0.1)
hold on
plot(tab_lambda,Cp8,'linewidth',0.1)
hold on
plot(tab_lambda,Cp9,'linewidth',0.1)
hold on
plot(tab_lambda,Cp10,'linewidth',0.1)
hold on
plot(tab_lambda,Cp11,'linewidth',0.1)
hold on
plot(tab_lambda,Cp12,'linewidth',0.1)

xlabel('lambda','fontsize',14)
ylabel('Cp','fontsize',14)
subplot(1,2,2)
plot(V,P,'linewidth',0.1)
grid
xlabel('windspeed(m/s)','fontsize',14)
ylabel('power(w)','fontsize',14)
%Grid side converter
cbus=80e-3;   %DC bus capacitance
Rg=20e-6;      %Grid side filter's resistance
Lg=400e-6;     %Grid side filter's inductance
kpg=1/(1.5*Vs*sqrt(2/3));
kqg=-kpg;
%PI regulator
tau_ig=Lg/Rg;
wnig=60*2*pi;

kp_idg=(2*wnig*Lg)-Rg;
kp_iqg=kp_idg;
ki_idg=(wnig^2)*Lg;
ki_iqg=ki_idg;
kp_v=-1000;
ki_v=-300000;
```